Modelling and optimized forecasting of volcanic ash and SO_2 dispersion

---

Thesis for the degree of Philosophiae Doctor

Birthe Marie Steensen

Faculty of Mathematics and Natural Sciences

University of Oslo

2017

Series of dissertations submitted to the
Faculty of Mathematics and Natural Sciences, University of Oslo
No. 1843

ISSN 1501-7710

Cover: Hanne Baadsgaard Utigard.
Print production: Reprosentralen, University of Oslo.

Acknowledgement

The research presented here has been carried at The Norwegian Meteorological Office, division of climate modelling and air pollution. Most of the work done for this thesis was funded by the Norwegian ash project financed by the Norwegian Ministry of Transport and Communications and AVINOR. Model and support is also appreciated through the Cooperative Programme for Monitoring and Evaluation of the Long-range Transmission of Air Pollutants in Europe (No: ECE/ENV/2001/003).

Most of all I would like to thank my supervisor Michael Schulz for giving me the opportunity to do a Ph.D. on this interesting topic. Thank you for all your support throughout the thesis. I also want to especially thank Nina Iren Kristiansen for always answering my questions and helping me. I also highly appreciate the support from my co-supervisor Jón Egill Kristjánsson and especially Kirstin Krüger for helping me towards the end.

I would like to thank all my co-workers for their moral support and technical help throughout my work.

Finally I would like to thank my family for support and especially Nils, you have always encouraged me and been patient during this period.

Contents

List of papers

Paper I

Steensen, B. M., Schulz, M., Theys, N., and Fagerli, H.: A model study of the pollution effects of the first 3 months of the Holuhraun volcanic fissure: comparison with observations and air pollution effects, Atmos. Chem. Phys., 16, 9745-9760, doi:10.5194/acp-16-9745-2016, 2016.

Paper II

Steensen, B. M., Schulz, M., Wind, P., Valdebenito, Á., and Fagerli, H.: The operational eEMEP model for volcanic SO_2 and ash forecasting, Geosci. Model Dev. Discuss., doi:10.5194/gmd-2016-315, in review, 2017.

Paper III

Steensen, B. M., Kylling, A., Kristiansen, N. I., and Schulz, M.: Uncertainty assessment and applicability of an inversion method for volcanic ash forecasting, Atmos. Chem. Phys. Discuss., doi:10.5194/acp-2016-1075, in review, 2017.

1. Introduction

Volcanic eruptions may cause changes in the atmospheric composition and radiative balance, and have significant environmental and economical effects. During eruption, volcanoes emit various sizes of rock fragments named tephra into the atmosphere, in addition to gases such as water vapor (H_2O), carbon dioxide (CO_2) and sulfur dioxide (SO_2). Close to the volcano, the gas emissions can lead to lethal concentrations and the large tephra particles, called blocks and bombs, fall out quickly after ejection and can cause major destruction. The finer particles such as coarse ash (2 mm > d > 64 µm), and especially the fine ash fraction of tephra (d < 64 µm) is light enough to be transported over large distances and consists of abrasive pulverized rock and glass that has a melting point lower than the cruising temperature of a jet engine. Aircrafts flying through ash clouds can therefore get exposed surfaces damaged, and jet engines may experience total failure (Casadewall, 1994). The effects of the volcanic gases emitted during volcanic eruptions are dependent on the injection height, high into the stratosphere the gases can alter the radiation budget globally and lead to changes in the Earth's climate that can last up to decades (Robock, 2000). Volcanic SO_2 emitted into the troposphere mainly increases pollution levels and longtime eruptions can cause acidification of lakes, soil and vegetation (Delmelle et al., 2002).

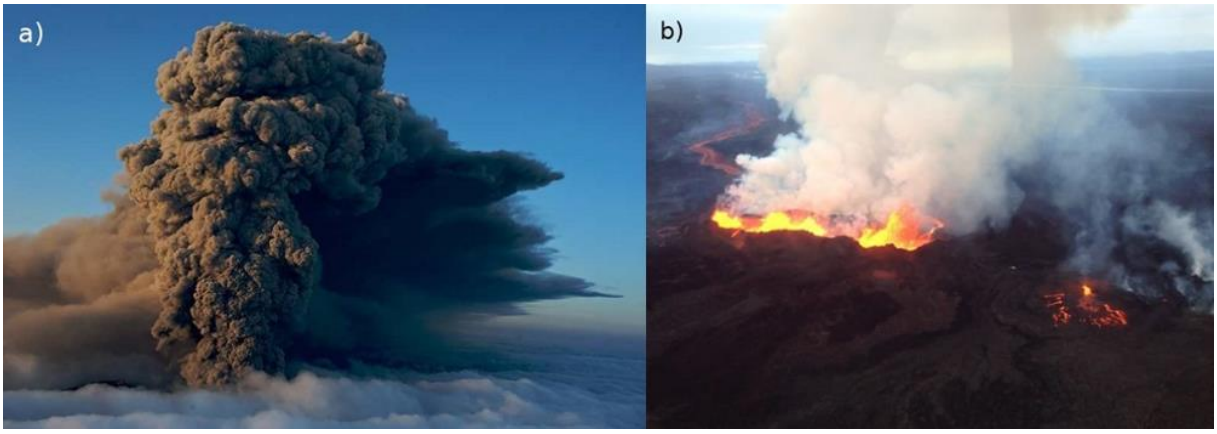

Figure 1.1: Volcanic eruptions on Iceland. a) The volcanic plume during the Eyjafjallajökull eruption 17 May 2010, with large amounts of ash emitted into the atmosphere (photo taken by Ólafur Sigurjónsson, from vedur.is). b) The eruption in the Barðarbunga volcanic system which lead to a fissure eruption on the Holuhraun plain with lava outpouring and high SO_2 emissions, 16 September 2014 (photo taken by Freysteinn Sigmundsson, from vedur.is).

Iceland is one of the most active volcanic regions on earth with around 20 large eruptions every century that have caused historical impacts (Thordarson and Höskuldsson, 2008). One example is the 1783-1784 Laki eruption that released an estimated total amount of 122 Tg of SO_2 into the atmosphere over eight months. Around 78 % of the SO_2 was emitted into the upper troposphere and lower stratosphere causing the emitted gas to be transported eastward by the polar jet stream (Thordarson and Self, 2003a). Sulfuric acid aerosol produced by oxidized SO_2 caused a haze that was observed over the entire Northern Hemisphere (Grattan et al., 1998). Thordarson and Self (2003a) found that the

three years following the eruption (1784-1786) had on average 1.3 °C colder surface temperatures over North America and Europe compared to the annual mean over the 31-year period from 1768 to 1798. Over the Northern Hemisphere, Angell and Korshover (1985) estimate a reduction in surface temperatures from 0.3-0.5 °C during the same three following years. The high increase in pollution levels also lead to increased mortality rates over northern Europe (Grattan et al., 2003; Witham and Oppenheimer 2004).

The first part of this thesis investigates the 2014-2015 Holuhraun eruption (Figure 1.1 b) with large lava volumes released over the Holuhraun plain. The eruption was much weaker than the Laki eruption both with respect to lava released and SO_2 emitted (Thordason and Self, 1993; Gìslason et al., 2015). This type of volcanic eruption, where lava and gas are released effusively through a linear volcanic vent is called a fissure eruption (Parfitt et al., 2009). During the Holuhraun event, high concentrations of SO_2 were reported over several stations in Europe (Schmidt et al., 2015; Gìslason et al., 2015), and the first paper of this thesis investigates how the increase in SO_2 emission affected pollution levels in Europe.

In the second and third paper of the thesis, the dispersion of volcanic ash emissions is studied. The effect of ash on air traffic was first recognized as a major hazard during the May 1980 Mount St. Helens eruption, where a jet airline experienced damage to engine parts and windshield abrasion (Miller and Casadewall, 2000). Ash emissions originating from the October 1982 Galunggung eruption caused engine failure on all four engines that powered a jet flying through the volcanic cloud. This latter case motivated the International Civil Aviation Organization (ICAO) to give guidelines to aircrafts for episodes of volcanic activity (ICAO, 2001). During the 1990s, ICAO established the Volcanic Ash Advisory Centers (VAACs), each with a responsibility for a geographical region, to issue warnings for flight levels where volcanic ash clouds can possibly endanger air traffic.

The third paper in the thesis will present the development and application of a dispersion model to forecast the transport of volcanic SO_2 and ash. The previous "zero" policy that did not allow flights in areas with any observed or predicted ash lead to numerous flight delays, cancellations and large economic cost during the 2010 Eyjafjalljökull eruption (Figure 1.1 a) (European Commission, 2011). The European civil aviation authorities changed the policy to include maximum ash concentrations levels defining the area into which jet airliners can fly safely (UK Civil Aviation Authority, 2016; ICAO, 2016). A low contaminated region is considered to be a region with ash concentrations less than 2 mg m^{-3}, a medium contaminated region has concentrations between 2 mg m^{-3} and 4 mg m^{-3}, and a highly contaminated region experiences concentrations exceeding 4 mg m^{-3}. There are different guidelines for air traffic depending on the ash concentrations and safety risk assessments, with the strictest restrictions applying for the most contaminated areas. The introduction of concentration thresholds for ash has produced a demand for high accuracy in modelling and forecasting of ash dispersion.

1.1 Research motivation

There has been an increase in research activity for both observations and modelling of volcanic ash and SO_2 following the 2010 Eyjafjallajökull and 2011 Grimsvötn Icelandic eruptions. Funding of the work carried out in this thesis mainly originate from the Norwegian National Ash project. One of the tasks was to set up and develop a pilot version of a dispersion model for performing forecasts of ash for the Norwegian airspace, in the event of a near-by volcanic eruption. Due to Iceland's location and the prevailing winds in this region, the volcanic ash and gases are predominantly transported into Northern and Western Europe (Gìslason et al., 2015). Another region in Europe with high volcanic activity is Italy. However, volcanic ash and gases from this region are rarely transported to Norway, and therefore this thesis will focus on recent volcanic activity in Iceland only.

During the work on this project, seismic activity increased in the Barðarbunga volcanic system, which resulted in the main volcanic eruption on the Holuhraun plain on 31 August 2014. The daily SO_2 released from the lava erupted amounted to around 4.5 times the daily anthropogenic emission for Europe in 2009 (Kuenen et al., 2014, Schmidt et al., 2015). Paper I studies how the volcanic SO_2 was spread over Europe during the first three months of the eruption, and compares model results with surface observations and satellite retrievals. For volcanic eruptions where both ash and SO_2 are emitted, SO_2 can act as a proxy for ash in the starting phases (Thomas and Prata et al., 2011; Sears et al., 2013), separation occurs due to density differences, as well as a possible different eruption height (Moxnes et al., 2014). Still validating model capabilities for transporting SO_2 from a volcanic eruption are important for gaining confidence in model results for future eruption scenarios, where volcanic ash may cause a problem for flight traffic. Studying a recent eruption also provides the possibility to use more state of the art meteorological data that would be available for future eruptions.

There are several sources of uncertainty that will be explored in connection with the dispersion of volcanic SO_2 and ash, especially with regards to being in a forecasting setup for operational use. Uncertainties associated with the transport of volcanic emissions due to inaccuracies in the numerical weather prediction data, grid resolution effects, and the description of ash transport in the model are addressed in Paper II. There are also large uncertainties connected to the ejection height and emission amount at the start of an eruption when available information is limited. The applicability of an inversion method (following Stohl et al., 2011) is tested to improve volcanic emissions in a forecasting setting in Paper III.

Satellite retrievals provide information about the current position of the volcanic SO_2 or ash clouds. A dispersion model is however needed to forecast the transport of the volcanic emissions. The European Monitoring and Evaluation Programme (EMEP) model developed at the Meteorological Synthesizing Centre - West (MSC-W), hosted by the Norwegian Meteorological institute since 1979, has been

extended to do dispersion forecasting of volcanic ash and SO_2. Historically, the EMEP MSC-W Eulerian model has been used to handle problems with acid deposition, tropospheric ozone and particles (Simpson et al., 2012). The EMEP MSC-W model is already in use in a forecast mode as one of the ensemble members of the Copernicus Atmospheric Monitoring Service (CAMS) daily ensemble production system for regional air quality forecasting (Marécal et al., 2015).

To model effectively dispersion of volcanic emissions for forecasting and hindcast purposes, some model adjustment has been made, such as the development of a reduced chemistry scheme only taking selected aerosol species, gases and reactions into account in order to reduce the computational time. Another addition to the model is the possibility to include more of the vertical layers available in the meteorological driver, thus increasing the vertical resolution and model top height for handling of the more explosive volcanoes. A specific development done for this thesis is to include the effect of gravitational settling of ash particles for all the model layers. In the standard EMEP MSC-W model, which included particles up to 10 μm in diameter, gravitational settling is only calculated in the lowest model layer. The new treatment is important for a more correct description of the transport of ash particles because differences in wind direction and strength over the column height increase the importance of correct vertical placement of the ash. The ash particles are also larger and released higher in the atmosphere than the particles normally included in the EMEP MSC-W model, such as dust and sea salt. This new version of the EMEP MSC-W model is called the emergency EMEP (eEMEP) model.

1.2 Objectives

Specific objectives of the thesis are:

a) Investigate the environmental impact on Europe of the 2014-2015 Holuhraun fissure eruption with its large amounts of SO_2 released into the atmosphere.
b) Develop and evaluate the eEMEP model capabilities to transport volcanic SO_2 and ash emissions and compare the results with observations.
c) Explore for a volcanic ash advisory system, how useful it is to assimilate satellite retrievals by an inversion algorithm, and find as well as apply the optimized ash source term quickly.
d) Document the uncertainties due to assumptions in the satellite retrievals, meteorological prediction uncertainty, resolution effects and the model description of volcanic ash and SO_2 transport in the eEMEP model.

Paper I focuses on objective (a) that deals with volcanic SO_2 transport. Objective (b) is addressed in paper II where the development of the eEMEP model is presented, as well as a validation of the simulated ash layer height. Paper III focuses on objective (c) where the ash dispersion calculated in the eEMEP model is used to evaluate the applicability of an ash assimilation technique. Objective (d) is addressed in all three papers: more specifically paper I studies emission height sensitivity, paper II

studies the gravitational settling sensitivity, and use ensemble meteorological data with different resolutions to explore uncertainties in the synoptic weather input data and how the dispersion of volcanic SO_2 concentrations are dependent on the model grid resolution. Paper III assesses uncertainties connected to the source terms and satellite retrievals.

The remainder of this thesis is structured as follows. Section 2 presents the scientific background of problems studied in this thesis. Section 3 gives a short description of the model, the observation data used and the inversion algorithm. Section 4 presents summaries of the findings in the papers and Section 5 gives an overall summary and an outlook for future work.

2. Scientific background

This chapter presents a short description of the scientific background related to the research topics investigated in the thesis. To give a broader understanding of the large diversity of volcanic eruptions, the first sections give a description of the eruption types studied here, the plume dynamics of volcanic eruptions and the source emissions. Since the study also addresses issues of dispersion modelling and assimilation, this is shortly described. Pollution levels that can be affected by volcanic eruptions are also presented.

2.1 Volcanic eruptions

Volcanic activity is caused by movements of tectonic plates that make up the Earth's lithosphere (the Earth's crust and mantle) (Perfit and Davidson, 2000). Volcanic activity on Iceland is caused by a divergence of the Eurasian and the North American plate, while for example the Italian volcanoes are produced by a convergence of the Eurasian and the African plate (Scarth and Tanguy, 2001). The types of volcanoes show a large structural variety from a crack in the ground to large stratovolcanoes (Thordarson and Larsen, 2007; Thordarson and Höskuldsson, 2008). Icelandic volcanism is diverse and involves a range of terrestrial magma types and different eruption styles.

Fissure eruptions

Fissure eruptions release lava from a linear vent, and gases such as water vapor, CO_2, SO_2 and halogens (chlorine and fluorine) that are dissolved in the magma are released into the atmosphere when reaching the surface. The gases expand due to the low pressure close to the surface and gas bubbles trapped in the lava cause an intensification of the outpouring of lava. Especially large bubbles of gas can lead to fire fountains that eject tephra when they reach the surface (Sparks et al., 1997). The ejection force and the higher temperature of the volcanic gas as compared to the ambient air, produce a thermal plume that in effect can place the emission of gases high in the atmosphere by convective transport. Flood lava eruptions in Iceland can last for months to years (Thordarson and Höskuldsson, 2008). There can be numerous eruption episodes caused by the formation of a new fissure that start with an explosive fire fountaining phase that is followed by a longer effusive phase.

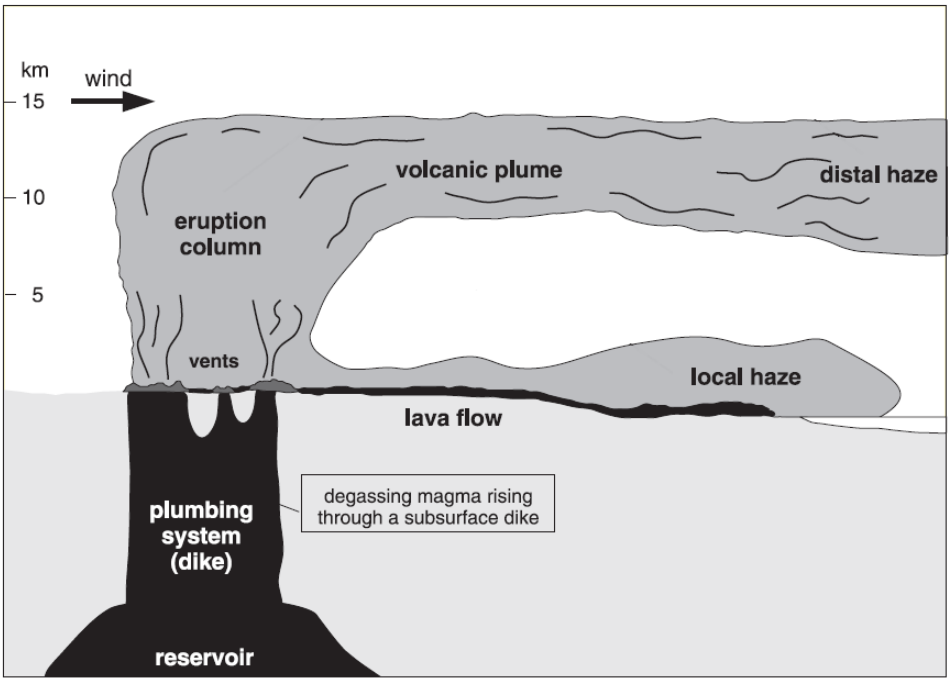

Figure 2.1: A schematic illustration of two-stage degassing during flood lava eruptions. Modified from Thordarson and Self (2003a).

Figure 2.1 shows the estimated vertical distribution of the sulfur emission from the strong Laki fissure eruption (Thordarson and Self, 2003a). Most of the SO_2 was released high into the atmosphere by eruptive episodes during the first five months of the eruption, which also released significant amounts of tephra (Thordarson and Self, 1993; Thordarson and Self, 2003a). The explosive phase was continued by a longer phase of flooding lava that released the gas at lower altitudes. During the 2014-2015 Holuhraun fissure, the first few weeks were characterized by fire fountaining with insignificant ash emissions followed by gas emissions from flooding lava.

Explosive eruptions

Gas dissolved in more viscous silicic magma, which does not flow so easily, can cause explosive volcanic eruptions. Higher crystal content and lower magma temperatures increase the viscosity (Sparks et al., 1997). Three out of four postglacial Icelandic volcanic eruptions have been explosive (Thordarson and Höskuldsson, 2008). The most active volcanic systems are covered by thick glaciers, and because of the proximity to the Atlantic Ocean and the high groundwater levels on Iceland most of these eruptions are hydromagmatic. When hot lava comes into contact with water, rapid conversion of water to steam can occur explosively. The explosive interactions depend on the water to magma ratio and increase the fine ash fraction of the tephra for these types of eruptions (Sigurdsson et al., 2000). Both the Eyjafjollajökull and the Grimsvötn volcanoes are situated under glaciers that the eruption plumes had to melt trough when the eruptions started, this caused increased fine ash emissions and also flooding (Gudmundsson et al., 2012; Liu et al., 2014).

There are several types of explosive volcanic eruptions, and the strength of an eruption can be measured with the Volcanic Explosivity Index (VEI) which is determined by the volume of ejecta, column height and qualitative observations (Newhall and Self, 1982). The index is logarithmic, starting from zero for effusive volcanic eruptions to eight for a supervolcanic eruption. The 2010 Eyjafjallajökull eruption has an estimated VEI of 3 (Gudmundsson et al., 2012), while the strong 1991 Mount Pinatubo eruption is estimated to have a VEI of 6 (Bluth et al., 1992).

2.1.1 Volcanic plumes

Plume dynamics of volcanic eruptions are complicated and are a large source of uncertainty when initiating a transport model. In particular is it a challenge to capture all the physical and dynamical aspects of an explosive eruption. A short description of how the plume can evolve during an eruption is presented here to give more insight into why the source term is difficult to estimate.

A volcanic plume consists of a mixture of tephra and gas that are discharged by explosive volcanic eruptions and shoot out of the vent at high speeds (Mastin et al., 2007). The ejection force from the volcano causes the plume to rise, although the emissions are denser than the surrounding air (Carey and Bursik, 2000). Negative buoyancy and turbulent interactions that entrain the surrounding air causes rising of the plume to slow down until it reaches neutral buoyancy. The entrained air becomes heated resulting in a decrease in plume density with height, and the plume may continue to rise as a hot air balloon. Volcanic emission can either form this convective plume reaching up tens of kilometers, or if the plume loses the discharge momentum before becoming buoyant, the plume can collapse and compose pyroclastic flows down the slopes of a volcano at high speeds (Sparks et al., 1997).

Weaker plumes with less ejection force can be distorted by horizontal wind (Carey and Bursik, 2000). Figure 2.2 shows how the rise of the plume is dependent on the average crosswind speed. For plumes with high rise rate compared to the crosswind speed, the plume is spread laterally as an umbrella shown in Fig. 2.2 (a). An increase in winds causes the umbrella to truncate on the upwind side (Fig. 2.2 (b)). A weaker plume with strong crosswinds compared to the rise rate causes the plume to bend over and no umbrella cloud is formed, as shown in Fig. 2.2 (c).

The height that a plume may reach is therefore mostly relying on the ejection force and atmospheric conditions, such as strong winds, low humidity and high stability of the troposphere, which may have a limiting effect on plume evolution (Carey and Bursik, 2000). More sophisticated plume models are available which include meteorological conditions and the effect of the plume height and dynamics as shown in Fig. 2.2 (Bursik et al., 2001; Costa et al., 2006; Mastin, 2007; Barsotti et al., 2008; Woodhouse et al., 2013; Mastin 2014). In-plume processes such as aggregation of ash particles by hydrometeors (water or ice), and capturing of fine ash particles by larger tephra particles falling through the plume can affect the plume evolution (Textor et al., 2006). Larger ash particles such as

lapilli (64 mm > d > 2 mm) and volcanic bombs (d > 64 mm) are more affected by gravitational effects and a separation of the ash and gas cloud may occur.

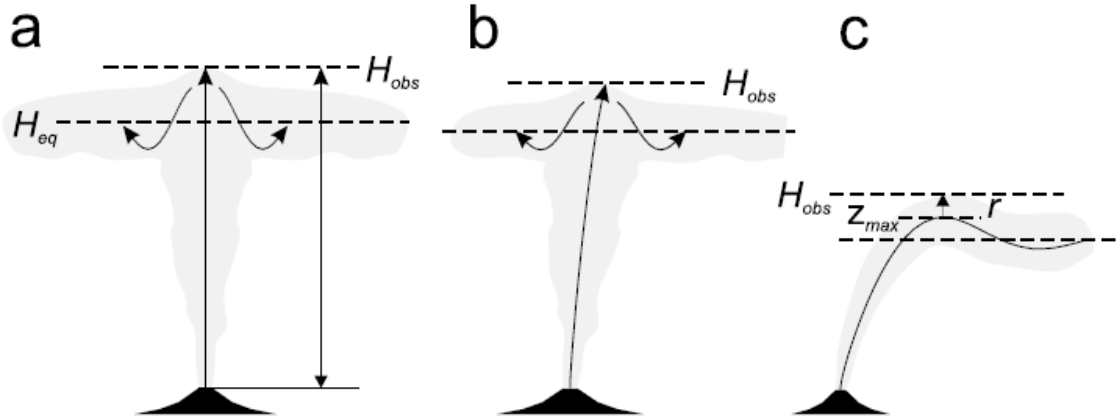

Figure 2.2: Illustrations of volcanic plumes for (a) a vertical plume with low crosswinds, (b) a lightly bent over plume in weak crosswinds, and (c) a bent over plume in strong crosswinds. H_{obs} represents the observed height of the plume, H_{eq} is the equilibrium height and z_{max} is the maximum elevation of the plume axis. From Mastin (2014).

2.1.2 Volcanic emission strength

There are several ways to calculate the volcanic emission strength of volcanic eruptions, for both ash and SO_2 emissions, with and without satellite observations. Although satellite images may give a good estimate of the amount of the SO_2 or the fine ash fraction of tephra released into the atmosphere (Brenot et al., 2014), empirical relationships are useful when no or a very limited number of satellite images are available, for example at the start of an eruption.

Estimates of SO_2 released from fissure eruptions such as at the Holuhraun plain are found by studying the properties of the lava released. This is known as the petrological method and is based on measuring the sulphur concentration in pristine melt or glass inclusions and in the quenched eruption products (Devine et al., 1984). Gìslason et al. (2015) found by using the relationship between iron concentrations and sulphur saturation presented in Blake et al. (2010), that the integrated SO_2 atmospheric mass loading from August to February from the lava released at Holuhraun was 10.7 ± 3 Tg, with an average emission rate of 56 ± 17 kt d^{-1} (148 kt d^{-1} for the first weeks). Thordarson et al. (2003b) presents an empirical approach based on the petrological method and a two stage degassing model (Thordarson et al., 1996). The first stage is due to the magma moving through the vent due to the pressure differences and gas expansion that leads to a high eruption column, and the second stage is caused by degassing of the lava (shown in Figure 2.1). Thordarson and Hartley found by using the Titanium Iron ratio in the lava a 5.3 kg SO_2 loading by each cubic meter of lava released on the plain. Daily SO_2 released to the atmosphere was found to reach 120 kt d^{-1} during the first two weeks, which were reduced to 30 kt d^{-1} in November.

For ash emissions, empirical relationships for a first guess of the ash emissions at the start of a volcanic eruption are found from historical volcanic eruptions. Several studies have investigated the relationships between the mass eruption rate (MER) of tephra and plume height H (given in km):

$$MER = \frac{H^{-e}}{d} \cdot \rho$$

MER is given in kg s^{-1}. ρ is the density of the ash particles, d and e represent the best fit coefficients between the MER and height relationship. Sparks et al. (1997) find a best fit for historical eruptions with the coefficients $d = 1.67$ and $e = 0.25$, while for the eruptions included in Mastin et al. (2009) a best fit is found for $d = 2.0$ and $e = 0.241$. The difference between these two studies is found to be statistically insignificant and the two lines are plotted in Figure 2.3 for the historical volcanic eruptions used in Mastin et al. (2009). Ash density (ρ) [kg m^{-3}] is another source of uncertainty, with values from 700 kg m^{-3} for the most porous part of the tephra to 3300 kg m^{-3} for crystals (Wilson et al., 2011). Observations of plume heights can be obtained from e.g. aircrafts or weather radars (Arason et al., 2011), as well as from satellite observations that can provide information in the vertical such as the Cloud-Aerosol Lidar with Orthogonal Polarization (CALIOP) instrument aboard the Cloud-Aerosol Lidar and Infrared Pathfinder Satellite Observations (CALIPSO) satellite (Winker et al., 2012).

Figure 2.3 shows the individual data points along with fitted eruption rates found from the empirical relationships described above. The scatter of the individual data points for the historical eruptions reflects the natural variability relating plume height and eruption rate but also the large uncertainty of the measured parameters such as the plume-height observations and inaccuracies in the eruption volume estimates. Including more recent volcanic eruptions with better observations can improve the relationship.

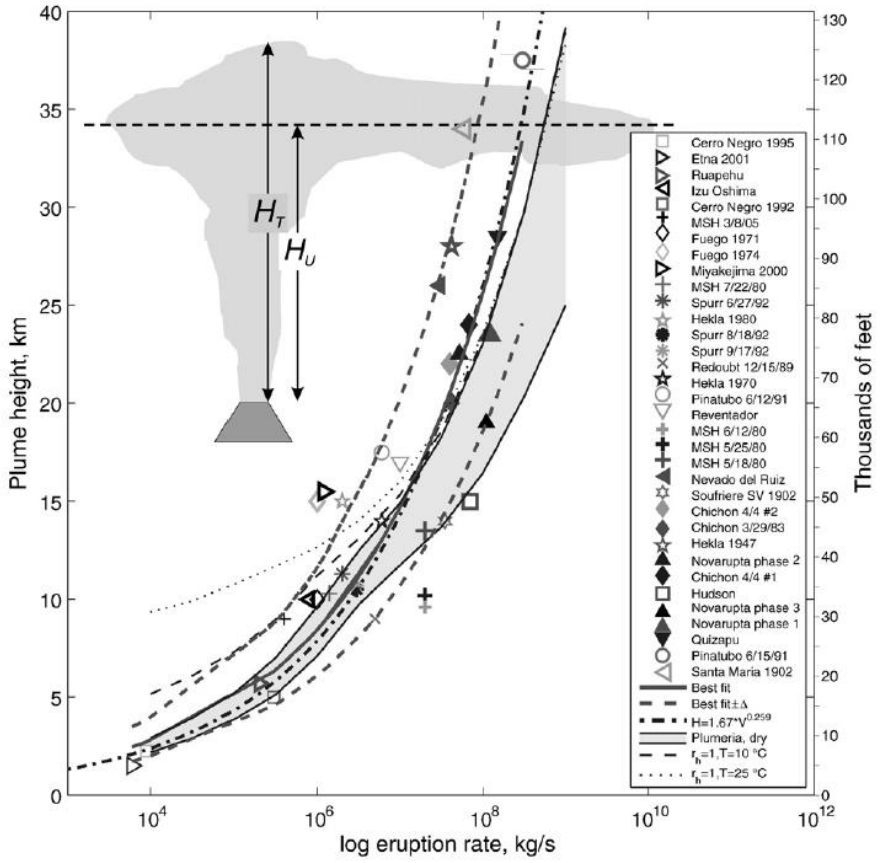

Figure 2.3: Plume height above vent versus mass eruption rate (kg s^{-1}) for the historic eruptions listed in the legend. The best fitted empirical relationship from Sparks et al. (1997) is given as the dash- dotted line. The solid line represents the empirical relationship found in Mastin et al. (2009), bold dashed lines enclose an error envelope of the Mastin et al. (2009) relationship corresponding to a 50 % confidence interval. The grey shaded region is calculated by the Plumeria model by Mastin (2007), using the height of the plume (H_T) and by using the height of the umbrella (H_U). The light dashed line and dotted lines are results from the same Plumeria model but with different atmospheric conditions. Figure from Mastin et al. (2009).

When released into the atmosphere, the amount of volcanic gas and fine ash can be observed by remote sensing that offer an independent way to estimate volcanic source strength. Since 1978 satellite retrievals of volcanic SO_2 column loads have been made possible by the Total Ozone Mapping Spectrometer (TOMS) (Krueger et al., 1995). More recent instruments such as thermal infrared sensors can also identify ash. Although there are large uncertainties connected to the detection and quantitative column load retrievals of both volcanic SO_2 and ash (see Thomas and Watson 2010, and a short description in section 3.2), various attempts have been made to develop methods for calculating emission fluxes from satellite retrievals for SO_2 that can also be applicable for ash (see Theys et al., 2013 for an overview of methods). All the methods are based on mass conservation, meaning that the satellite retrieval for a given day reflects the budget of volcanic emissions and losses since the start of the eruption period. The box method considers the SO_2 mass concentrations within a box (or circle) that has the dimensions corresponding to the total distance traveled by the plume in one day (Lopez et

al., 2013). The traverse method considers the flux of SO_2 passing through imagined vertical cross sections (Meruccie et al., 2011). Both these methods require knowledge about the wind fields, while another method (Delta-M) relies only on a series of SO_2 mass obtained by successive satellite overpasses (Krueger et al., 1996). Most earth orbiting satellite instruments observe the volcanic cloud only over a short period of time and the area is restricted by the swath of the satellite. Parts of the volcanic clouds can therefore be missed and high frequency variations in the emission sources may also be unresolved by these methods. For SO_2 emissions, considerations about the lifetime and losses dependent on atmospheric conditions also have to be taken into account.

Finally inversion methods are developed to optimally exploit the satellite retrievals to find the volcanic source term by the use of volcanic transportation and dispersion models for both SO_2 and ash emissions (Eckhardt et al., 2008; Stohl et al., 2011; Boichu et al., 2013). This study will evaluate the application of such an inversion technique, based on work presented in Stohl et al. (2011), in a forecasting setting. More information on this method will be given in Section 3.3.

There are limitations for all these methods used to calculate the volcanic source terms. They may be applicable for different types of volcanic emissions and at different times during the eruption (Theys et al., 2013). The empirical relationships are useful at the start of eruption, before any satellite observations are available. When satellite data are available, the box and traverse method can be used for young plumes. The Delta-M method is best suited for long lived plumes at high altitudes. Over long eruptions with changes in the emission flux, the inversion method is considered to calculate the most accurate source term.

Paper III uses the empirical relationship for ash emissions with the Mastin et al. (2009) coefficients to produce a priori emissions for the inversion calculations. In this case, the a priori estimate was reduced by around 50 % by the inversion calculations indicating the uncertainties in the empirical relationships.

2.2 Volcanic dispersion and transportation models

The use of numerical models to forecast and study the transport of volcanic emission has been increasing over the last decades. The models calculate the transport of trace substances by using meteorological data input from numerical weather prediction (NWP) models. Modelling ash and SO_2 dispersion can be complex, as there are many uncertainties. This section will give a small introduction to the methods of modelling transport of volcanic emission from plumes that have persisted for a sufficiently long time, so that the volcanic ash or SO_2 have become fully subjected to atmospheric motions and therefore further transport is independent of the uncertainties connected to the plume dynamics and emission term.

There are two principal ways to model transportation; (i) Lagrangian particle models compute trajectories of a large number of particles to describe the transport and diffusion of pollutants in the atmosphere (Stohl et al., 2005). (ii) Eulerian models, like the eEMEP calculate the mass concentration of the tracers as a function of space and time trough fluxes between grid boxes. Most VAACs use Lagrangian models, e.g. NAME (Jones et al., 2007) at the London VAAC, or HYSPLIT (Draxler and Hess, 1997) at the Washington and Anchorage VAAC. Other well-known Lagrangian models used for ash dispersion are FLEXPART (Stohl et al., 2005) and PUFF (Searcy et al., 1998), the latter is also used as backup by the Washington and Anchorage VAAC. Some Eulerian models used for ash dispersion are MOCAGE (Josse et al., 2004) used at VAAC Toulouse, Fall3d (Folch et al., 2009) and Ash3d (Schwaiger et al., 2012). All the models, whether they are of Lagrangian or Eulerian type, treat the processes dispersion, turbulence, deposition and convective mixing differently. A last method is by tracking volcanic ash and SO_2 directly online in the numerical weather prediction models (Webley et al., 2012, Flemming et al., 2013). By doing this during the simulation, the NWP models can account for changes in the atmospheric conditions due to the volcanic emissions. This method will not be discussed is this work.

The Lagrangian models have advantages for operational runs as they are usually computationally less expensive, display less numerical diffusion, and can therefore produce quick results for the dispersion of the volcanic emission clouds. Concentrations in Lagrangian models are typically calculated by the density of the multiple particles released. The results can however exhibit uncertainties in regions with a low number of particles. Concentrations are calculated more directly in the Eulerian model frame as the transport is calculated at every grid point in the model domain from the actual emitted mass. This causes the concentrations to be dependent on the resolution of the model as concentrations are mixed within the grid box. This effect, called numerical diffusion is dependent on grid resolution, advection scheme, gradients in the tracer field and numerical precautions taken, and will be studied here for volcanic transportation modelling. There are several methods for computational efficient advection calculations with limited numerical diffusion effects. For the eEMEP model, the numerical solution for the advection equation is based on the Bott scheme (1989 a,b). The Bott scheme uses higher order polynomial fitting to obtain a better fitting of the advected field. With increasing computational resources, Eulerian model calculations have become feasible in operational settings using model calculations with higher model grid resolution (Schwaiger et al., 2012).

An advantage of the Eulerian models is that the loss of the pollutants is treated more consistently with a dynamic atmospheric chemistry environment and other deposition processes. SO_2 is lost in the atmosphere by oxidation to form sulfate either in the gas-phase with the hydroxyl radical (OH) or in the aqueous phase (in-cloud) mainly be hydrogen peroxide (H_2O_2). In the Eulerian model frame, since it can handle several tracers at the same time, the concentration of OH or that of oxidants in cloud droplets can be controlled by local chemistry (Simpson et al., 2011). Paper I uses this possibility on

the eEMEP model to calculate the increase on sulfuric acid aerosol. Other process such as fine ash aggregation to coarser particles can also be parameterized by actual model concentrations in an Eulerian model (Costa et al., 2006).

2.3 Data assimilation

The goal of data assimilation is to combine model results with observations to increase the model performance (Daley 1993; Kalnay 2003). Model simulations, and especially predictions, are initial-value problems where an estimate of the present state of the atmosphere has to be given to start a realistic model forecast simulation. Both the meteorological data used as input to the dispersion model and the pollutants transported in the model pose initial state problems. For volcanic eruptions the initial state problems relate to the source term and thus the concentration of volcanic emission in the atmosphere. While the meteorological driver initial value problem is related to meteorological variables such as atmospheric pressure, wind, temperature and humidity.

A first guess of the initial state is often used to prepare the calculations (Gneiting and Raftery, 2005). For a NWP this best guess can be a climatology or more commonly a previous short range forecast. Then assimilation is often done by minimizing a cost function by combining the model background or the best guess assumption with the observations to obtain the best possible initial conditions for the actual forecast. For the solution, to not become ill-conditioned and difficult to solve, enough observations are needed. The uncertainty of the initial state of the NWP forecast translates into uncertainties further into the weather prediction. Probability forecasts based on ensemble modeling with multiple numerical prediction model simulations started with slightly perturbed initial conditions can be used to quantify this uncertainty.

Observations which constrain volcanic emissions can be assimilated into dispersion models by calculating an optimized emission term by e.g. an inversion method or by directly changing the model concentrations to observed satellite values. An example of the latter is the insertion method presented by Wilkins et al. (2016), where a series of satellite observations is used to initialize a forecast of volcanic ash dispersion. This method requires no knowledge of the source term in the model. It does, however, include the uncertainties in the satellite retrieval. This method also has uncertainties connected to the height and vertical extension of the ash cloud, as the satellite data often detect horizontal distribution only. Since the winds can vary with height, a correct placement of the cloud is important for further predictions. The inversion method used in this study fist applied on volcanic eruptions by Eckhard et al. (2008), combines model results with observations, both concentrations and the vertical placement of the emissions are matched with the satellite retrievals. Stohl et al. (2011) did additional development to the method to produce a time and height resolved source term. A further

description of this method is presented in section 3.3. A similar inversion method was also used by Boichu et al. (2013).

2.4 Pollution levels

Although the largest strain from volcanic emissions is felt close to the volcano, where the concentrations are high, tephra and SO_2 transported far away from the volcanic source can also increase the pollution to critical levels (Baxter 2000; Schmidt et al., 2015).

The World Health Organization (WHO) has set concentration limits for SO_2 for both short term and long term exposure due to health effects on the respiratory system. A limit for a ten minute mean exposure is set to 500 µg m^{-3} and a daily 24-hour mean exposure is recommended to be below 20 µg m^{-3} (WHO, 2005). The European Union has agreed on their own concentration limits; a high hourly average of 350 µg m^{-3} that should not to be exceeded more than 24 times within a calendar year (EU Directive, 2008). During the 2014-2015 Holuhraun eruption, the 350 µg m^{-3} hourly concentration limits were exceeded repeatedly on Iceland (Gíslason et al., 2015).

Particulate matter (PM) also has a range of health effects, mostly related to the respiratory and cardiovascular systems. Especially exposure to high concentrations of fine ash may cause nasal, throat, eye and skin irritation (www.ivhhn.org). Exposure to PM can also increase the risk of lung cancer (Raaschou-Nielsen et al., 2013). In addition to the fine ash released from volcanic eruptions, the increase in sulfuric acid aerosol production due to increase in SO_2 contributes to the PM concentration. WHO has concentration limits on the part of particulate matter with mass diameters up to 10 µm (PM_{10}) and particulate matter with mass diameters up to 2.5 µm ($PM_{2.5}$). An annual mean PM_{10} limit is set at 20 µg m^{-3} and a 24-hour mean limit at 50 µg m^{-3} that should not be exceeded more than three days in a year. For $PM_{2.5}$, the annual mean limit is set at 10 µg m^{-3} and a 24-hour mean limit is at 25 µg m^{-3}, exceeded no more than three days per year.

Sulfur deposition causes acidification of ecosystems as well as lakes and rivers (Tørseth et al., 2012). Plants can be exposed to damage due to acidification from sulfur by and wet deposition above the ground and by pollution in the soil (Reuss and Johnson, 2012). Acidification of waters has led to fish death in Scandinavia (Hindar, 1994). Emission restrictions have decreased the anthropogenic sources of SO_2 since 1980s, as shown in Figure 2.4. A clear decrease is seen as a result of the reduced emissions over this time period, especially over central Europe. High concentrations are still measured over Poland and Hungary in 2009, while the stations in central Norway and western Sweden have the lowest measured concentrations. An increase in SO_2 caused by volcanic eruptions over time may again increase the acidification level, and the increase in sulfur deposition due to the Holuhrun 2014-2015 eruption is studied in Paper I.

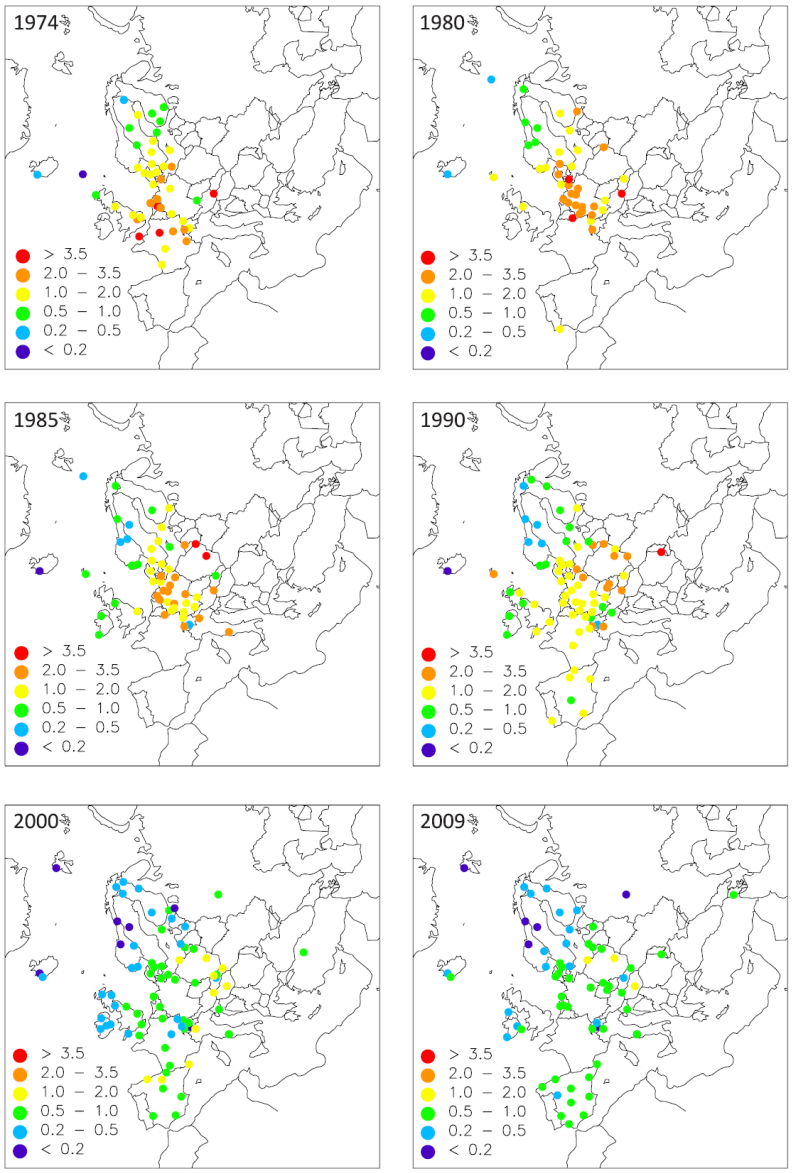

Figure 2.4: Annual mean concentrations of SO_4^{2-} in aerosol from 1974 to 2009, units are given in µgS m^{-3}. Modified from Tørseth et al. (2012).

3. Methods

This chapter presents a short description of the eEMEP model used to calculate dispersion in the thesis, methods to detect and retrieve SO_2 and ash by satellite observations and other observational data used, and a short presentation of the inversion method.

3.1 Model

The EMEP MSC-W model is a chemical transport model (CTM) developed at the Norwegian Meteorological Institute. Since first described in Eliassen et al. (1982), the model has been expanded to include more physical processes, chemical compounds and photo-oxidants (Simpson et al., 2012). Throughout the years the model has also been converted from a Lagrangian modelling frame to an Eulerian with optional horizontal resolution dependent on the meteorological input data. Updates to the model are described in the yearly EMEP reports (e.g. EMEP Status Report, 2016). Paper II presents additions to the model to describe the transport of volcanic SO_2 and ash which especially were done as a part of this thesis. This version of the model is called the emergency EMEP (eEMEP).

A development for the eEMEP model is the change from sigma coordinates to hybrid eta (η) levels the vertical levels description. With this change, the model is capable of including more vertical levels, if available in the meteorological input data, in order to improve the vertical resolution and increase the model height of the top level for large volcanic plume heights. The eta levels are a function of reference pressure P_0= 1013.5 hPa, and two time-independent coefficients denoted by A and B that only vary in the vertical, $\eta = A/P_0 + B$. The pressure levels are defined as: $p = A + BP_0$.

Each pollutant in the model is transported forced by information from the meteorological driver. If χ represents the mass mixing ratio of any pollutant, e.g. kg pollutant per kg air, the continuity equation can be written as:

$$\frac{\partial}{\partial t}(\chi p^*) = -m_x m_y \frac{\partial}{\partial x}\langle \frac{u}{m_y}\chi p^* \rangle - m_x m_y \frac{\partial}{\partial y}\langle \frac{v}{m_x}\chi p^* \rangle - \frac{\partial}{\partial \eta}\langle \dot{\eta}\chi p^* \rangle + \frac{\partial}{\partial \eta}\left[K_\eta \frac{\partial}{\partial \eta}(\chi p^*)\right] + \frac{p^*}{\rho}S$$

The first three terms on the right hand side describes the flux divergence of the advective transport, u and v are the horizontal wind components, and $m_x$and m_y are the map factors in the x and y directions. The vertical velocity is denoted by $\dot{\eta} = d\eta/dt$ and $p^* = \partial\eta/\partial p$. The fourth term represents the vertical eddy diffusion, and K_η represents the vertical eddy diffusion coefficient in η-coordinates. The fifth term represents the source and sinks (S) of the tracer due to chemical reactions and emissions, and ρ represent the air density.

The advection scheme has a numerical solution based on the Bott's scheme (1989a,b), with the fourth order scheme in horizontal directions and a second order version applied on the variable grid distances in the vertical direction.

Air is also advected (χ_{air}=1), and inconsistencies in the wind field may result in "air concentration" different from 1. New mixing ratios need to be found after each advection step to keep mass conservation. The advected air ($\chi_{air}^{t+\Delta t}$) is used to renormalize the mixing ratio of the advected pollutants. This is done by dividing the results obtained with the Bott-scheme with the new air concentration: $(\chi_x)^{t+\Delta t} = \frac{(\chi_x p^*)^{t+\Delta t}}{\chi_{air}^{t+\Delta t}}$, where $(\chi_x p^*)^{t+\Delta t}$ is the result of the Bott-scheme in the x-direction after a time step Δt.

Time steps used in the advection scheme are dependent on the model grid resolution. Since the model needs meteorology data to drive the dispersion and should be flexible for different users, the eEMEP model is adapted to run with input from several NWPs. As described above, horizontal resolution is dependent on the resolution of the meteorological driver, and simulations with resolutions varying from a very fine (few km) to 1x1 degree are possible. Temporal resolution is typically 3-hourly for the meteorology data. Although model calculations require some data (see table 2 in Simpson et al., 2012) from the meteorological driver, the model can calculate missing fields if they are required and not included in the data (e.g. 3-d precipitation, vertical velocity).

The chemical species, reactions as well as emissions included in the model have been developed over time, and the model can be run with different complexity of chemistry and allows reduction in the number of tracers. To perform quick simulations of the spread of volcanic ash and SO_2, additional pollutants and reactions are excluded in the model calculations in order to reduce the computational time. For the study in Paper I, where the increase in sulfate production due to the volcanic SO_2 emission is investigated, full standard EMEP MSC-W chemistry was used in order to account for sulfur production and the contribution to $PM_{2.5}$ concentrations.

Treatment of volcanic emissions during transport

There are different loss processes in the model determining the fate of volcanic emissions in the atmosphere; SO_2 is lost by oxidation to form sulfuric acid aerosols, while the fine ash particles are deposited mainly due to gravitational settling. Depositions due to wet scavenging are included for sulfur and ash. Both in-cloud and below-cloud removal are taken into account. Below-cloud scavenging rates are calculated based on Scott (1979). Dry deposition of SO_2 in the model is only calculated in the surface flux layer of the model, closest to the ground, and is parameterized for different land types, temperatures and humidity over the canopy.

Sulfuric acid aerosol is formed by oxidation of SO_2 in both gas and aqueous phase. In gas phase the oxidation is initiated by OH that is controlled by local photochemistry. In aqueous phase, the oxidants ozone, hydrogen peroxide and oxygen catalyzed by metal ions contribute to the oxidation. If the cloud evaporates, the sulfuric acid aerosol formed in the cloud is assigned to the airborne particulate phase.

Dry deposition of sulfuric acid aerosol in the model is done in a similar way to the dry deposition of SO_2, except with different parameterizations for the land types.

Paper II in this study presents the addition of gravitational settling for volcanic ash included in the eEMEP model, one as part of the work on this thesis. Ash particles are heavier and denser than other pollutants included in the standard EMEP MSC-W model (> 10μm) and therefore the gravitational settling for volcanic ash in all layers is added to the model. Wilson and Huang (1979) give a description of gravitational settling where the drag coefficient is modified to include the shape of the ash particle, this parameterizatio is also used in Ash3d (Schwaiger et al., 2012) and as one of four possibilities in Fall3d (Folch et al., 2009). Further information about gravitational settling is presented in Paper II.

Volcanic emission

Volcanic emission parameters for both SO_2 and the fine ash fraction of tephra are read from a source term file containing flux (kgs^{-1}), vertical position and time of release. The location of the volcano is read in from a separate file. If the vertical distribution of the emissions is given in height intervals, the emissions are spread uniformly between the appropriate vertical levels in the model. More sophisticated emission descriptions from e.g. plume models that use atmospheric conditions like Plumeria (Mastin, 2007), or emissions calculated from inversion techniques (Stohl et al., 2011), can therefore be used, if provided as input. Model results of these types of volcanic emission terms are presented in Paper II and III. If only the height of the emission top is given, the emissions are distributed uniformly over the emission column down to the height of the volcano top. This type of simplified emission is used in Paper I.

3.2 Observations

Several types of volcanic SO_2 and ash observations are compared with the eEMEP model results in this thesis. Retrievals of column burdens from satellite observations are especially valuable for volcanic eruptions and are used in all the studies. Ash satellite retrievals are also applied to constrain the ash source term in the model. A short presentation of observed surface concentrations and vertical lidar retrievals are also described here.

3.2.1 Satellite observations

Satellite measurements provide global observations of volcanic activity and sometimes early detection of eruptions (Thomas and Watson, 2010; Hufford et al., 2000). Retrievals can give information about the concentrations, transport and even height of the volcanic clouds for some instruments (Winker et al., 2012). This section provide a short overview of available satellite products and what is used in this

study for detecting ash and SO_2, and a simple description of the assumptions made to retrieve the column loads.

SO_2 retrievals

Vertical Column Densities (VCD) of SO_2 can be retrieved from infrared (IR) sensors like AIRS (Atmospheric Infrared Sounder) and IASI (Infrared Atmospheric Sounding Interferometer), and ultraviolet (UV) visible satellite measurements from e.g. OMI (Ozone Monitoring Instrument) and GOME-2 (Global Ozone Monitoring Experiment-2). Both types of instruments detect SO_2 due to absorption over distinct wavelengths (Brenot et al., 2014). There is an uncertainty in the IR retrievals due to competing water vapor absorption over the wavelength of interest and a low thermal contrast between the volcanic cloud and the ground (Thomas and Watson, 2010). The UV spectrometers measure sunlight backscattered from the atmosphere and observations are therefore only available during sunlight hours. Clouds over the SO_2 can obscure the retrieval with IR, and detection over cold surfaces such as snow or high cirrus clouds can also be difficult because of the low temperature contrast (Prata et al., 2003). Retrievals are also sensitive to the presence of water and ice clouds for UV instruments (Yang et al., 2007; Theys et al., 2015).

Retrievals from UV spectrometer are used in this thesis. The sensitivity of backscattered radiation by SO_2 molecules decreases towards the ground and therefore the retrieval algorithm assumes an a priori plume height distribution (Yang et al., 2007). If the assumed plume height distribution does not match the real plume height, the retrieved VCD values are not representative of the actual values, and therefore difficult to compare directly with model VCD. Averaging kernels provide the vertical information of the weighting of the a priori plume height and noise in the satellite retrieval from clouds. Paper I compares VCD of SO_2 from model simulations and satellite retrievals by applying the averaging kernel from OMI retrievals (Theys et al., 2015) to the model layers. Paper II compares the SO_2 VCDs calculated by ensemble model results to the same OMI retrieval.

Ash retrievals

IR satellite retrievals are most commonly used to find the column loads of volcanic ash in the atmosphere. UV-visible sensors can only indicate the increased presence of absorbing aerosols in the atmosphere by the absorbing aerosol index (AAI) (Brenot et al., 2014). The Spinning Enhanced Visible and Infrared Imager (SEVIRI) aboard the geosynchronous Meteosat Second Generation (MSG) satellite provide retrievals every 15 minutes over an earth disk, providing continuous monitoring capabilities for volcanic ash (Schmetz et al., 2002). These retrievals are used in Paper III.

Ash is identified in pixels if the brightness temperature difference (BTD) between the infrared channels 10.8 μm and 12.0 μm are above a certain threshold after applying the water vapor absorption correction by Yu et al. (2002). The threshold is typically given between -0.5 K to -1 K. Ice gives positive BTDs and water clouds give BTDs closer to zero. Ash pixels can therefore be contaminated

by the presence of water and ice clouds (Prata and Prata, 2012). The ash detection can falsely classify ash in regions where there is no ash over land due to spectral land surface emissivity, and for pixels with large viewing angles close to the edge of the SEVIRI coverage. To calculate the ash column loads, several assumptions are made that increases the uncertainty, which is further described in Paper III.

A distinct assumption that is studied in Paper III is the effect of the change in size distribution dependent on the geometric standard deviation (σ_{PSD}). The dependency is given in Francis et al. (2012), eq. 14:

$$n(r) = \frac{N_d}{\sqrt{2\pi}} \frac{1}{\ln(\sigma_{PSD})} \exp(-\frac{(\ln r - \ln r_o)^2}{2(\ln \sigma_{PSD})^2})$$

Where N_d is the total number density, r is the particle radius, r_0 is the geometric mean radius, and $n(r)$ is the size distribution over the radius range. Varying the geometric standard deviation will have impact on the retrieved effective radius as well as the total retrieved ash mass.

3.2.2 Surface observations

Measurements of SO_2 and $PM_{2.5}$ surface concentrations and SO_X wet depositions are used in Paper I to validate the eEMEP model simulation. There are several measurement sites over Europe that measure pollutants. These have over the years changed both with respect to number of stations and geographical coverage. In this study SO_2 and $PM_{2.5}$ surface concentrations are collected from the European Environment Agency (EEA) through the European Environment Information and Observation Network (EIONET) (http://www.eionet.europa.eu/aqportal), state spring 2006. SO_X deposition data are collected from the EBAS database (ebas.nilu.no).

3.2.3 Lidar

Lidar (light detection and ranging) measures the vertical placement of molecules, aerosol and water/ice clouds in the atmosphere. The lidar sends out short pulses of laser light into the atmosphere that is scattered by the atmospheric components. Some of the scattered light is backscattered into a detector that measures the received data. Based on the small delays in time from the backscattered light at the different altitudes, the distance from the pulse can be obtained and the position of backscattering material estimated.

The dataset used in Paper II, described in Pappalardo et al. (2013), includes measurements of the ash layer during the 2010 Eyjfjallajökull eruption from the European lidar network EARLINET (European Aerosol Research Lidar Network). An alert went out to the lidar stations at 15 April 2010 10 UTC to start continuous measurements of the ash layer during the volcanic eruption. The ash cloud was first detected over Hamburg at altitudes of 3 to 6 km on the early morning of 16 April. After a while, the ash layer was mixed in with the planetary boundary layer (PBL). After the ash gets mixed within the boundary layer, this part of the ash is no longer present in the dataset. To compare to model results, the

height of the observed boundary layer have to be taken into account. There are several methods to determine the height of the PBL in lidar profiles: i) By assuming a higher aerosol burden in the boundary layer, the height of the maximum difference in backscattered energy will indicate where the boundary layer lies (Endlich et al., 1979). This method may fail in detecting the boundary layer when plumes above or below the PBL can disturb the backscatter profile. ii) Identify the PBL as where the backscatter exceeds a clear air value by an assumed small value (Melfi et al., 1985). This approach is however very dependent on the assumed value, which also causes uncertainty in the retrieved height. The method used in the Eyjafjallajökull dataset is described by Steyn et al. (1999). The PBL is found by fitting an idealized profile to the observed profile of the measured backscatter. This is found to give robust PBL height for most atmospheric conditions.

For the classification of type for the different aerosol above the PBL, backward trajectory model-output were used to identify from which region the aerosol originated.

3.3 Inversion algorithm

The thesis explores the possibility of using an inversion method to assimilate satellite retrievals for ash dispersion forecasting. The inversion constrains the source term by satellite retrievals with the purpose to obtain an optimized emission term used in the model, so that the dispersed ash fields in the model are more similar to satellite observations. With the constrained source term, the method should provide a better starting point for a further forecast. The source term over the forecasting period is still however uncertain, and this is also explored further in the thesis.

The inversion algorithm is based on previous work from Seibert (2000), where the technique was used to calculate emissions from major emission areas in Europe. Eckhardt et al. (2008) developed the algorithm to produce emission estimates with vertical distributions from volcanic eruptions, and Stohl et al. (2011) expanded it further to calculate both height and time resolved emissions for the 2010 Eyjafjallajökull eruption. Seibert et al. (2011) presents further development of the algorithm to derive a posteriori uncertainties by propagating the uncertainties in the a priori emissions. This is done to identify where the emission estimate uncertainties are reduced. This latter version of the equations was used in the thesis and will be presented here.

Especially at the start of an eruption, the number of satellite observations may be too small to constrain the a posteriori solution, thereby causing the problem to be ill-constrained. Using an a priori emission estimate reduces the unphysical solutions that could result from insufficient observational data. A priori emissions can be calculated by using the empirical relationships described in section 2.1.2 for observed plume height, and should be given on the same time and height resolution as the a posteriori.

The algorithm needs input from model simulations and satellite observations of the volcanic cloud. To produce the source receptor matrix with the model results, eEMEP is initiated with a unit emission (1 kg s^{-1}) that is released as a pulse over each of the emission heights and times. Unit emissions are used to later scale the results with the a priori emissions. The multiple model simulations are then matched with hourly satellite retrievals for each grid point for the corresponding model time. The time sampling of satellite observations and the time and height resolution of the source emissions are variable, and in the thesis 19 height intervals and three hourly emission pulses are used to match with hourly satellite data.

The inversion finds an a posteriori source emission x with n elements by solving the problem:

$$M(x - x^a) \approx y^o - Mx^a$$

Here the elements of x^a represent the best guess a priori emission estimate and y^o represent the satellite observations, M is the mxn source receptor matrix calculated with the dispersion model. This solution can be abbreviated to

$$M\tilde{x} \approx \tilde{y}$$

The inversion is calculated by minimizing a cost function $J = J_1 + J_2 + J_3$. The difference between model and observation given the standard error of observations σ_o is given by J_1:

$$J_1 = (M\tilde{x} - \tilde{y})^T diag(\sigma_o^{-2})(M\tilde{x} - \tilde{y}),$$

where the operator $diag$ places the elements of σ_o along the diagonal of a matrix. J_2 gives the deviation from a priori values

$$J_2 = \tilde{x}^T diag(\sigma_x^{-2})\tilde{x},$$

where σ_x is the standard error of the a priori values. J_3 is a measure of the deviation from smoothness.

$$J_3 = \varepsilon(D\tilde{x})^T D\tilde{x}$$

D is a tridiagonal matrix with elements on the main diagonal equal to -2 and elements on the diagonal above and below equal to 1, and works as an operator for calculations of second derivatives, which are small for a smooth profile. ε determines the weight of this smoothness constraint.

Minimizing the cost function leads to a linear system of solutions for the a posteriori.

$$G\tilde{x} = \sigma_o^{-2} M^T \tilde{y}$$

Here G is the matrix:

$$G = M^T diag(\sigma_o^{-2})M + diag(\sigma_x^{-2}) + \varepsilon D^T D$$

To prevent unphysical negative emission in the a posteriori calculations, penalties are placed on negative values by increasing σ_x for these emission times and heights. This is done by iteration until

the solution converges so that the negative values sum up to maximum 1 % of the total released mass. Small negative values are then set to 0.

Further into the eruption period, more observations become available and the solution becomes more confident. Paper III studies how the a posteriori solution changes with an increasing amount of observations as it would during a real event. The effect the uncertainties connected to the observations (σ_o) and a priori emissions(σ_x) are also studied.

4. Presentation of findings

Paper I: Steensen, B. M., Schulz, M., Theys, N., and Fagerli, H.: A model study of the pollution effects of the first 3 months of the Holuhraun volcanic fissure: comparison with observations and air pollution effects, Atmos. Chem. Phys., 16, 9745-9760, doi:10.5194/acp-16-9745-2016, 2016.

This paper studies the impact of the first three months of the 2014-2015 Holuhraun volcanic fissure. The eruption produced a total lava field of 85 km^2 over the Holuhraun plain (Pedersen et al., 2017) and released around 11 (±5) Tg of SO_2 (Gíslason et al., 2015). The daily emissions from the lava field were 4.5 times the daily anthropogenic emission from the 28 European Union countries, which for 2009 is estimated to be 13.9 kt d^{-1} (Kuenen et al., 2014; Schmidt et al., 2015). This is also the anthropogenic emission estimate used in this paper.

The main purpose of the study is to investigate the increase in pollution levels over Europe due to the eruption on the Holuhraun plain, by using the eEMEP model set up with chemistry and anthropogenic emissions. The model simulations are initiated with a constant emission estimate of 65 kt d^{-1} released for sensitivity testing in three different heights. Model results are compared to OMI satellite retrievals over the first two months (September and October 2014), to observations of SO_2 and $PM_{2.5}$ concentrations over three episodes when the volcanic emissions were transported to surface stations in Europe, as well as to observations of SO_X wet deposition. For the satellite observation comparison, an averaging kernel is applied to the model data to correct for the height dependent sensitivity of the satellite UV detection of SO_2. The base model simulations with emissions released from the ground up to 3 km match better with satellite retrievals than the other two model simulations with emissions released lower or higher in the atmosphere (0-1 km and 3-5 km). The comparison at ground stations shows that at times there are large discrepancies between the peak concentrations of model and observed concentrations. The timing of the peaks in concentration level is however good, and for most of the stations the model simulation with volcanic SO_2 released into a 0-3 km column height matches best with the observations. Both Schmidt et al. (2015) and Boichu et al. (2016) studied the Holuhraun eruption by use of dispersion model simulations in both Lagrangian and Eulerian modeling frames and found that there is too little exchange of pollutants to the PBL. The model surface concentrations of SO_2 are therefore too low for stations in the United Kingdom, Ireland and France in September 2014 explaining some of the discrepancies found here in Paper I.

Even though surface concentration stations measured higher-than-normal concentrations, exceedances of SO_2 concentrations were only measured frequently during the period on Iceland (Gíslason et al., 2015). Iceland is also found to be the region which is most sensitive to variations in emission height. PM exceedances are calculated for Europe using a threshold of a 24 hour average for $PM_{2.5}$ concentration of 25 µg m^{-3} (WHO, 2005). By using the model calculations, the result shows that the

Barðarbunga eruption increased the number of PM exceedance days by up to two days over the three months studied for the already polluted Benelux region. Only one exceedance day due to the volcanic eruption were found by studying model calculations over Iceland, and none at the coast of Norway, even though these two regions experienced the largest percentage increase in PM concentrations. The model results also show high relative and absolute increases of SO_X deposition over the coast of Northern Norway and Northern Scotland. These regions are under normal conditions among the least polluted regions over Europe, and the increase in pollution due to the Holuhraun volcanic fissure increased the SO_X deposition levels to values similar to the most polluted regions in Europe. Overall the model results and observations show that Barðarbunga eruption had little effect on the average sulfur concentration levels in Europe outside Iceland over the three months, with only short periods exhibiting high concentrations.

Paper II: Steensen, B. M., Schulz, M., Wind, P., Valdebenito, Á., and Fagerli, H.: The operational eEMEP model for volcanic SO_2 and ash forecasting, Geosci. Model Dev. Discuss., doi:10.5194/gmd-2016-315, in review, 2017.

This paper presents the additions and developments for the EMEP MSC-W model to improve the transport calculations of volcanic emissions and especially ash in the model. To include volcanic emission from explosive eruptions with a high plume the model top is increased from the standard 16 km to a more flexible height based on the vertical levels available in the meteorological data driving the model. By increasing the number of vertical levels the resolution is also improved. Gravitational settling for ash tracers is newly included and added to all model layers. The operational set up of the model is presented.

An efficient dispersion model for forecasting volcanic emissions needs to balance both the complexity of the model and a sufficient high resolution. The inherent numerical diffusion in Eulerian models caused by the instant mixing of tracers within a grid box is studied to see the importance of resolution for simulations where peak concentrations need to be predicted for ash advisory decision making. Dispersion forecasts are initiated over three days at the beginning of the 2014 Holuhraun fissure eruption, driven by ensemble meteorology members on three different horizontal resolutions. Ensemble meteorology consists of forecast simulations with several members that have differences caused by small changes in the initial conditions and different physical model descriptions. The goal of ensemble forecasts is to quantify the uncertainty of the forecast and to produce probability forecasts for certain events based on the occurrence of the events in the different members. Frequency change over the thresholds dependent on the different resolutions is therefore studied.

High resolution dispersion simulations have members with high concentrations further into the forecast and also a larger spread between the members. Forecast simulations with the lowest resolution

show more agreement and therefore gain little from ensemble forecasting. High resolution also matches slightly better with observations, but have a much higher computational cost. Less information is found to be lost between the high and mid resolution than between the mid and low model resolution, and therefore the mid resolution setup (20x20km) is found to be sufficient when it is critical to obtain results in time. To perform an even quicker forecast of dispersion from volcanic eruptions, where peak concentration calculations are not crucial, a low resolution is found to be sufficient.

To study the effect of gravitational settling in the calculations, two model simulations with and without gravitational settling of ash particles are compared to lidar observations of the ash layer over central European stations during the 2010 Eyjafjollajökull eruption (Pappalardo et al., 2013). The model simulations use the same emission estimate from Stohl et al. (2011) and the same meteorology. Gravitational settling causes the center of mass to be about 1 km closer to the ground than the model simulation with no gravitational settling included. However, the descending layer caused by a high pressure system over Europe in the studied time interval has a larger effect. The height variations of the ash layer caused by real weather situations are not captured perfectly well by either of the two simulations, playing down the role of gravitation parameterization imperfections. The eEMEP model result of ash center of mass calculated with gravitational settling show higher correlation with those from the lidar observations compared to the results from the model simulation with no gravitational settling at four of the six stations studied used in the study. Although a physical correct model description of volcanic ash and SO_2 dispersion is advantageous, other factors such as model resolution, details of the source term and the model setup, whether it includes assimilation or not, are evaluated as more important for safety assessments.

Paper III: Steensen, B. M., Kylling, A., Kristiansen, N. I., and Schulz, M.: Uncertainty assessment and applicability of an inversion method for volcanic ash forecasting, Atmos. Chem. Phys. Discuss., doi:10.5194/acp-2016-1075, in review, 2017.

This paper presents the applicability of an inversion method to find an optimized source term to forecast ash dispersion for two periods during the 2010 Eyjafjallajökull eruption. The first period in April is characterized by narrow ash clouds with high concentrations visible in the satellite data, while for the period in May the observed ash clouds are more extensive with lower concentrations. The inversion is performed with four different satellite data sets with different assumptions for the size distribution. The effect of weighting the uncertainties associated with the a priori emissions and the mass load uncertainties for the satellite retrievals on the a posteriori results is also studied. The inversion technique is at last tested in a forecasting environment where more satellite observations are added gradually as it would happen during a real volcanic eruption.

The default fine ash fraction of 0.4 for silicate-type standard volcanoes like Eyjafjollajökull given in Mastin et al. (2009) used in an operational setting and in this study to calculate the a priori emissions, is found to be too high for this eruption. All the a posteriori solutions calculated with the different satellite sets and uncertainties are therefore reduced compared to the a priori source term. This is in agreement with Stohl et al. (2011) and Kristiansen et al. (2012) where a lower fine ash fraction of 0.1 is used. The reductions are dependent on the ash column loads retrieved in the satellite data set used as input for the calculations. The spread in a posteriori results found by changing the uncertainty connected to the a priori is found to be larger than by changing the satellite mass load uncertainty.

The quality of using the inversion in a forecasting environment is tested by adding gradually, with time, more observations to improve the estimated height versus time evolution of Eyjafjallajökull ash emissions. We show that the initially too high a priori emissions are reduced effectively when using just 12 hours of satellite observations. More satellite observations (>12h), in the Eyjafjallajökull case, place the volcanic injection at higher altitudes. Adding additional satellite observations (>36h) changes the a posteriori emissions to only a small extent for May and minimal for the April period, because the ash is transported effectively out of the domain during this period. A forecast emission term is tested where the last 12 hours of the a posteriori term are averaged and released over the forecast period. Using this emission the forecast simulations show better results than forecasts with a zero emission estimate for periods with a continued volcanic activity.

Compared to using only the a priori emissions the forecast simulations with the a posteriori emission have column loads more comparable to observed ash, and with loads more confined to regions where satellite observations show ash to be present. Because of undetected ash in the satellite retrieval and diffusion in the model, the forecast simulations still generally contain more ash than the observed fields and the model ash is more spread out. Overall, using the a posteriori emissions in our model reduces the uncertainties connected to both the satellite observations and the a priori estimate to perform a more confident forecast in both amount of ash released and emission heights.

5. Summary and conclusion

This chapter presents the conclusions in connection with the research objectives of this thesis, in order to obtain a more comprehensive understanding of the scientific findings attained in this thesis. The objectives were to

a) Investigate the environmental impact on Europe of the 2014-2015 Holuhraun fissure eruption with its large amounts of SO_2 released into the atmosphere.

SO_2 from the Holuhraun fissure eruption was measured at several stations over Europe, and especially observations of surface concentrations from Ireland, the United Kingdom and France show short periods with high concentrations. Averaged over three months, the increase in SO_2 concentrations compared to concentration levels experienced during recent years was small, except over Iceland. There was also found an increase of observed sulfate in wet deposition measurements and of $PM_{2.5}$ surface concentrations. This increase is seen especially over Northern United Kingdom and Scandinavia, and there is a notably high increase (over 1000 times) in sulfate wet deposition over the coast of western Norway due to the high precipitation frequency over this region. Sensitivity simulations in which the emissions are released over a lower or higher emission column are also shown to have little effect on the increase in mean pollution levels, except in the regions close to the source.

Even though the SO_2 emissions from the fissure are over 4 times the daily anthropogenic European emission, Iceland is found to be situated too far away in this case to cause an impact on European air quality. The much stronger 1783-1784 Laki eruption would have led to a higher increase as well as a stronger climate effect than the Barðarbunga eruption, where most of the emissions were at low altitudes in the troposphere. A longer lasting eruption than the Barðarbunga emission period can also cause an increase in acidification over time.

b) Develop and evaluate the eEMEP model capabilities to transport volcanic SO_2 and ash emissions and compare the results with observations.

To prepare the model to handle dispersion of volcanic emissions, several improvements were carried out within this thesis. The eEMEP model can handle a more sophisticated description of the volcanic emissions, and the height of the top layer was increased, making it possible to include more layers from the meteorological driver. A simplified chemistry is prepared to minimize computational costs for eruptions where chemical reactions are not important.

Of special interest in this study is the addition of gravitational settling for ash particles. The effect of adding this process is validated by investigating the ash layer observed by lidar over Central Europe during the 2010 Eyjafjallajökull eruption. For the model simulations with gravitational settling, the ash layer is found to be at times up to 1 km lower in the atmosphere over the lidar stations, compared to the model simulation without gravitational settling. The model ash layer with gravitational settling

also shows a slightly higher correlation with the observed layer for most of the lidar stations. However, the height variations in the ash layer caused by weather situations are not captured well, whether gravitational settling is included or not, implying a reduced importance of the role of gravitation parameterization imperfections.

Model results with Barðarbunga emissions are compared also to observed surface concentrations of SO_2 and $PM_{2.5}$ and measured SO_X depositions in Paper I. All three papers use satellite observations to study the column burdens and horizontal extent of the volcanic gas or ash clouds compared to the model-simulated clouds. Common for all these comparisons is the importance of understanding the underlying assumptions behind the retrievals of observable quantities. This is especially important for the satellite retrievals, where several assumptions are made that affect the retrieved values. Detection limits and instrument failure may also affect the observations. For most of the comparisons studied, our eEMEP model simulations match well with the observations and the discrepancies will be further discussed in future work.

c) Explore for a volcanic ash advisory system, how useful it is to assimilate satellite retrievals by an inversion algorithm, and find as well as apply the optimized ash source term quickly.

For more accurate ash dispersion forecasting, especially for ash advisory purposes, an assimilation setup for the eEMEP model is tested, with an inversion algorithm to calculate a new source term. The results are found to have large uncertainties due to assumptions made for the satellite retrieval, which affects the retrieved ash amount, as well as due to assumptions made in the a priori estimate. For episodes when the ash clouds are well observed, only 12 hours of hourly satellite observations are needed to find a better solution for the volcanic emissions than a priori. When the satellite retrieval yields low concentrations of the ash cloud, the a priori emissions are reduced with only a small amount of observational data. After 36 hours of assimilated satellite observations, additional observations to the inversion calculations have minimal effect on the a posteriori emission term.

Enough satellite observations are needed to avoid making the a posteriori solution ill-constrained. This is especially a challenge at the start of a forecast and over periods with no ash in the satellite retrievals. For these periods, the solution falls back on the a priori emissions, leading to an increase in dependency on this initial best guess estimate. To increase the confidence of the forecast, further considerations are needed, and this will be explained more below when suggesting possible future work.

d) Document the uncertainties due to assumptions in the satellite retrievals, meteorological prediction uncertainty, resolution effects and the model description of volcanic ash and SO_2 transport in the eEMEP model.

The satellite retrieval algorithm used in the Barðarbunga study for SO_2 retrievals, applies an assumed plume height to retrieve column loads. Information about this height and water and ice clouds are

found in the averaging kernel. Resulting retrieved column loads values are therefore dependent on both the concentrations and vertical placement of the volcanic SO_2 cloud, and to compare model results to the satellite data the model data needs to be weighted with the same averaging kernel. As shown in the study, applying the satellite averaging kernel on model column loads from three simulations with different emission heights gives a large change both in the resulting values as well as the differences on column loads between the three simulations. Because of the weighting, the validation of the model simulations compared to the satellite data is difficult without any further information about the height or amount of the emissions for the volcanic plume.

Assumptions in the satellite retrieval also have a large effect on the retrieved ash column loads. This uncertainty also has an effect on the a posteriori emission term calculated by the inversion algorithm. This a posteriori emission term is then later used to calculate a forecast emission term and most significantly the model predictions of the ash cloud. Uncertainty in the satellite ash retrieval is therefore translated into uncertainties in the model concentrations.

Model simulations with volcanic ash and SO_2 also have model uncertainties caused by other sources: i) Error in the initials condition and physical description of dynamical processes in the meteorological driver influence the dispersion model and therefore affects the transport of pollutants, ii) the model grid resolution affects the meteorological information and numerical diffusion, and iii) simplifications and parameterizations in the treatment of the tracer dispersion in the model. The latter is investigated by studying the effect of gravitational settling. Point i) and ii) are studied by running dispersion forecasts with ensemble meteorology on three different resolutions. Lower resolution causes the volcanic emissions to be diluted faster, so that lower concentrations are found for a larger area. Higher resolution ensemble forecasts yield a higher number of members with high concentrations further away from the emission source. Running dispersion simulations on low resolution also causes loss of meteorological information that is only resolved at high resolution in the NWP.

These effects are important when interpreting model results and when setting up an operational forecast model. This is especially the case when studying the current concentration limits for flight avoidance in areas with concentrations greater than 4 mg m^{-3} (ICAO, 2016). Forecast simulations with low grid resolution would exhibit a smaller area for the no flight zone. Therefore a sufficiently high resolution model is needed in an advisory set up. Compared to the uncertainties connected to weather and model parameterization, the volcanic source term is more important for concentration thresholds and has a high uncertainty. The inversion technique is found to place the ash effectively at the heights that matches the transport of the observed ash, and in more comparable concentrations to the satellite retrieval than what is found by empirical relationships. This also causes the model concentrations to be dependent on the satellite retrieval and to the a priori emission when satellite retrievals are insufficient. More knowledge about the size distribution of tephra is found to be especially important for both the a priori and a posteriori estimate.

5.1 Future work

During the work presented in this study, some inaccuracies and weaknesses in the methods are found that should be explored further.

i) The eEMEP model results does not show the high surface concentrations observed in UK and France after transport of SO_2 from Iceland during the Barðarbunga event. This is probably caused by missing transport of the volcanic SO_2 into the PBL. A good description of both the height of the PBL as well as the exchange between troposphere and the PBL is important for calculating the impact these types of eruptions may have on the pollution levels. As the model errors accumulate over time during the length of the model simulations, the discrepancy as found in the study can therefore have a large impact on the long-range transport of the volcanic pollutants.

ii) A high resolution model is found to be important for realistically modelling meteorological features such as maximum wind speeds and convection, and for reducing numerical diffusion. However, high resolution adds to the computational time of the forecasts. The advection scheme in the EMEP MSC-W model is considered less computational demanding and takes only up to 20% of the computational time for ash transport with simplified chemistry. Compared to the simulations normally performed by the model that go over a year, short range dispersion forecasts add an increased requirement on mass conservations on the hourly time steps that are considered for these simulations. This is especially important for the input simulations to the inversion routine, where small numerical errors are multiplied with the a priori estimate. Exploring other assumptions than the current advection scheme (following Schwaiger et al. (2012)) could be beneficial to obtain better forecasts.

iii) The inversion method (Seibert et al., 2000; Eckhardt et al., 2008; Stohl et al., 2011) constrains the emission source by using satellite observations. If the satellite observations do not contain any ash the solution is not altered from the best guess a priori emission. This is particularly observed for the dispersed ash that is not matched by any satellite detected ash. The satellite-sets used in Paper III differentiate between unidentified pixels, where the retrieval is unable to determine whether ash is present or not, and in pixels where the retrieval with certainty does not find any ash. Since the retrieval has no certain information, the ash column values for these unidentified regions are also set to zero. Another source of uncertainty is the 0.2 μg m^{-2} detection limit for ash in the satellite retrieval (Prata and Prata, 2012). Ash pixels with no ash could therefore still possibly include ash, either small amounts under detection limit or contaminated by water and ice. Exploring possibilities for the inversion algorithm to differentiate between the unidentified

satellite retrievals and regions with possible ash but below the detection limit would be beneficial in a forecasting setting as it would constrain the solution better.

The possibility of using zero or low emissions as a priori are discussed in Paper III in order to reduce ash emissions for emission times with no observed ash. However, in a strictly operational setting without manual interpretation it is difficult to know if there are no emissions supported by enough satellite observations to constrain the solution or if the solution is highly relying on the a priori result. An a priori solution with ash emission is therefore considered more conservative in an operational forecasting setting.

iv) Including fine ash aggregation in the model description. Aggregation increases the gravitational settling and reduces the atmospheric residence time for ash (Brown et al. 2011) and could improve the treatment of ash in the model.

References

Angell, J. K., & Korshover, J: Surface temperature changes following the six major volcanic episodes between 1780 and 1980. *Journal of Climate and Applied Meteorology*, *24*(9), 937-951, 1985.

Arason, P., Petersen, G. N., and Bjornsson, H.: Observations of the altitude of the volcanic plume during the eruption of Eyjafjallajökull, April–May 2010. Earth System Science Data, 3(1), 9-17, 2011.

Baxter, P. J: Impacts of eruptions on human health. *Encyclopedia of volcanoes*, 1035-1043, 2000.

Barsotti, S., Neri, A. and Scire, J.S.: The VOL-CALPUFF model for atmospheric ash dispersal: 1. Approach and physical formulation, J. Geophys. Res., 113, B03208, doi:10.1029/2006JB004623, 2008.

Blake, S., Self, S., Sharma, K., & Sephton, S: Sulfur release from the Columbia River Basalts and other flood lava eruptions constrained by a model of sulfide saturation. *Earth and Planetary Science Letters*, *299*(3), 328-338, 2010.

Bluth, G. J., Doiron, S. D., Schnetzler, C. C., Krueger, A. J., & Walter, L. S.: Global tracking of the SO2 clouds from the June, 1991 Mount Pinatubo eruptions. *Geophysical Research Letters*, *19*(2), 151-154, 1992.

Boichu, M., Menut, L., Khvorostyanov, D., Clarisse, L., Clerbaux, C., Turquety, S., & Coheur, P. F.: Inverting for volcanic SO_2 flux at high temporal resolution using spaceborne plume imagery and chemistry-transport modelling: the 2010 Eyjafjallajökull eruption case-study. Atmospheric Chemistry and Physics, 13(17), 8569-8584, 2013.

Boichu, M., Chiapello, I., Brogniez, C., Péré, J. C., Thieuleux, F., Torres, B., ... & Söhne, N.: Current challenges in modelling far-range air pollution induced by the 2014-2015 Bárðarbunga fissure eruption (Iceland). Atmospheric Chemistry & Physics, 16(17), 2016.

Bott, A.: A positive definite advection scheme obtained by nonlinear re-normalization of the advection fluxes, Mon. Weather Rev., 117, 1006–1015, 1989a.

Bott, A.: Reply, Mon. Weather Rev., 117, 2633–2636, 1989b.

Brenot, H., Theys, N., Clarisse, L., Van Geffen, J., Van Gent, J., Van Roozendael, M., ... & Valks, P.: Support to Aviation Control Service (SACS): an online service for near real-time satellite monitoring of volcanic plumes. Natural hazards and earth system sciences, 14(5), 1099-1123, 2014.

Brown, R.J., Bonadonna, C. and Durant, A.J.: A review of volcanic ash aggregation. Phys. Chem. Earth 45-46. 65-78, 2011.

Bursik, M.: Effect of wind on the rise height of volcanic plumes. Geophysical Research Letters, 28(18), 3621-3624, 2001.

Carey, S., & Bursik, M: Volcanic plumes. *Encyclopedia of volcanoes. Academic Press, San Diego*, 527-544, 2000.

Casadevall, T.J: Volcanic ash and aviation safety: Proceedings of the First International Symposium on Volcanic Ash and Aviation Safety, U.S. Geol. Surv. Bull., 2047, 450 pp, 1994.

Costa, A., Macedonio, G., & Folch, A: A three-dimensional Eulerian model for transport and deposition of volcanic ashes. *Earth and Planetary Science Letters*, *241*(3), 634-647, 2006.

Daley, R. *Atmospheric data analysis*. No. 2. Cambridge university press, 1993.

Delmelle, P., Stix, J., Baxter, P. et al.: Atmospheric dispersion, environmental effects and potential health hazard associated with the low-altitude gas plume of Masaya volcano, Nicaragua Bull Volcanol : 423. doi:10.1007/s00445-002-0221-6, 2002.

Devine, J. D., Sigurdsson, H., Davis, A. N., & Self, S: Estimates of sulfur and chlorine yield to the atmosphere from volcanic eruptions and potential climatic effects. *Journal of Geophysical Research: Solid Earth*, *89*(B7), 6309-6325, 1984.

Draxler, R.R. and Hess, G.: Description of the HYSPLIT_4 modeling system NOAA Tech. Memo. ERL ARL-224, NOAA Air Resources Laboratory, Silver Spring, MD 24 pp, 1997.

Eckhardt, S., Prata, A. J., Seibert, P., Stebel, K., & Stohl, A.: Estimation of the vertical profile of sulfur dioxide injection into the atmosphere by a volcanic eruption using satellite column measurements and inverse transport modeling. Atmospheric Chemistry and Physics, 8(14), 3881-3897, 2008.

Eliassen, A., Saltbones, J., Stordal, F., Hov, Ø., Isaksen, I. S., & Stordal, F.: A Lagrangian long-range transport model with atmospheric boundary layer chemistry. Journal of Applied Meteorology, 21(11), 1645-1661, 1982.

EMEP Status Report 1/2015: Transboundary particulate matter, photo-axidants, acidifying and eutrophying components, EMEP MSC-W & CCC & CEIP, Norwegian Meteorlogical Institute (EMEP MSC-W), Oslo, Norway, 2015.

EMEP Status Report 1/2016: Transboundary particulate matter, photo-axidants, acidifying and eutrophying components, EMEP MSC-W & CCC & CEIP, Norwegian Meteorlogical Institute (EMEP MSC-W), Oslo, Norway, 2016.

Endlich, R. M., F. Ludwig, and E. E. Uthe, 1979: An automated method for determining the mixing depth from lidar observations. Atmos. Environ., 13, 1051–1056.

EU: Directive 2008/50/EC of the European Parliament and of the Council on ambient air quality and cleaner air for Europe., Official Journal of the European Union L 152, 11 June 2008, pp. 1-44., L 152, 1–44, URL http://faolex.fao.org/docs/pdf/eur80016.pdf, 2008.

European Commission, Frequently Asked Questions 26 May 2011 (available at http://europa.eu/rapid/press-release_MEMO-11-346_en.htm) 2011.

Flemming, J., & Inness, A.: Volcanic sulfur dioxide plume forecasts based on UV satellite retrievals for the 2011 Grímsvötn and the 2010 Eyjafjallajökull eruption. Journal of Geophysical Research: Atmospheres, 118(17), 2013.

Francis, P. N., Cooke, M. C. and Saunders, R. W.: "Retrieval of physical properties of volcanic ash using Meteosat: A case study from the 2010 Eyjafjallajökull eruption." *J. Geophys. Res* 117, D00U09, 2012.

Folch, A., Costa, A., Macedonio, G.: FALL3D: A computational model for transport and deposition of volcanic ash, Comput. Geosci, 35(6) 1334-1342, doi:10.1016/j.cageo.2008.08.008, 2009.

Gíslason, S. R., Stefánsdóttir, G., Pfeffer, M. A., Barsotti, S., Jóhannsson, T., Galeczka, I., Bali, E., Sigmarsson, O., Stefánsson, A., Keller, N. S., Sigurdsson, Á., Bergsson, B., Galle, B., Jacobo, V. C., Arellano, S., Aiuppa, A., Jónasdóttir, E. B., Eiríksdóttir, E. S., Jakobsson, S., Guðfinnsson, G. H., Halldórsson, S. A., Gunnarsson, H., Haddadi, B., Jónsdóttir, I., Thordarson, T., Riishuus, M., Högnadóttir, T., Dürig, T., Pedersen, G. B. M., Höskuldsson, Á., and Gudmundsson, M. T.: Environmental pressure from the 2014–15 eruption of Bárðarbunga volcano, Iceland, Geochem. Persp. Lett., 1, 84–93, 2015.

Gneiting, T. and Raftery, A.E.: "Weather forecasting with ensemble methods." *Science* 310.5746, 248-249, 2005.

Gudmundsson, M. T., Thordarson, T., Höskuldsson, Á., Larsen, G., Björnsson, H., Prata, F. J., ... & Hayward, C. L. Ash generation and distribution from the April-May 2010 eruption of Eyjafjallajökull, Iceland. *Scientific reports*, *2*, 572, 2012.

Grattan, J., Durand, M., and Taylor, S.: Illness and elevated human mortality in Europe coincident with the Laki Fissure eruption. *Geological Society, London, Special Publications*, *213*(1), 401-414, 2003.

Grattan, J: The distal impact of Icelandic volcanic gases and aerosols in Europe: a review of the 1783 Laki Fissure eruption and environmental vulnerability in the late 20th century. *Geological Society, London, Engineering Geology Special Publications*, *15*(1), 97-103, 1998.

Hindar, A: Acid water and fish death. *Nature, 372*, 327-328, 1994.

Hufford, G., Simpson, J. J., Salinas, L., Barske, E., & Pieri, D. C: Operational considerations of volcanic ash for airlines. *Bulletin of the American Meteorological Society*, *8*(4), 745-755, 2000.

ICAO, 2001. Manual on Volcanic Ash, Radioactive Material and Toxic Chemical Clouds, Second Edition, ICAO Document 9691-AN/954.

ICAO, 2016 EUR Doc 019, NAT Doc 006, Part II – EUR/NAT VACP, Edition 2.0.0 — July 2016, available at http://www.skybrary.aero/bookshelf/books/357.pdf

Jones, A., Thomson, D., Hort, M. and Devenish, B.: The UK Met Office's next generation atmospheric dispersion model, NAME III, in Air Pollution Modelling and its Application XVII, edited by C. Borrego and A.-L. Norman, pp. 580–589, Springer, New York, 2007.

Josse, B., Simon, P. and Peuch, V.-H.: Radon global simulationswith the multiscale chemistry and transport model MOCAGE, Tellus,Ser. B, 56(4), 339–356, doi:10.1111/j.1600-0889.2004.00112.x, 2004. Kain, J. S. The Kain-Fritsch Convective Parameterization. Anupdate. J. Appl. Meteorol. 43, 170–181, 2004. Kain, J. S. and Fritsch, J. M.: A one-dimensional entraining/detraining plume model and its application in convective parameterization. J. Atmos. Sci., 47, 2784–2802, 1990.
Kalnay, E.: *Atmospheric modeling, data assimilation and predictability*. Cambridge university press, 2003.

Kristiansen, N. I., A. Stohl, Prata, A. J., Bukowiecki, N., Dacre, H., Eckhardt, S., Henne, S., Hort, M. C., Johnson, B. T., Marenco, F., Neininger, B., Reitebuch, O., Seibert, P., Thomson, D. J., Webster, H. N. and Weinzierl, B.: Performance assessment of a volcanic ash transport model mini‐ensemble used for inverse modeling of the 2010 Eyjafjallajökull eruption. Journal of Geophysical Research: Atmospheres 117.D20, 2012.

Krueger, A. J: Sighting of El Chichon sulfur dioxide clouds with the Nimbus 7 total ozone mapping spectrometer. *Science*, *220*(4604), 1377-1379, 1983.

Krueger, A. J., Walter, L. S., Bhartia, P. K., Schnetzler, C. C., Krotkov, N. A., Sprod, I. T., & Bluth, G. J. S: Volcanic sulfur dioxide measurements from the total ozone mapping spectrometer instruments. *Journal of Geophysical Research: Atmospheres*, *100*(D7), 14057-14076, 1995.

Krueger, A.J., Schnetzler, C.C., and Walter, L.S.: The December 1981 eruption of Nyamuragira volcano (Zaire), and the origin of the 'mystery cloud' of early 1982, J. Geophys. Res., 101, 15191-15196, 1996.

Kuenen, J. J. P., Visschedijk, A. J. H., Jozwicka, M., and Denier van der Gon, H. A. C.: TNO-MACC_II emission inventory; a multiyear (2003–2009) consistent high-resolution European emission inventory for air quality modelling, Atmos. Chem. Phys., 14, 10963–10976, doi:10.5194/acp-14-10963-2014, 2014.

Liu, E. J., Cashman, K. V., Beckett, F. M., Witham, C. S., Leadbetter, S. J., Hort, M. C. and Guðmundsson, S.: Ash mists and brown snow: Remobilization of volcanic ash from recent Icelandic eruptions. *Journal of Geophysical Research: Atmospheres*, *119*(15), 9463-9480, 2014.

Lopez, T.M., Carn, S.A., Werner, C., Kelly, P.,Doukas, M., Pfeffer, M., Fee, D., Webley, C., Cahill, C., and Schneider, D.J.: Evaluation of Redoubt volcano's sulfur dioxide emissions by the Ozone Monitoring Instrument, J. Volcanol. Geotherm. Res., 259, 290-307, 2013.

Marécal, V., Peuch, V. H., Andersson, C., Andersson, S., Arteta, J., Beekmann, M., ... & Chéroux, F.: A regional air quality forecasting system over Europe: the MACC-II daily ensemble production. Geoscientific model development, 8(9), 2777-2813, 2015.

Mastin, L.G.; A user-friendly one-dimensional model for wet volcanic plumes. Geochemistry, Geophysics, Geosystems 8.3, 2007.

Mastin, L. G., Guffanti, M., Servranckx, R., Webley, P., Barsotti, S., Dean, K., ... & Schneider, D.: A multidisciplinary effort to assign realistic source parameters to models of volcanic ash-cloud transport

and dispersion during eruptions. Journal of Volcanology and Geothermal Research, 186(1), 10-21, 2009

Mastin, L.G.: Testing the accuracy of a 1-D volcanic plume model in estimating mass eruption rate. Journal of Geophysical Research: Atmospheres 119.5: 2474-2495, 2014.

Melfi, S. H., J. D. Spinhire, S.-H. Chou, and S. P. Palm, 1985: Lidar observation of vertically organized convection in the planetary boundary layer over the ocean., J. Climate Appl. Meteor., 24, 806–821.

Merucci, L., Burton, M.R., Corradini, S., and Salerno, G.G.: Reconstruction of SO2 flux emission chronology from space-based measurements, J. Volcanol. Geotherm. Res., 206, 80-87, 2011.

Miller, T.P., Casadevall, T.J: Volcanic Ash Hazards to Aviation. In: Sigurdsson, H., Houghton, B.F., McNutt, S.R., Rymer, H., Stix, J. (Eds.), Encyclopedia of Volcanoes. Academic Press, San Diego, pp. 915–930, 2000

Moxnes, E. D., Kristiansen, N. I., Stohl, A., Clarisse, L., Durant, A., Weber, K., and Vogel, A.: Separation of ash and sulphur dioxide during the 2011 Grimsvötn eruption, J. Geophy. Res.-Atmos., 119, 7477–7501, 2014

Newhall, C. G., & Self, S.: The volcanic explosivity index (VEI) an estimate of explosive magnitude for historical volcanism. *Journal of Geophysical Research: Oceans*, *87*(C2), 1231-1238, 1982

Pappalardo, G., Mona, L., D'Amico, G., Wandinger, U., Adam, M., Amodeo, A., Ansmann, A., Apituley, A., Alados Arboledas, L., Balis, D., Boselli, A., Bravo-Aranda, J. A., Chaikovsky, A., Comeron, A., Cuesta, J., De Tomasi, F., Freudenthaler, V., Gausa, M., Giannakaki, E., Giehl, H., Giunta, A., Grigorov, I., Groß, S., Haeffelin, M., Hiebsch, A., Iarlori, M., Lange, D., Linné, H., Madonna, F., Mattis, I., Mamouri, R.-E., McAuliffe, M. A. P., Mitev, V., Molero, F., Navas-Guzman, F., Nicolae, D., Papayannis, A., Perrone, M. R., Pietras, C., Pietruczuk, A., Pisani, G., Preißler, J., Pujadas, M., Rizi, V., Ruth, A. A., Schmidt, J., Schnell, F., Seifert, P., Serikov, I., Sicard, M., Simeonov, V., Spinelli, N., Stebel, K., Tesche, M., Trickl, T., Wang, X., Wagner, F., Wiegner, M., and Wilson, K. M.: Four-dimensional distribution of the 2010 Eyjafjallajökull volcanic cloud over Europe observed by EARLINET, Atmos. Chem. Phys., 13, 4429-4450, doi:10.5194/acp-13-4429-2013, 2013.

Parfitt, L., & Wilson, L. *Fundamentals of physical volcanology*. John Wiley & Sons. 2009.

Pedersen, G. B. M., Höskuldsson, A., Dürig, T., Thordarson, T., Jónsdóttir, I., Riishuus, M. S., . & Sigmundsson, F: Lava field evolution and emplacement dynamics of the 2014–2015 basaltic fissure eruption at Holuhraun, Iceland. *Journal of Volcanology and Geothermal Research*, *2017*.

Perfit, M. R., & Davidson, J. P: Plate tectonics and volcanism. *Encyclopedia of Volcanoes*, 89-113, 2000.

Prata, A. J., and A. T. Prata: Eyjafjallajökull volcanic ash concentrations determined using Spin Enhanced Visible and Infrared Imager measurements, J. Geophys. Res., 117, D00U23, doi:10.1029/2011JD016800, 2012.

Raaschou-Nielsen, O., Andersen, Z. J., Beelen, R., Samoli, E., Stafoggia, M., Weinmayr, G., ... & Xun, W. W.: Air pollution and lung cancer incidence in 17 European cohorts: prospective analyses from the European Study of Cohorts for Air Pollution Effects (ESCAPE). The lancet oncology, 14(9), 813-822, 2013.

Reuss, J. O., and Dale W. J.: Acid deposition and the acidification of soils and waters. Vol. 59. Springer Science & Business Media, 2012.

Robock, A.: Volcanic eruptions and climate. *Reviews of Geophysics*, *38*(2), 191-219, 2000.

Scarth, A., and Tanguy, J.-C. *Volcanoes of Europe*. Oxford University Press, USA, 2001.

Schwaiger, H. F., Denlinger, R. P. and Mastin, L. G.: Ash3d: A finite-volume, conservative numerical model for ash transport and tephra deposition, J. Geophys. Res., 117, B04204, doi:10.1029/2011JB008968, 2012.

Scott, B. C.: Parameterization of sulphate removal by precipitation, J. Appl. Met., 17, 11375–11389, 1979.

Schmetz, J., Pili, P., Tjemkes, S., Just, D., Kerkmann, J., Rota, S., & Ratier, A: An introduction to Meteosat second generation (MSG). *Bulletin of the American Meteorological Society*, *83*(7), 977-992, 2002.

Schmidt, A., Ostro, B., Carslaw, K. S., Wilson, M., Thordarson, T., Mann, G. W., & Simmons, A. J: Excess mortality in Europe following a future Laki-style Icelandic eruption. *Proceedings of the National Academy of Sciences*, *108*(38), 15710-15715, 2011.

Schmidt, A., Leadbetter, S., Theys, N., Carboni, E., Witham, C. S., Stevenson, J. A., ... & Delaney, L. Satellite detection, long-range transport, and air quality impacts of volcanic sulfur dioxide from the 2014–2015 flood lava eruption at Bárðarbunga (Iceland). Journal of Geophysical Research: Atmospheres, 120(18), 9739-9757, 2015.

Searcy, C., Dean, K., and Stringer, W.: PUFF: A high-resolution volcanic ash tracking model, Journal of Volcanology and Geothermal Research, 80, 1-16, 1998.

Sears, T. M., Thomas, G. E., Carboni, E., A Smith, A. J., and Grainger, R. G.: SO2 as a possible proxy for volcanic ash in aviation hazard avoidance, J. Geophys. Res.-Atmos., 118, 5698– 5709, 2013.

Seibert, P.: Inverse modelling of sulfur emissions in Europe based on trajectories. Inverse Methods in Global Biogeochemical Cycles, 147-154, 2000.

Seibert, P., Kristiansen, N. I., Eckhardt, S., Prata A. J., Richter, A., and Stohl, A.: Uncertainties in the inverse modelling of Sulphur dioxide eruption profiles, Geomatics, Natural Hazards and Risk, submitted, 2011.

Sigurdsson, H., Houghton, B., McNutt, S., Rymer, H., & Stix, J. (Eds.). *The encyclopedia of volcanoes*. Elsevier, 2000.

Simpson, D., Benedictow, A., Berge, H., Bergström, R., Emberson, L. D., Fagerli, H., Flechard, C. R., Hayman, G. D., Gauss, M., Jonson, J. E., Jenkin, M. E., Nyíri, A., Richter, C., Semeena, V. S., Tsyro, S., Tuovinen, J.-P., Valdebenito, Á., and Wind, P.: The EMEP MSC-W chemical transport model – technical description, Atmos. Chem. Phys., 12, 7825-7865, doi:10.5194/acp-12-7825-2012, 2012.

Sparks, R. S. J., Bursik, M. I., Carey, S. N., Gilbert, J., Glaze, L. S., Sigurdsson, H., & Woods, A. W. *Volcanic plumes*. Wiley. 1997

Steyn, D., Baldi, G. M., and Hoff, R. M.: The Detection of Mixed Layer Depth and Entrainment Zone Thickness from Lidar Backscatter Profiles, J. Atm. Oceanic Tech., 16, 953–959, 1999.

Stohl, A., Forster, C., Frank, A., Seibert, P., & Wotawa, G.: Technical note: The Lagrangian particle dispersion model FLEXPART version 6.2. Atmospheric Chemistry and Physics, 5(9), 2461-2474, 2005.

Stohl, A., Prata, A. J., Eckhardt, S., Clarisse, L., Durant, A., Henne, S., Kristiansen, N. I., Minikin, A., Schumann, U., Seibert, P., Stebel, K., Thomas, H. E., Thorsteinsson, T., Tørseth, K., and Weinzierl, B.: Determination of time- and height-resolved volcanic ash emissions and their use for quantitative ash dispersion modeling: the 2010 Eyjafjallajökull eruption, Atmos. Chem. Phys., 11, 4333-4351, doi:10.5194/acp-11-4333-2011, 2011.

Textor, C., Graf, H. F., Herzog, M., Oberhuber, J. M., Rose, W. I., & Ernst, G. G: Volcanic particle aggregation in explosive eruption columns. Part I: Parameterization of the microphysics of hydrometeors and ash. *Journal of Volcanology and Geothermal Research*, *150*(4), 359-377, 2006.

Theys, N., Campion, R., Clarisse, L., Brenot, H., van Gent, J., Dils, B., Corradini, S., Merucci, L., Coheur, P.-F., Van Roozendael, M., Hurtmans, D., Clerbaux, C., Tait, S., and Ferrucci, F.: Volcanic SO2 fluxes derived from satellite data: a survey using OMI, GOME-2, IASI and MODIS, Atmos. Chem. Phys., 13, 5945-5968, doi:10.5194/acp-13-5945-2013, 2013.

Theys, N., De Smedt, I., Gent, J., Danckaert, T., Wang, T., Hendrick, F., ... & Krotkov, N.: Sulfur dioxide vertical column DOAS retrievals from the Ozone Monitoring Instrument: Global observations and comparison to ground-based and satellite data. Journal of Geophysical Research: Atmospheres, 120(6), 2470-2491. 2015.

Thomas, H. E. and Prata, A. J.: Sulphur dioxide as a volcanic ash proxy during the April–May 2010 eruption of Eyjafjallajökull Volcano, Iceland, Atmos. Chem. Phys., 11, 6871–6880, doi:10.5194/acp-11-6871-2011, 2011.

Thordarson, T., & Self, S: The Laki (Skaftár Fires) and Grímsvötn eruptions in 1783–1785. *Bulletin of Volcanology*, *55*(4), 233-263, 1993.

Thordarson, T., Self, S., Oskarsson, N., & Hulsebosch, T: Sulfur, chlorine, and fluorine degassing and atmospheric loading by the 1783–1784 AD Laki (Skaftár Fires) eruption in Iceland. *Bulletin of Volcanology*, *58*(2), 205-225, 1996.

Thordarson, T., and Self, S: " Atmospheric and environmental effects of the 1783–1784 Laki eruption: A review and reassessment." *Journal of Geophysical Research: Atmospheres* 108.D1 (2003a).

Thordarson, T, and Self, S., and Miller D.J., Larsem, G., and Vilmundardóttir: "Sulphur release from flood lava eruptions in the Veidivötn, Grímsvötn and Katla volcanic systems, Iceland." Geological Society, London, Special Publications 2131, 103-121, 2003b

Thordarson, T., & Larsen, G: Volcanism in Iceland in historical time: Volcano types, eruption styles and eruptive history. *Journal of Geodynamics*, *43*(1), 118-152, 2007.

Thordarson, T. and Höskuldsson, Á.: "Postglacial volcanism in Iceland." *Jökull* 58: 197-228, 2008.

Thomas, H. E., and I. Watson, M.: Observations of volcanic emissions from space: current and future perspectives. *Natural Hazards* 54.2: 323-354, 2010.

Tørseth, K., Aas, W., Breivik, K., Fjæraa, A. M., Fiebig, M., Hjellbrekke, A. G., ... & Yttri, K. E.: Introduction to the European Monitoring and Evaluation Programme (EMEP) and observed atmospheric composition change during 1972–2009. Atmospheric Chemistry and Physics, 12(12), 5447-5481, 2012.

UK Civil Aviation Authority (2016). A history of ash and aviation [online] Available at: https://www.caa.co.uk/Safety-initiatives-and-resources/Safety-projects/Volcanic-ash/A-history-of-ash-and-aviation/ [Accessed 8 Feb. 2016].

Webley, P. W., Steensen, T., Stuefer, M., Grell, G., Freitas, S., & Pavolonis, M.: Analyzing the Eyjafjallajökull 2010 eruption using satellite remote sensing, lidar and WRF-Chem dispersion and tracking model. Journal of Geophysical Research: Atmospheres, 117(D20), 2012.

WHO: Air quality guidelines. Global update 2005. Particulate matter, ozone, nitrogen dioxide and sulfur dioxide, URL http://www.who.int/phe/health_topics/outdoorair/outdoorair_aqg/en/, World Health Organisation, European Centre for Environment and Health Bonn Office, ISBN 92 890 2192, 2005.

Wilkins, K. L., Watson, I. M., Kristiansen, N. I., Webster, H. N., Thomson, D. J., Dacre, H. F., & Prata, A. J.: Using data insertion with the NAME model to simulate the 8 May 2010 Eyjafjallajökull volcanic ash cloud. Journal of Geophysical Research: Atmospheres, 121(1), 306-323, 2016.

Wilson, L. and Huang, T.C.: The influence of shape on the atmospheric settling velocity of volcanic ash particles, Earth and Planetary Sci. Lett., 44,311-324, 1979.

Wilson, T.M., Stewart, C., Sword-Daniels, V, Leanard, G.S., Johnston, D.M., Cole, J.W., Wardman, J., Wilson, G. and Barnard, S.T.: Volcanic ash impacts on critical infrastructure. J. Phys. Chem. Earth, doi:10.1016/j.pce.2011.06.006, 2011.

Winker, D. M., Liu, Z. Omar, A. Tackett, J. and Fairlie, D.: CALIOP observations of the transport of ash from the Eyjafjallajökull volcano in April 2010, J. Geophys. Res., 117, D00U15, doi:10.1029/2011JD016499, 2012.

Witham, C. S., & Oppenheimer, C: Mortality in England during the 1783–4 Laki Craters eruption. *Bulletin of Volcanology*, *67*(1), 15-26, 2004.

Woodhouse, M. J., Hogg, A. J., Phillips, J. C. and Sparks , R. S. J. Interaction between volcanic plumes and wind during the 2010 Eyjafjallajökull eruption, Iceland, J. Geophys. Res. Solid Earth, 118, 92–109, doi:10.1029/2012JB009592, 2013.

Yang, K., Krotkov, N. A., Krueger, A. J., Carn, S. A., Bhartia, P. K., & Levelt, P. F: Retrieval of large volcanic SO2 columns from the Aura Ozone Monitoring Instrument: Comparison and limitations. *Journal of Geophysical Research: Atmospheres*, *112*(D24), 2007.

Yu, Tianxu, William I. Rose, and A. J. Prata. Atmospheric correction for satellite-based volcanic ash mapping and retrievals using "split window" IR data from GOES and AVHRR. Journal of Geophysical Research: Atmospheres 107.D16, 2002.

6. Scientific papers

I

Atmos. Chem. Phys., 16, 9745–9760, 2016
www.atmos-chem-phys.net/16/9745/2016/
doi:10.5194/acp-16-9745-2016

Atmospheric Chemistry and Physics Open Access EGU

A model study of the pollution effects of the first 3 months of the Holuhraun volcanic fissure: comparison with observations and air pollution effects

Birthe Marie Steensen[1], Michael Schulz[1], Nicolas Theys[2], and Hilde Fagerli[1]

[1]Division for climate modelling and air pollution, Norwegian Meteorological Institute, Postbox 43 Blindern, 0313 Oslo, Norway
[2]Atmospheric composition, Belgian Institute for Space Aeronomy, Ringlaan-3-Avenue Circulaire, 1180 Brussels, Belgium

Correspondence to: Birthe Marie Steensen (birthems@met.no)

Received: 9 November 2015 – Published in Atmos. Chem. Phys. Discuss.: 25 January 2016
Revised: 13 June 2016 – Accepted: 9 July 2016 – Published: 3 August 2016

Abstract. The volcanic fissure at Holuhraun, Iceland started at the end of August 2014 and continued for 6 months to the end of February 2015, with an extensive lava flow onto the Holuhraun plain. This event was associated with large SO_2 emissions, amounting up to approximately 4.5 times the daily anthropogenic SO_2 emitted from the 28 European Union countries, Norway, Switzerland and Iceland. In this paper we present results from EMEP/MSC-W model simulations to which we added 750 kg s^{-1} SO_2 emissions at the Holuhraun plain from September to November (SON), testing three different emission heights. The three simulated SO_2 concentrations, weighted with the OMI (Ozone Monitoring Instrument) satellite averaging kernel, are found to be within 30 % of the satellite-observed SO_2 column burden. Constraining the SO_2 column burden with the satellite data while using the kernel along with the three simulated height distributions of SO_2, we estimate that the median of the daily burdens may have been between 13 and 40 kt in the North Atlantic area under investigation. We suggest this to be the uncertainty in the satellite-derived burdens of SO_2, mainly due to the unknown vertical distribution of SO_2. Surface observations in Europe outside Iceland showed concentration increases up to > 500 µg m^{-3} SO_2 from volcanic plumes passing. Three well identified episodes, where the plume crossed several countries, are compared in detail to surface measurements. For all events, the general timing of the observed concentration peaks compared quite well to the model results. The overall changes to the European SO_2 budget due to the volcanic fissure are estimated. Three-monthly wet deposition (SON) of SO_x in the 28 European Union countries, Norway and Switzerland is found to be more than 30 % higher in the model simulation with Holuhraun emissions compared to a model simulation with no Holuhraun emissions. The largest increases, apart from extreme values on Iceland, are found on the coast of northern Norway, a region with frequent precipitation during westerly winds. Over a 3-month average (during SON 2014) over Europe, SO_2 and $PM_{2.5}$ surface concentrations, due to the volcanic emissions, increased by only ten and 6 % respectively. Although the percent increase of $PM_{2.5}$ concentration is highest over Scandinavia and Scotland, an increase in PM exceedance days is found over Ireland and the already polluted Benelux region (up to 3 additional days), where any small increase in particulate matter concentration leads to an increase in exceedance days.

1 Introduction

Increased seismic activity in the Bárðarbunga volcano was recorded by the Icelandic Met Office from the middle of August 2014 (http://en.vedur.is/earthquakes-and-volcanism/volcanic-eruptions/holuhraun/). The activity continued in the volcano but some tremors also appeared towards the Holuhraun plain, a large lava field north of the Vatnajökull ice cap, the latter covering the Bárðarbunga and Grimsvötn volcano. On 31 August a continuous eruption started at Holuhraun with large amounts of lava pouring onto the plain and large amounts of sulfur dioxide (SO_2) emitted into the at-

mosphere (Sigmundsson et al., 2015). Thordarson and Hartley (2015) estimated SO_2 emissions from the magma at Holuhraun to range between 30 and 120 kt d^{-1} over the first 3 months of the eruption, with a maximum during the first 2 weeks of September. Schmidt et al. (2015) also found that among several model simulations with different emission fluxes, the model simulations with the largest emission (120 ktd^{-1}) compared best with satellite observations at the beginning of September. In comparison, Kuenen et al. (2014) estimated the daily anthropogenic emission from the 28 European Union countries for 2009 to be 13.9 ktd^{-1}, while the 2013 estimate is 9.8 ktd^{-1} (EMEP, 2015). The eruption ended in February 2015 and during the 6 months of eruption a total of approximately 11 ($\pm$5) Tg SO_2 may have been released (Gíslason et al., 2015), and the total lava field from the fissure measured 85 km^2 in area with a lava volume estimated to amount to 1.4 km^3 (vedur.is). It is of interest to investigate the impact of these volcanic emissions on SO_2 levels in Europe in 2014. In the last decades, measures have been taken to reduce SO_2 emissions, triggered by the Convention on Long-range Transboundary Air Pollution (LRTAP), in Europe. Significant reductions of 75 % in emission between 1980 and 2010 are confirmed by observations (Tørseth et al., 2012). The impact of volcanic eruptions with SO_2 emissions can thus perturb the European atmospheric sulfur budget to a larger extent than before and potentially lead to new acidification of lakes and soils if the eruption lasts over a long time period.

For comparison, the big 1783 Icelandic Laki eruption lasted 8 months and released a total amount of estimated 120 Tg of SO_2. The resulting sulfuric acid caused a haze observed in many countries in the Northern Hemisphere and increased mortality in northern Europe (Grattan et al., 2003; Thordarson and Self, 2003; Schmidt et al., 2011). The fissure at Holuhraun was much weaker than the Laki fissure, both in terms of amount of SO_2 released and probably also the height of the eruptive column. Thordarson and Self (1993) estimated that the Laki erupted at emission heights up to 15 km, while the observations of the Holuhraun eruptive cloud saw the plume rising up to 5 km (vedur.is). Ground-level concentrations exceeded the Icelandic hourly average health limit of 350 µgm^{-3} over large parts of Iceland (Gíslason et al., 2015). The World Health Organization (WHO) has a 10 min limit of 500 µgm^{-3} and a 24 h limit of 20 µgm^{-3}. High hourly mean surface concentrations of SO_2 were measured in Ireland (524.2 µgm^{-3}), then also in Austria (247.0 µgm^{-3}) and Finland (180 µgm^{-3}) (Schmidt et al., 2015; Ialongo et al., 2015).

A climate impact of high SO_2 emissions may be suspected, such as a cooling of climate due to an increase in aerosol burdens. Gettelman et al. (2015), using a global climate model, found a small increase in cloud albedo due to the Holuhraun emissions resulting in a -0.21 Wm^{-2} difference in radiative flux at the top of the atmosphere. If the event had happened earlier in the summer, a larger radiative effect could be expected (-7.4 Wm^{-2}). Understanding the atmospheric sulfur budget associated to such events is thus of great interest also for climate science. Unlike the two previous big eruptions in Iceland, Eyjafjallajökull in 2010 and Grímsvötn in 2011, this eruption did not emit significant amounts of ash. However, uncertainties in volcanic source estimates, time-varying emissions from a volcano type of point source and dependence of transport on initial injection height are similar problems for SO_2 and ash plumes. For eruptions in which both ash and SO_2 are emitted, SO_2 can act as a proxy for ash (Thomas and Prata et al., 2011; Sears et al., 2013), however separation will occur because of density differences and different eruption heights (Moxnes et al., 2014). Proven capability of modelling the transport of a volcanic plume can be useful for judging future eruption scenarios where SO_2 or ash can cause a problem.

The Holuhraun eruption is worth being analysed for several gas and aerosol transport and transformation processes, this study will mainly focus on simulated air quality effects and the perturbed sulfur budget due to the volcanic SO_2 emissions during the first 3 months of the eruption. Several stations in Europe reported high concentrations of SO_2 during this time and case studies are chosen to evaluate simulated plume development over Europe. The transport is modelled with the EMEP MSC-W chemical transport model, one of the important models used for air quality policy support in Europe over the last 30 years (Simpson et al., 2012). The first 2 months of the eruption are well covered by satellite observations. Both station and satellite data are compared to model results to understand the amplitude and magnitude of the sulfur budget perturbation. The effect of the injection height on the model results is studied by sensitivity simulations. Finally the perturbed European sulfur budget is documented and discussed to investigate the impact of increased SO_2 emission from a Icelandic volcano on European pollution levels.

2 Methods

2.1 Model description

The model simulations of the transport of the SO_2 Holuhraun emissions are created with the 3-D Eulerian chemical transport model developed at the Meteorological Synthesizing Centre – West (MSC–W) for the European Monitoring and Evaluation Programme (EMEP). The EMEP MSC-W model is described in Simpson et al. (2012). SO_2 is oxidized to sulfate in both gas and aqueous phase. In gas phase the oxidation is initiated by OH and is controlled by local chemistry. In aqueous phase the oxidants ozone, hydrogen peroxide and oxygen catalysed eventually by metal ions contribute to the oxidation. The dry deposition in the model is parameterized for different land types. Both in-cloud and subcloud scavenging are considered for wet deposition.

The simulations use the EMEP-MACC (Monitoring Atmospheric Composition and Climate) model configuration. The horizontal resolution of the model simulations is 0.25° (longitude) × 0.125° (latitude). There are 20 vertical layers up to about 100 hPa, with the lowest layer around 90 m thick. The model is driven by meteorology from the European Centre of Medium-Range Weather Forecasts (ECMWF) in the MACC model domain (30° W to 45° E and 30 to 76° N). Iceland is in the upper north-western corner of the domain, which implies losses of sulfur from the regional budget terms in sustained southerly and easterly flow regimes. The meteorology fields used have been accumulated in the course of running the MACC regional model ensemble forecast of chemical weather over Europe (http://macc-raq-op.meteo.fr), of which the EMEP MSC-W model is a part. For our hindcast-type simulations here, only the fields from the first day of each forecast are used. The meteorology is available with a 3 h interval. All model simulations are run from September through to November 2014.

Emission from the Holuhraun fissure is set to a constant 750 kgs^{-1} SO_2 (65 ktd^{-1}) for the entire simulation from the total 2.0 ± 0.6 Tg SO_2 emitted in September estimated in Schmidt et al. (2015). For all model runs the anthropogenic emissions are standard for our EMEP MACC model configuration. Table 1 shows an overview of the four different model runs that are used in this study. The column height observed both at ground and airborne instruments, varied during the eruption (Schmidt et al., 2015), the mean height was however around 3 km over the period. For the best guess, base case simulation, called bas_hol, volcanic emissions at Holuhraun are distributed equally from the ground up to a 3 km emission column height. To test the sensitivity towards emission height, two additional model simulations are carried out. One simulation in which the volcanic emission is distributed from the ground up to 1 km called low_hol, and a simulation in which the volcanic emission is distributed between 3 km and 5 km called high_hol. To derive the impact purely due to the emissions from Holuhraun, a simulation with no Holuhraun emissions is performed, called no_hol. Sensitivity runs with an almost doubled constant emission rate of 1400 kgs^{-1}, and a time-varying emission term given in Thordarson and Hartley (2015) were also studied. These resulted in an almost linear increase in concentrations and deposition and did not compare better to observations and will therefore not be presented here. The sensitivity to height of the emission appeared to be more important and is shown here in more detail.

Anthropogenic SO_2 emissions in the model are described in Kuenen et al. (2014). There is a yearly total SO_2 emission of 13.2 $Tg\,a^{-1}$ corresponding to 2009 conditions, the same year that is used in the reference MACC model configuration. The difference to actual 2014 conditions is assumed to be unimportant here. The inventory includes 2.34 Tga^{-1} SO_2 in yearly ship emissions over the oceans. Over the continents the yearly emissions are 5.08 Tga^{-1} SO_2 for the 28 EU countries and 5.53 Tga^{-1} SO_2 for the non-EU countries in the MACC domain (including Iceland) covered by the MACC domain.

2.2 Observations

The satellite data used in this study stem from the Ozone Monitoring Instrument (OMI) aboard NASA AURA (Levelt et al., 2006). The satellite was launched in July 2004 as part of the A-train earth-observing satellite configuration and follows a sun-synchronous polar orbit. The OMI measures backscattered sunlight from the Earth's atmosphere with a spectrometer covering UV and visible wavelength ranges. Measurements are therefore only available during the daytime. The background SO_2 concentrations are often too low to be observable, but increases in SO_2 from volcanic eruptions can produce easily distinguishable absorption effects (Brenot et al., 2014). Pixel size varies between 13 km × 24 km at nadir and 13 km × 128 km at the edge of the swath. OMI satellite data are affected by "row anomalies" due to a blockage affecting the nadir viewing part of the sensor, which affects particular viewing angles and reduces the data coverage. The zoom-mode of OMI reduces the coverage on some days. The coverage is also reduced by missing daylight, e.g. winter observations from high latitudes are absent. Therefore data from only the first 2 months from September until the end of October are used in this study.

The retrievals are described in Theys et al. (2015). The sensitivity of backscatter radiation to SO_2 molecules varies with altitude (generally decreasing towards the ground level), therefore the algorithms use an assumed height distribution for estimating the integrated SO_2 column density. Since often little information is available at the time of eruption and the retrievals produce results daily (even for days with no eruption), an assumed a priori profile is used for the vertical SO_2 distribution. The satellite retrievals used here assume an a priori profile with a plume thickness of 1 km that is centred at 7 km, similar to the method described in Yang et al. (2007). As found in Schmidt et al. (2015), this is too high for the Bárðarbunga eruption. Therefore, the retrieved SO_2 column densities may be too low. To compare the vertical column density (VCD) from the model to the one from satellite retrievals, the averaging kernel from the satellite has to be used. Each element of an averaging kernel vector defines the relative weight of the true partial column value in a given layer to the retrieved vertical column (Rodgers, 2000). Cloud cover also changes the averaging kernel and a spatio-temporally changing kernel is part of the satellite data product (an averaging kernel is provided for each satellite pixel).

To apply the averaging kernel on model data, the satellite data are regridded to the model grid so that those data from satellite pixels nearest to any given model grid point are used for that grid point. A smaller area than the whole model domain was chosen to study and be compared to the satellite data, 30° W to 15° E and 45 to 70° N (red boxes in

Table 1. Overview of model runs and the Holuhraun SO_2 emission height assumptions and flux; given are also medians of daily mass burdens of SO_2 for September to October 2014 in the North Atlantic as described along with Figs. 2 and 3.; last column contains scaled mass burdens, assuming 7.0 kt of SO_2 burden derived from satellite data (see text in discussion).

Model simulation name	Emission injection layer [km]	Emission flux ($kg\,s^{-1}$)	Burden original (kt)	Burden kernel weighted (kt)	Mass burden scaled (kt)
bas_hol	0–3	750	22.5	7.4	21.4
low_hol	0–1	750	25.4	4.4	40.3
high_hol	3–5	750	15.9	8.3	13.4
no_hol		0			

Fig. 1). The Aura satellite makes five overpasses over the domain during the daytime and swaths are partly overlapping in the northern regions. For the grid cells where the swaths overlap, the satellite observations are averaged to produce daily average fields. There are also regions that are not covered by satellite observation that will not be taken into account in the model data post processing. To make comparable daily averages of the model data, the closest hour in the hourly model output are matched to the satellite swath time and only grid points that are covered by satellite are used. The profiles for the averaging kernel in the satellite product are given on 60 levels and the values from these levels are interpolated to model vertical levels. The newly adjusted model VCD is then calculated by multiplying the interpolated averaging kernel weights to the SO_2 concentration in each model layer, integrating all layers with the height of each model layer.

Because of noise in the satellite data small retrieved VCD values are highly uncertain. A threshold limit is sought to identify those regions that have a significant amount of SO_2. Standard deviation for the satellite data is calculated over an apparently SO_2 free North Atlantic region (size $10 \times 15°$ lat lon respectively) and is found to be around 0.13 DU. Effects of varying cloud cover are ignored. An instrument detection limit is 3 times the standard deviation of a blank, so we assume that with a threshold value set to 0.4 DU we exclude satellite data below the detection limit. Any grid point with a value above this threshold in the satellite data is used along with the corresponding model data. Daily mass burdens for the North Atlantic region are calculated by summing up all SO_2 VCD in the grid cells above the threshold. Finally we convert Dobson units to mass burdens here and there in the paper to facilitate comparison to models and mass budgets. One Dobson unit is 2.69×10^{20} molecules per square metre, which corresponds to a column burden of 28.62 milligrams SO_2 per square metre (mgm^{-2}).

Data of SO_2 and $PM_{2.5}$ surface concentrations are collected by the European Environment Agency (EEA) through the European Environment Information and Observation Network (EIONET). We make use of two preliminary subsets of this data, one obtained from work within the MACC project to produce regular air quality forecasts and reanalysis (only SO_2) and a second one obtained from EEA, a so called up-to-date (UTD) air quality database, state spring 2016. The two different subsets cover observation data from different countries, and have not been finally quality assured at the time of writing this paper. We use only station data, which contain hourly data. However, there are missing data and some stations have instruments with high detection limits, making it difficult to create a continuous measurement series with good statistics. Therefore, in this study only some outstanding episodes with high concentrations of SO_2 and documented transnational transport of a volcanic plume are analysed. For the first 6-day period between 20 and 26 September 2014, high concentrations of SO_2 were measured over Great Britain and countries further to the south. For the second 6-day period, a month later (20 to 26 October), the plume was also detected over Great Britain, but was transported further east towards Germany. For the last plume studied, lasting from 29 October to 4 November, the volcanic emission was transported eastward to the coast of Norway and countries to the south. Recent daily deposition data are taken from the EBAS database (ebas.nilu.no) for those stations for which the data are already available. Model data to represent the station values are picked from hourly data at model surface level in the grid cell where the station is located.

3 Results

3.1 Comparison to satellite data

Observations by satellite provide information about SO_2 location and column density. Figure 1a shows as an example the VCD from the OMI satellite overpasses on 24 September 2014. Figure 1b and c show the modelled and the kernel-weighted VCD from the base simulation (bas_hol). The observed satellite SO_2 cloud and the model-simulated SO_2 cloud show similar shape and location. The kernel-weighted model column densities are smaller than the original model VCDs. More weight is given by the averaging kernel to model layers higher up, close to the reference height of 7 km, where there is less SO_2 in our case, with emissions and transport happening in the lower part of the troposphere. The re-

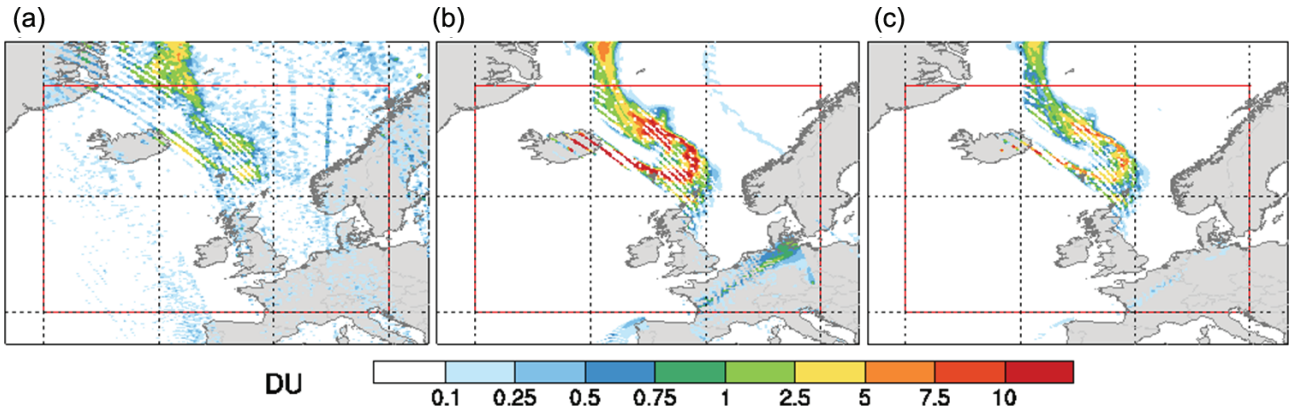

Figure 1. SO_2 column density: **(a)** for the satellite swaths on 24 September 2014; **(b)** for corresponding, consistently colocated original model data in the base simulation bas_hol; **(c)** for these model data with the satellite averaging kernel applied. The red box indicates the area where the statistics of satellite and model data in Figs. 2 and 3 are acquired.

duced kernel-weighted column densities are closer to the column densities observed by the satellite. There are, however, some spatial differences regarding where the maximum column densities are located.

A quantitative comparison is attempted here by integrating all satellite – and corresponding model data – above the North Atlantic, between Iceland and Europe, into daily mean column burdens. Figure 2 shows the time series from September to October of daily satellite coverage and daily mass burdens considered over the area where satellite VCD values exceed the 0.4 DU detection limit as explained above. The area covered by valid satellite observations at the beginning of the period is around 70 % of the domain used here (red boxes in Fig. 1). Towards the end of the period, the satellite coverage is only around 40 % because of the increasing solar zenith angle (a satellite zenith angle cut-off of 75° is used for the satellite data). On some days, the satellite cover is even lower because of the OMI zoom mode. The percentage of the satellite data that is above the detection limit is low over the entire 2-month period, only reaching around 10 % at the end of September and beginning of October.

On most days, the satellite daily mass burden is above the model value, ignoring the days when the OMI zoom mode is responsible for a small coverage. The average satellite-derived SO_2 mass burden assuming a 7 km reference height is 11.2 kt, while the kernel-weighted model burden in bas_hol is 8.7 kt SO_2. The highest values are found at the beginning of the period, 42.1 kt SO_2 on 7 September, for the model, and 37.4 kt SO_2, on 20 September for the satellite. Taking into account the area in which the satellite-observed SO_2 is found above detection limit, the satellite average column loadings are calculated to reach 70 mgm^{-2} for September. Furthermore, the peaks in the middle of October, visible in Fig 2b, exhibit a satellite average column loading of 62 mgm^{-2}.

The daily values of SO_2 mass burden are decreasing over time, especially during October. There is also a positive bias of the model against the satellite at the end of October. At the same time the satellite coverage is decreasing along with an increasing solar zenith angle. To further investigate whether this is responsible for the general decrease in mass burdens and the increasing bias of the simulated vs. observed VCDs, a new aggregation domain further south is used. All the areas where satellite observations may be possible up to the end of October (61.25° N) are used to calculate another set of daily column burdens for satellite and model data (see Fig. 2c). Satellite coverage in this southerly domain is not decreasing over time, but it is also not covering Iceland, so the SO_2 from Holuhraun first needs to be transported south before it can be detected. The plume is transported that far south 4 times over the 2-month period as the peaks in column burden values in Fig. 2c show. In this southerly area the daily accumulated mass burdens are similar in September and in October, supporting the hypothesis that the apparent decrease in mass burden in Fig. 2b is due to reduced satellite coverage.

Percentile values from the distribution of the daily mass burden in September and October 2014 from all three model simulations, original and kernel weighted, are shown in Fig. 3. Note that the mass burdens are accumulated in the same area in the North Atlantic, where at least 0.4 DU SO_2 was observed by OMI. Looking at the original model data, the model simulation with emissions in the lowest kilometre (low_hol) has the highest daily mass burden values (median: 25.4 kt), followed by the best-guess simulation, bas_hol (median: 22.5 kt), while the run with the emission highest in the atmosphere (high_hol) exhibits the smallest mass burden (median: 15.9 kt). The higher values in the low_hol simulation can be explained by less wind and dispersion at low altitudes and thus a more concentrated SO_2 cloud than in the two other model simulations.

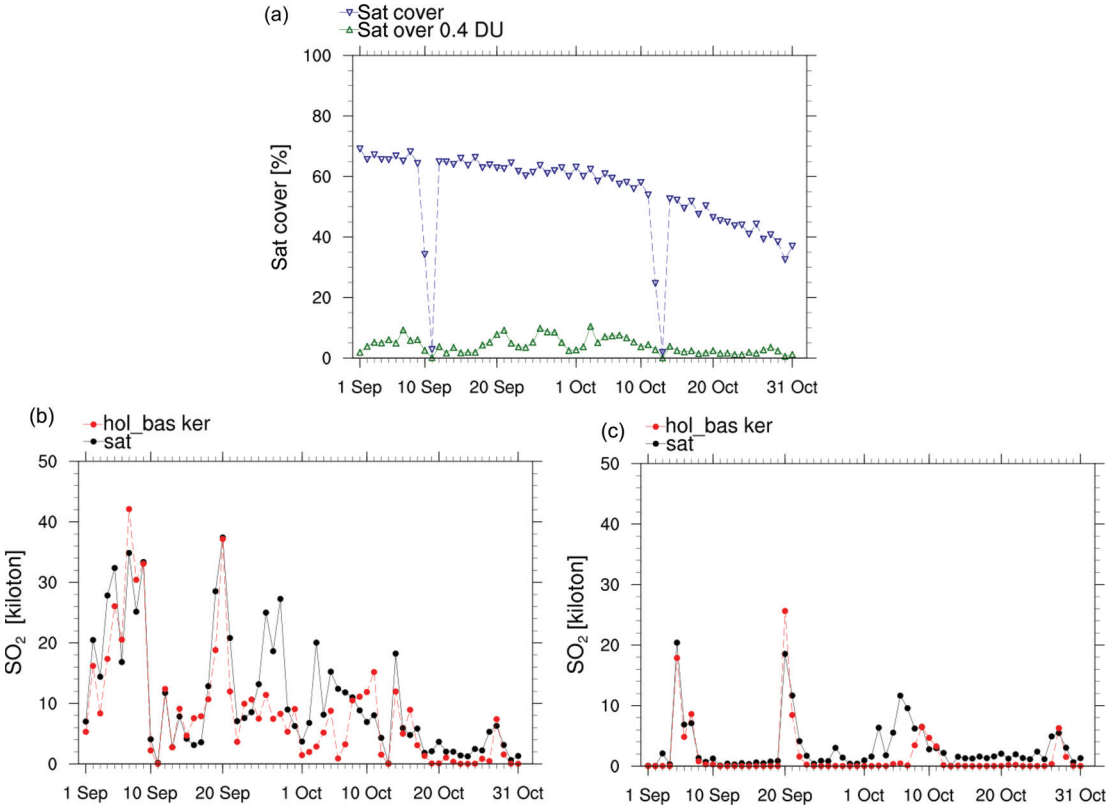

Figure 2. (a) Time series of the daily reference area covered by valid satellite observations (blue triangles) in percent of the total area of the domain used for the statistics (30° W to 15° E and 45–70° N, see Fig. 1). Green triangles show the reference area in percent where satellite-derived SO_2 VCD is above 0.4 DU; **(b)** Time series of accumulated daily SO_2 mass burdens in reference area from satellite data ("sat", black dots) and from model base run with averaging kernel applied ("hol_bas ker", red dots; **(c)** Shows the same as **(b)** but over a smaller area just south of 61.15° N.

The kernel-weighted model data represent what can be directly compared to the satellite data. As shown in Fig. 3, and illustrated already in Fig. 1, the kernel-weighted model column burden values are much smaller than the original ones, because the SO_2 plume was simulated to be far below 7 km altitude. The impact of the kernel weighting is quite different for the three model simulations. After the averaging kernel has been applied to the model data, the high_hol model simulation exhibits the highest daily burdens compared to the other two model simulations. The median for the bas_hol, low_hol and high_hol daily mass burden are 7.4, 4.4 and 8.4 kt respectively, while the satellite mass burden median value is 7.0 kt. High burdens retrieved from satellite data, and high kernel-weighted model burdens reflect that volcanic SO_2 is present at high concentrations and/or at high altitudes.

Analysis of the distribution of daily mass burdens allows for investigating how many days with very high burdens were present. Comparing the satellite data to the kernel-weighted model data, we find that the satellite's 75th percentile is larger than any of the model simulation's 75th percentiles. The satellite data contain some high daily burden values that result in a higher average burden and a higher 75th percentile. From testing different emission heights in our three-model simulations, the best-guess bas_run has the most similar distribution of daily burdens compared to the satellite data over the first 2 months.

3.2 Surface concentrations

SO_2 from the volcanic eruption on Holuhraun was measured at several surface stations during the period. Three different episodes with clear peaks in observed concentrations at stations around Europe are described in the following paragraphs. Exemplary comparisons are shown and additional comparisons at other stations are available in the Supplement.

A particular episode with very high surface concentrations of up to 500 $\mu g m^{-3}$ SO_2 in Ireland at the beginning of September was studied by Schmidt et al. (2015). However, just very few Irish station data were in the data extract we obtained from the EEA for this episode, and we decided to document the comparison for this episode in the Supplement. The comparison supports, however, that our emission flux in-

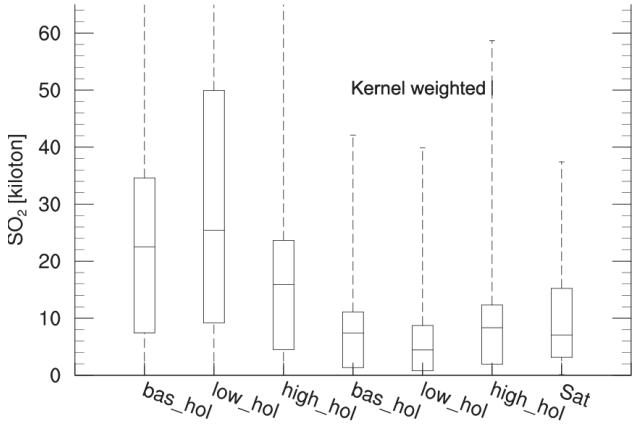

Figure 3. Distribution of daily SO_2 mass burden values in the area where satellite-derived SO_2 exceeds 0.4 DU (# 61; values from Fig. 2) as box-and-whisker plots; shown for the model simulations are original data (3 left boxes) and kernel-weighted data (3 following boxes) and the satellite data. The boxes shown represent the 25th percentile, the median, and the 75th percentile values, lower whiskers the minimum value and upper whiskers the maximum value.

deed might have been too small in the first days of September 2014.

Figure 4 shows the hourly time series for two stations over Great Britain and France from 20 September to 26 September. A maximum concentration of 44.3 μgm^{-3} SO_2 was measured on 21 September 16 UTC at a station situated in Manchester (53.48° N and 2.24° W) near the west coast of Britain. None of the three model simulations reach the observed maximum values. However, the simulated concentration field shows areas south of the station near Manchester, where the volcanic SO_2 concentrations are around 50 μgm^{-3}. Interestingly, the agreement of the model-derived volcanic SO_2 time series is better in agreement with measurements than the total simulated SO_2 concentration (grey curve), indicating that the model may not resolve SO_2 transport from nearby pollution sources and that the station for these days is rather representative of long-range transported volcanic SO_2. Observed $PM_{2.5}$ concentrations at the station show that, over the period, the highest concentration (52.1 μgm^{-3}) – probably anthropogenic – is measured at the start of the period, when the model did not simulate any volcanic sulfur contribution. The next day, the plume moved further south over France. The station is situated on the west coast of France in Saint-Nazaire (47.25° N and 2.22° W). The measurements show three peaks over 3 days, with the highest one (38 μgm^{-3}) measured on the 23 September at 12:00 UTC. All three model simulations have peak concentrations which are earlier than the observed ones, and the concentrations from the model are lower than observed. The three simulations do, however, show increased concentrations at the site due to the volcanic eruption over the 3 days. The map shows that large parts of France had an increase in SO_2 surface concentrations during this time.

Figure 5 shows the time series for three stations over Scotland and Germany a month later, from 20 to 26 October. The high_hol simulation shows low concentrations over the Scottish Grangemouth station (56.01° N and 3.70° W), but the bas_hol and low_hol have a plume with high concentrations over the station on 20 October. There are no measurements at this time with which to compare the model values. The timing of the second plume on 21 October for the two models is a few hours early and the modelled concentrations higher than observed (6.09 μgm^{-3}), especially in the low_hol simulation. The map shows a narrow plume from Iceland southwards to Scotland and the station lies on the edge of this plume. On 22 October, the volcanic SO_2 is measured at stations in Germany. Figure 5d shows the plume reaching from Iceland into the North Sea, transported east and south compared to the situation from the day before. The two stations Kellerwald (51.15° N and 9.03° E) and Bremerhaven (53.56° N and 8.57° E) experience the plume differently. While for Bremerhaven the observed peak (41.0 μgm^{-3}) is short in duration, the peak lasts for 1 day at Kellerwald with an observed maximum of 10.2 μgm^{-3}. The map shows that the plume is narrow for all three stations and the local spatial gradient is large.

A third plume is illustrated in Fig. 6 over northern Europe, occurring from the end of October to the beginning of November. Figure 6a shows the measured SO_2 concentrations at a station in Oslo, Norway (59.92° N and 10.76° E). There are four peaks measured from 29 to 31 October, with the highest one on 29 October (50.4 μgm^{-3}). The models runs show a contribution from Holuhraun SO_2 over the same 3 days, but do not reach the high measured concentrations and the first plume is especially underestimated. On October 30, the plume is transported south-east to Poland. The Polish station in Sopot (54.43° N and 18.58° E) experiences a short peak indicating that the model simulation happens a few hours earlier. The bas_hol simulation exhibits the most similar concentration evolution among the three model experiments.

Figure 7 shows wet deposition for the whole 3-month period at the Kårvatn station (62.78° N and 8.88° E) in Norway. There are high levels, both observed and modelled during the last part of September. The model exhibits a clear peak value on 27 September, while the observations record deposition spread out over several days. Summed over the whole period, the observed deposition amounts to 15.9 $gSm^{-2}\,yr^{-1}$ while the model simulated 20.0 $gSm^{-2}\,yr^{-1}$. Comparisons at other stations in Norway show similar results (Supplement).

3.3 Effects of the eruption on European pollution

The above results show that, despite the Holuhraun eruption releasing large amounts of SO_2, the stations in Europe often measured an increase in SO_2 concentration only as

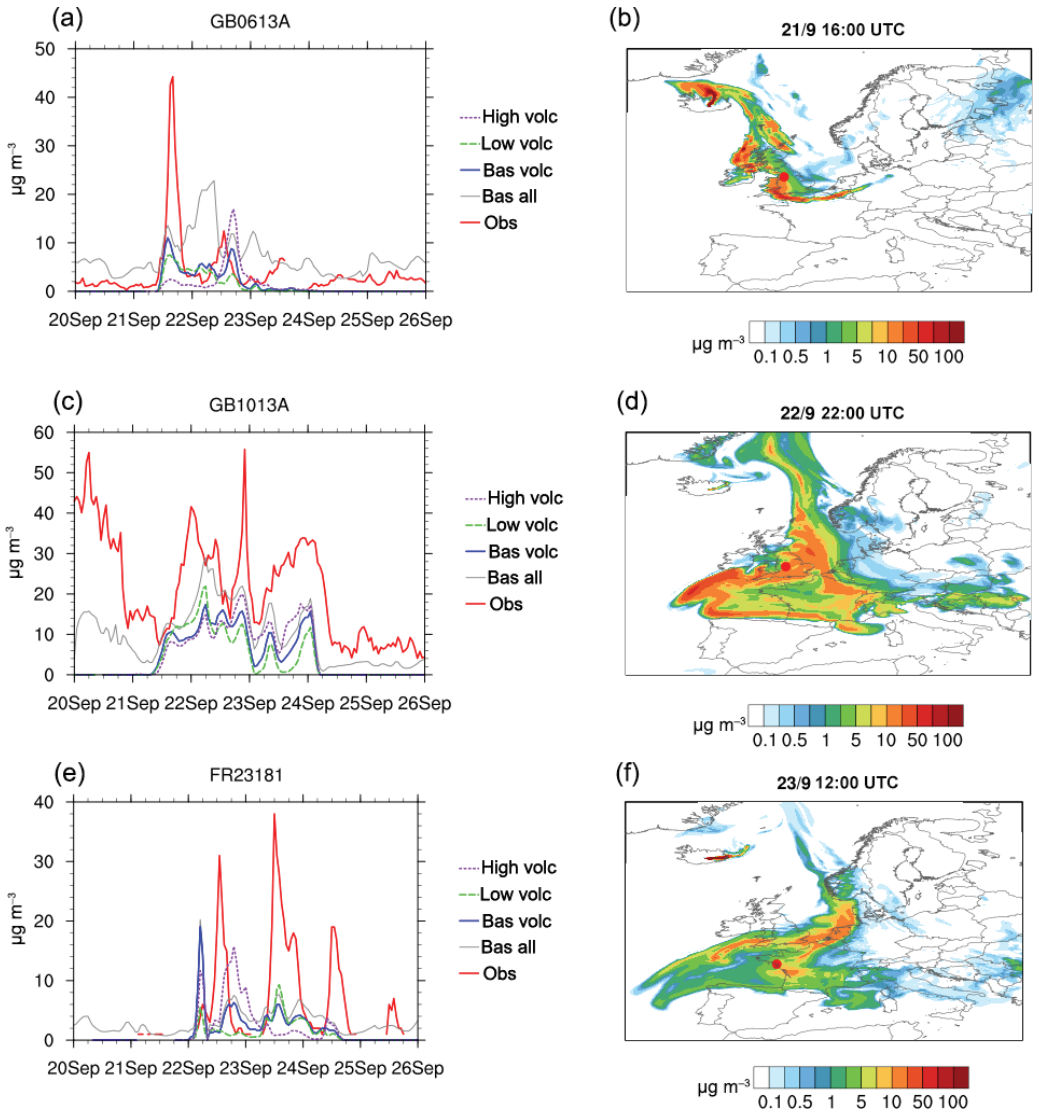

Figure 4. Left panels: time series of surface concentrations from 20 to 26 September 2014 for two stations, GB0613A, Manchester, SO_2 (top), $PM_{2.5}$ (middle) and FR23181, Saint-Nazaire, SO_2 (bottom). The red line shows the measured surface concentrations, the grey line represents the modelled surface concentration in bas_hol ("bas all"). By subtracting from the modelled surface concentrations in the three model runs (bas_hol, low_hol and high_hol) the no_hol simulation values, the concentration due to volcanic eruption is calculated and shown in the blue, green and pink lines respectively. Right panels: corresponding map of simulated surface concentration due to the volcanic eruption from bas_hol, corresponding to the blue line in the left panels, for the time of the maximum observed concentration. The red dot on the map marks the position of the station.

short peaks (Gíslason et al., 2015; Schmidt et al., 2015). The model makes it possible to investigate the general impact on European air quality by Holuhraun volcanic emissions. Table 2 summarizes characteristic SO_x budget terms and surface concentrations for the European continental land area in the countries mentioned in Table 2. Concentration and deposition over the oceans are not included. To isolate the effect of the Holuhraun eruption on Iceland itself, the deposition and concentrations over Iceland are given in brackets.

The table shows that the Holuhraun emission flux in the study period corresponds to over 4.5 times the anthropogenic emission from the 31 European countries considered here (not including ship emissions). The anthropogenic emissions from Iceland are only 18 kt, while the SO_2 emissions from Iceland increase by more than 300 times.

Over the 3 months, there is 1.32 times more SO_x wet deposition for the base run with Holuhraun emission than the reference simulation with no Holuhraun emission (no_hol). Table 2 shows that wet deposition over Europe is quite depen-

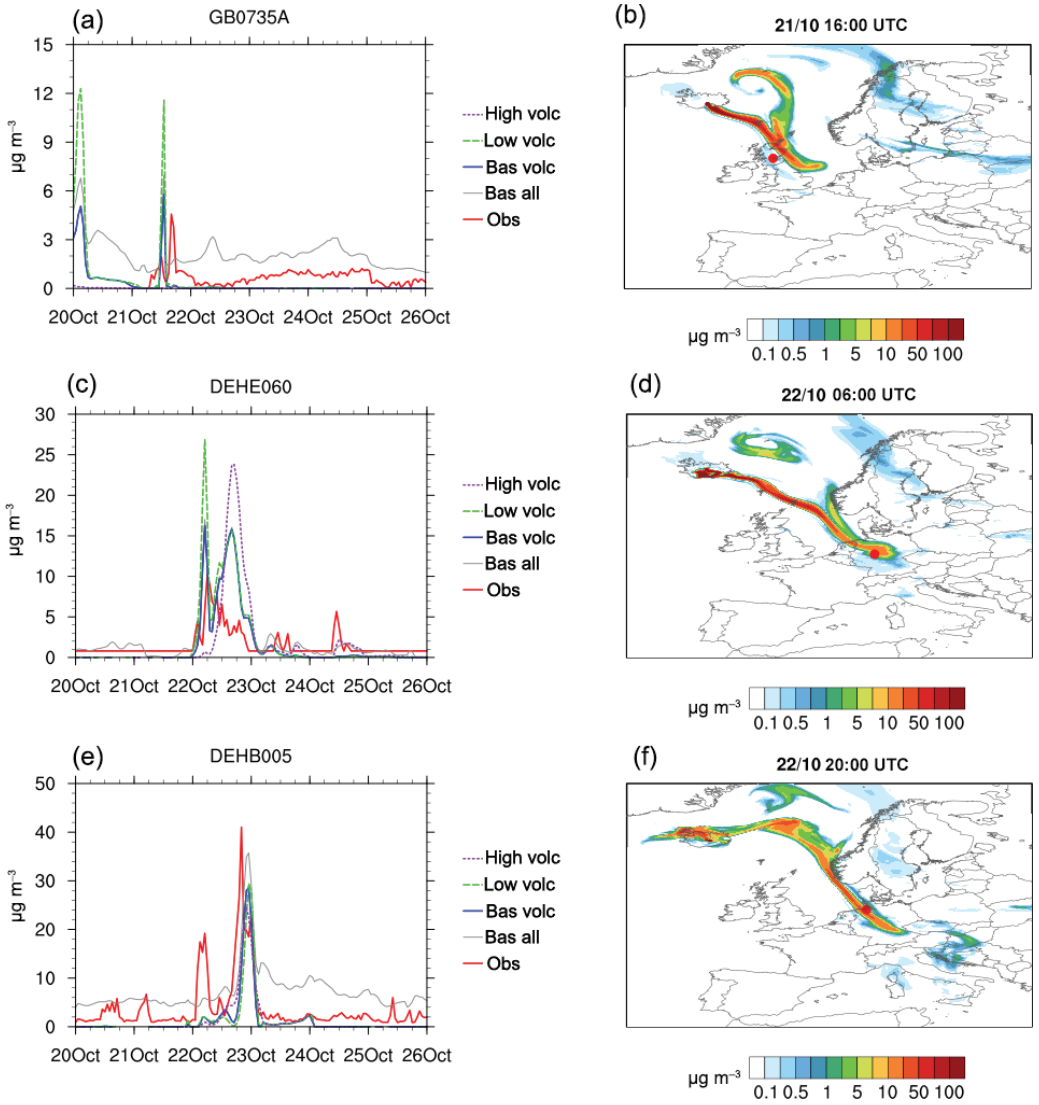

Figure 5. The same as Fig. 4, but from 20 to 26 October 2014 for three different stations GB0735A Grangemouth in Scotland, DEHE060 Kellerwald and DEHB005 Bremerhaven in Germany, all SO_2.

dent on the emission height. The simulation with the emission highest in the atmosphere (high_hol) exhibits the highest wet deposition in Europe. For dry deposition, a 10 % increase over Europe is found for all three model simulations with Holuhraun emissions. Close to the source, over Iceland, the deposition levels are very dependent on emission height, with dry deposition ranging from 8 to 409 kt.

Figure 8 shows the total deposition over Europe for the standard MACC model simulation with no Holuhraun emission (no_hol), the base model simulation (bas_hol) and the percent increase between these two model runs. Areas that experience the highest percent increase are also areas that have low levels in the model simulation with no emission at Holuhraun. Due to the Holuhraun emissions, Iceland has the highest SO_x deposition in Europe, and the coast of northern Norway shows depositions on the same level as the more polluted eastern Europe. Even though the previous section indicated that the model has higher wet deposition levels in northern Norway than observed, it also showed that it is very likely that the observed increases in SO_x deposition levels are due to the Holuhraun emissions.

The averaged SO_2 surface concentration over Europe is higher than over Iceland under normal conditions. The volcanic emission caused the concentration level over Iceland to increase by a factor of 177 (for the low_hol simulation). Over the rest of Europe, the increase is about the same for all three Holuhraun simulations, even though the time series showed that the different simulations had peaks often arriv-

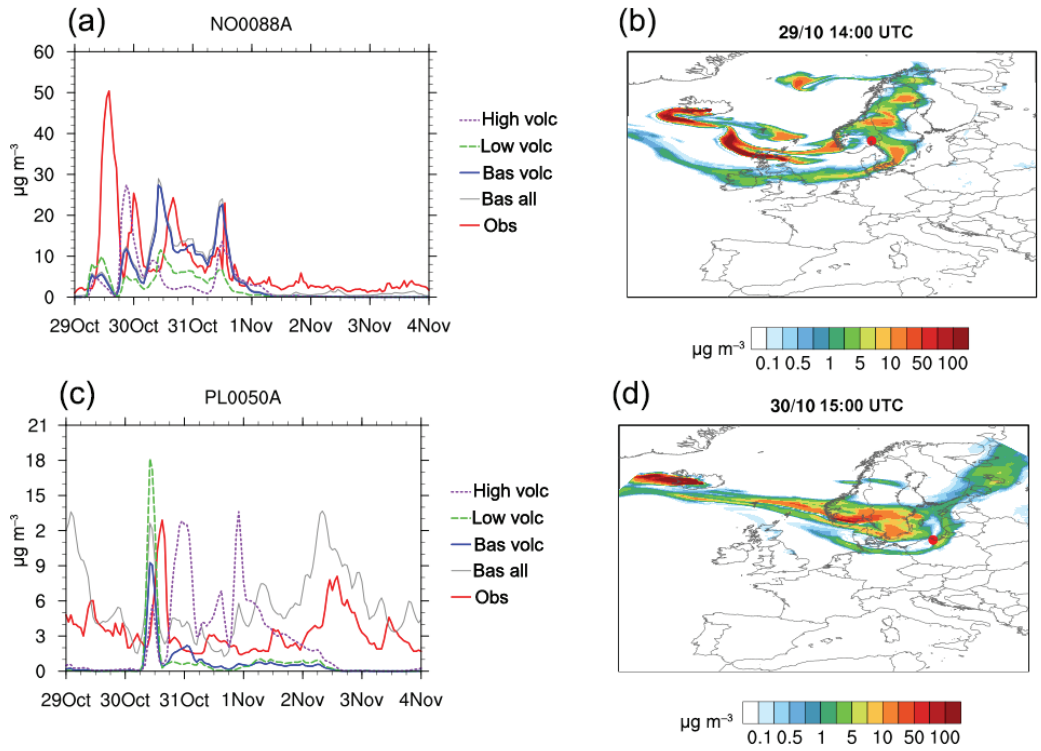

Figure 6. The same as Fig. 4 but from 29 October to 4 November 2014 for NO0088A Oslo, Norway and PL0050A in Sopot Poland, both SO_2.

Table 2. Emissions, depositions and concentrations for the 28 European Union member states, Norway and Switzerland for the 3 months September, October, November 2014; emissions and depositions are totalled over the 3 month period, concentrations are the mean over the period for the 31 countries. Numbers in brackets are the contribution from Iceland, for emission and deposition. For concentrations, the number represents the average over Iceland. See simulation names and set-up in Table 1.

Simulations:	no_hol	bas_hol	low_hol	high_hol	bas_hol/no_hol
Emissions SO_2	1257	1257	1257	1257	1
(kt)	(18)	(5980)	(5980)	(5980)	(5.68)
SO_x Wet deposition	1043	1382	1285	1465	1.32
(kt)	(11)	(1122)	(1491)	(472)	(2.37)
SO_x Dry deposition	481	529	524	526	1.10
(kilotons)	(4)	(151)	(409)	(8)	(1.40)
Mean SO_2 surface conc.	1.39	1.58	1.56	1.56	1.13
($\mu g\,m^{-3}$)	(0.59)	(38.95)	(105.91)	(1.81)	(66.17)
Mean $PM_{2.5}$ surface conc.	5.86	6.20	6.09	6.28	1.06
($\mu g\,m^{-3}$)	(0.82)	(2.50)	(3.13)	(1.12)	(3.06)

ing at different times. Vertical mixing, on average, levels off initial differences in emission height for volcanic plumes arriving in Europe.

The small increases in $PM_{2.5}$ concentrations over Europe, as shown in Table 2, are due to increased sulfate production from volcanic SO_2. However, $PM_{2.5}$ is a collection of all aerosols under 2.5 µm, and the volcanic sulfate is changing total aerosol mass therefore relatively little. The table shows that Iceland has a lower average concentration than the rest of Europe for all four runs, even though Iceland is the source for the increase in aerosol pollution levels. The high_hol model simulation has a higher increase in $PM_{2.5}$ concentration over Europe than the two other simulations. By contrast, the low_hol simulation finds the highest sulfate and SO_x deposition on Iceland itself, and possibly over the nearby ocean, which will lead to a smaller contribution to pollution levels over the rest of Europe.

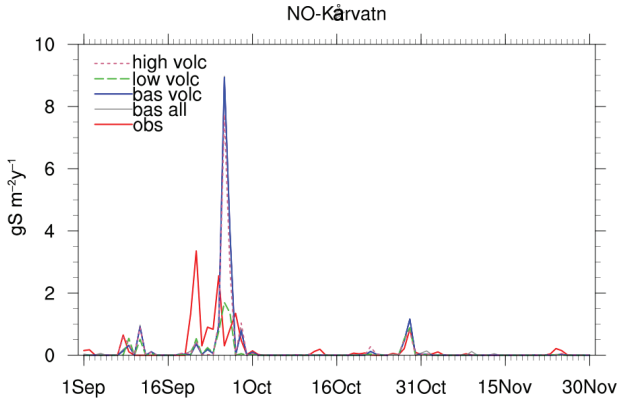

Figure 7. The same as Fig. 4, but September–November 2014 daily time series of SO_x total deposition at the Kårvatn station in Norway.

The distribution of $PM_{2.5}$ from the no_hol and bas_hol simulation, plotted in Fig. 9, shows the same polluted and clean areas as in Fig. 8, although the increase is lower. Over north-western Norway and northern Norway, the increase is over 100 %. Figure 9b shows that although the percentage increase is high, the $PM_{2.5}$ concentrations in these areas are still among the least polluted in Europe. The high deposition levels in this region indicate that some of the $PM_{2.5}$ is scavenged out.

WHO recommends a 24 h average mean concentration level of 25 μgm^{-3} for $PM_{2.5}$ not to be exceeded over 3 days in a year (WHO, 2005). Figure 10a shows that over the Benelux region, northern Germany and northern Italy this limit value is exceeded by up to 10 days during the 3 months studied. As the previous plot showed, these are regions with high average $PM_{2.5}$ concentrations. Because the daily concentrations are already high, any increase in days in the model bas_hol simulation due to the Holuhraun emissions is also occurring in these regions, and the areas with the highest percent increase do not experience any days over the limit. The figure also shows that Northern Ireland experienced up to 2 exceedance days due to the volcanic eruption.

4 Discussion

The bias and variances between the model data and the satellite observations can be due to several factors. (a) The model emission flux may be under- or overestimated compared to the real emissions, model VCDs are therefore too low/too large compared to the observed ones. (b) The areas for which the column mass burdens have been computed depend on the VCD detection limit and the actual satellite data, so the retrieved model burdens depend on the position of the identified and observed SO_2 cloud. If a simulated plume is displaced into an area where the satellite does not show any valid signal or no signal above detection limit, then this part of the model plume is ignored and may lead to underestimates by the model. (c) The presence of clouds can increase the uncertainty of the satellite retrieval. (d) The fluctuating real height of the SO_2 plume may introduce additional bias between model and satellite VCDs. Schmidt et al. (2015) presented IASI (Infrared Atmospheric Sounding Interferometer) plume heights for the Bárðarbunga SO_2 plume between 5.5 and 1.6 km derived from an area of 500 km around the volcanic location, and a mean IASI centre of mass height between 2.7 and 0.6 km.

Schmidt et al. (2015) presented a comparison between model, satellite and ground observations for September. Mass burdens from OMI were derived using observed plume heights from the IASI instrument on the MetOp satellite. Both satellite data sets were compared with the model NAME (Numerical Atmospheric-dispersion Modelling Environment), a Lagrangian model, which was run for September, with sensitivity runs testing both emission height and emission flux. The model simulation with a plume height of 3 km and doubled emission flux ($\sim 1400\,kgs^{-1}$) matched well with the OMI satellite data for the first days, while for the rest of September another simulation matched better, when emissions were similar to the constant emission term used in our study ($\sim 700\,kgs^{-1}$). Their study and ours show that for the first days and at the end of September, the satellite data exhibit higher values than a model using an emission rate of 700–750 kgs^{-1} SO_2. Our Holuhraun emission term in the three model simulations is constant throughout the simulations both with respect to the respective three emission heights and emission flux (see Table 1). Maximum fluxes of 1300 kgs^{-1} were reported by Barsotti (2014). Gíslason et al. (2015) estimated a 2.5 times above-average emission term during the first 2.5 weeks of the eruption. Our assumption of a constant emission term is thus certainly a simplification.

However, here we suggest that overall understanding of the height of the plume is as important to achieve model agreement with the satellite data as emission intensity variations. The emission height is also variable, dependent on initial volcanic eruption characteristics and meteorological conditions like wind speed and stratification (Oberhuber et al., 1998). Table 1 contains the original mass burdens and the kernel-weighted mass burdens as described in Sect. 3.1. It also contains a scaled burden estimate, assuming that each of the three simulations should be corrected for bias against the satellite-derived burden. This scaling assumes that in each model simulation the height distribution may be correct. The resulting mass burdens from the three simulations differ by 60 %, computed as standard deviation. This may be seen as an uncertainty estimate associated with our limited knowledge of the real height of emission and dispersion of the SO_2 plume from Bárðarbunga.

A better source estimate for the eruption is beyond the scope of this study, however, the fluctuations both in flux magnitude and emission height can explain some of the differences between satellite-observed and simulated concentrations, especially in the first days of September.

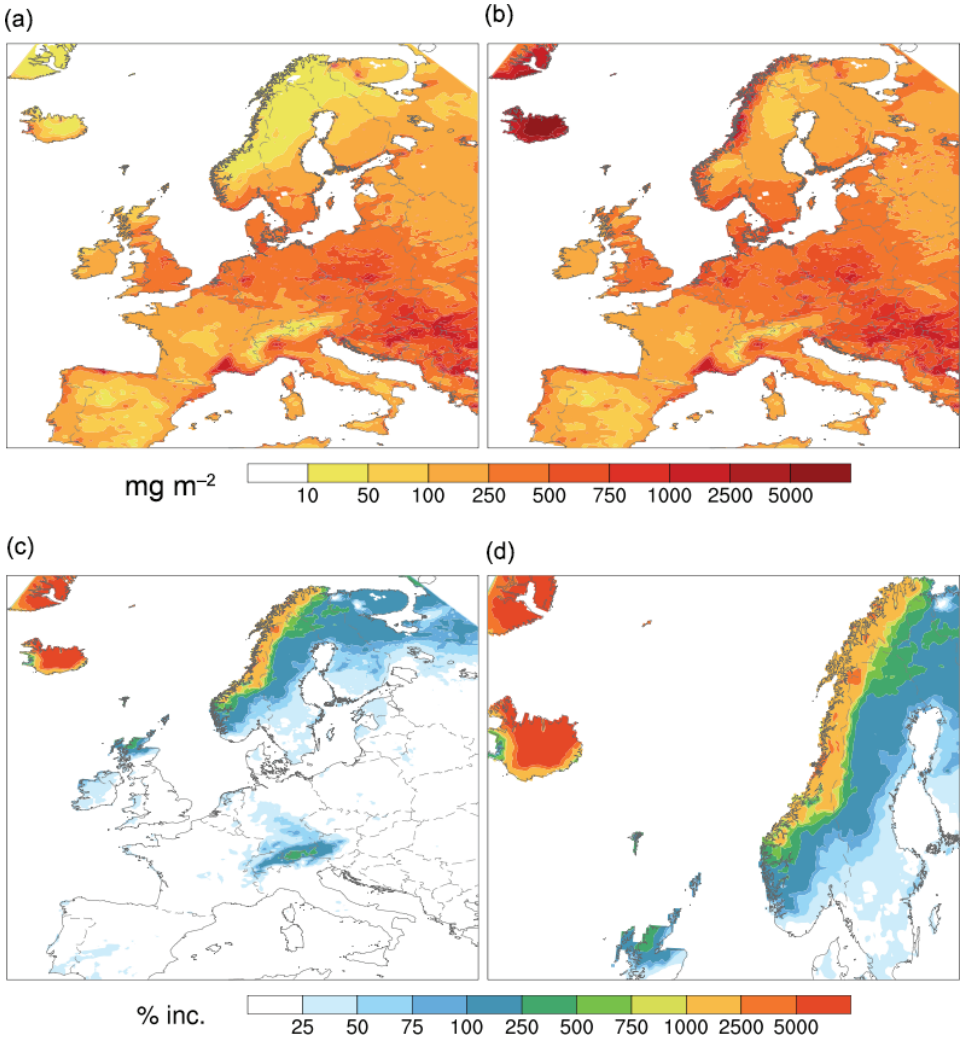

Figure 8. **(a)** Simulated total deposition of SO_x (wet and dry) over Europe from September to November 2014 for no_hol and **(b)** bas_hol simulations; **(c)** percent increase in SO_x deposition due to the Holuhraun emissions; **(d)** shows the same as **(c)** but zoomed into Norway and northern Europe.

Surface concentration comparisons presented in this study and in the Supplement show that the volcanic SO_2 was observed as short singular peaks lasting a few hours or as a sequence of several peaks spread over a few days. Three episodes are picked where transnational transport is documented. The biggest difference between simulated and measured concentrations is found for the first of the three studied plumes during 20 to 26 September in Manchester (station GB0613A), Great Britain and Saint-Naizaire (station FR23181), France, with up to a factor of four differences. Both the measured and simulated concentrations during the September event were higher than the two later events, pointing to a more efficient transport of SO_2 in this event. Higher emission fluxes up to a factor of 2 are supported by the satellite comparison on some of the days at the end of September. Changes in emission flux for the EMEP/MSC-W have been shown to have an almost linear change in concentrations (not shown here); even with doubled emissions during this event the model would still simulate surface concentrations well below those observed. Station data comparisons presented in Schmidt et al. (2015) for these days are similar, indicating that models have difficulties representing this period.

The discrepancies found between the model and observations suggest that the volcanic SO_x budget terms and average European surface concentrations presented in Table 2 contain errors. The model surface concentrations seem to be especially low compared to the observations; however the map plots in Figs. 4, 5, 6 show that sometimes modelled concentrations near the stations reached the observed levels. The area-averaged volcanic concentration contribution presented in Table 2 may therefore be close to reality. A more thorough study with a completed quality controlled data set is

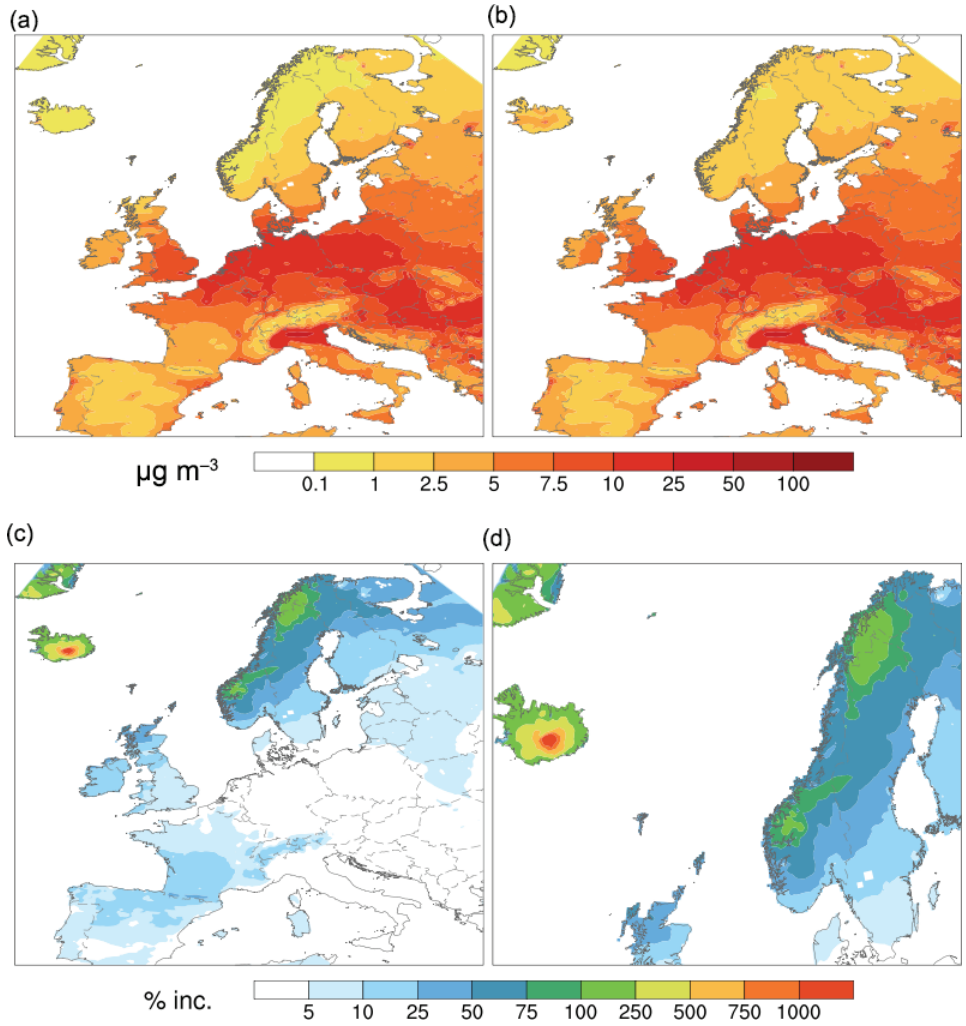

Figure 9. Shows the same as Fig. 8, but for average $PM_{2.5}$ concentration over the 3 months.

needed to better estimate the increase in SO_2 concentrations due to the eruption at the stations in the 2014 volcanic eruption episode.

Transport from an Icelandic volcano to Europe is caused by northerly and north-westerly winds. For the first plume, from 20 to 26 September, when the model shows low concentrations compared to the observations, there had been southerly winds for some time before strong northerly winds transported the SO_2 cloud southward over Great Britain and France. Compared to the other two episodes, the SO_2 surface concentration due to Holuhraun are higher over a larger area during this episode. The difficulty of the model in simulating the SO_2 transport correctly is connected to the uncertainty in the emission term, the meteorology fields, the chemical reactions and deposition. Overall the comparison to observations shows, that our best-guess bas_hol model simulation matches best with the observed satellite column burdens, their time evolution and for some stations with the magnitude and timing of the observed surface concentration peaks.

The results in this study show that the sulfur deposition from September to November over northern Norway was at the same level as found in the most polluted regions in Europe. The emission ceiling's aim, set by the Gothenburg Protocol, was to reduce the SO_x emissions by 63 % by 2010 from the 1990 levels in the European area of the convention of long-range transport of air pollutants (EMEP, 2015). Most countries have accomplished these reductions, and the sulfur deposition levels over Europe have decreased. The Holuhraun eruption changed the picture in some areas. Comparing observed deposition levels at Tustervatn station in central Norway, the simulated deposition is higher than the yearly observed averages since 1980. Monthly observed values at this station during the 2011 Grimsvötn eruption show almost as high values as the bas_hol simulation. The time series from the Kårvatn station also shows that the in-

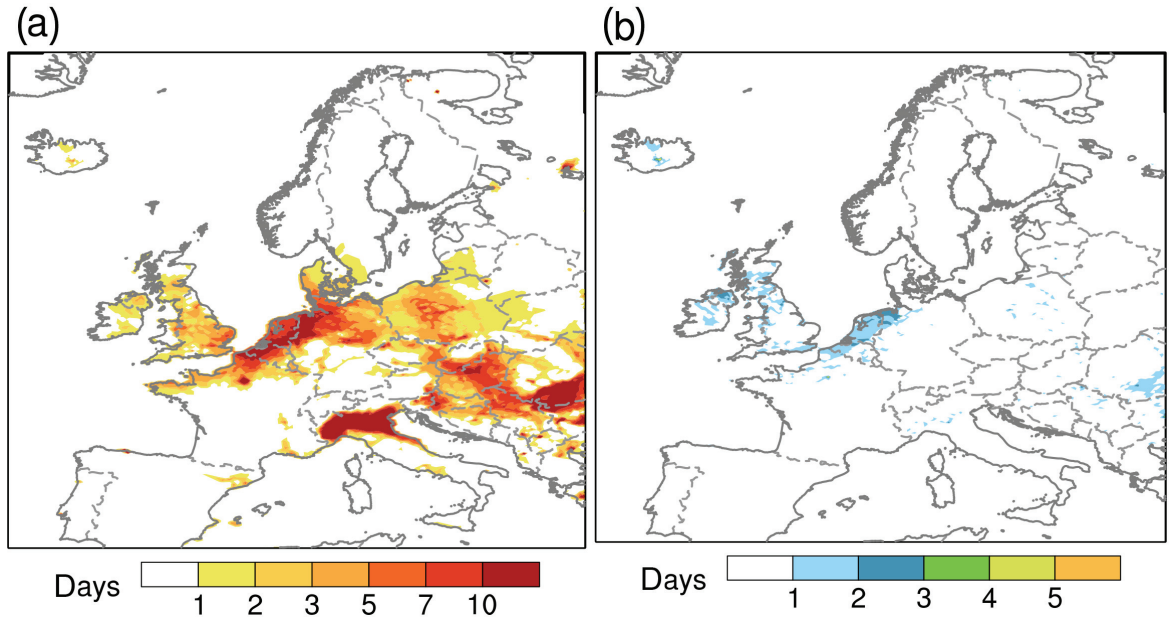

Figure 10. **(a)** Number of days with exceedances of $PM_{2.5}$ in the period September through to November 2014, for the bas_hol model simulation. **(b)** The increase in days of $PM_{2.5}$ exceedance from no_hol to bas_hol simulation, attributable to volcanic emissions.

creases are due to the Holuhraun volcanic eruption. Northern Norway is more susceptible for volcanic impact because of its geographical position, in addition to high frequency of precipitation on the western coast of Norway. Comparing the mean deposition levels over the 3 months in 2014 over Norway to model simulations with emissions from previous years, they are double those from the early 1990s (EMEP, 2015). Southern Norway experienced a sulfur deposition decrease of 40 % from 1980 to 1995 due to emission abatement in Europe (Berge et al., 1999). The highest contributors to high deposition levels over southern Norway were the UK and Germany (18 and 15 % respectively). Norway also experienced a high percent increase in $PM_{2.5}$ concentrations in 2014. The $PM_{2.5}$ levels over Scandinavia are low, and a small increase in the concentrations leads to high percent increases. The increase over land shows a similar pattern as the results found in Schmidt et al. (2011) for a hypothetical Laki eruption. Even though the highest increase is over Scandinavia and Scotland, the concentrations are too low to exceed the 25 µg m^{-2} limit. Already polluted regions like the Benelux region experience more days with exceedances as well as Northern Ireland.

5 Conclusions

The increase in emitted SO_2 to the atmosphere caused by the volcanic eruption at Holuhraun was observed by satellite and detected at several stations over Europe (Schmidt et al., 2015; Gíslason et al., 2015). Model simulations with the EMEP MSC-W model with emissions from Holuhraun over the period from September to November 2014 have been carried out to investigate the model capability to simulate such events, and also to study the impact of the increased emissions on concentrations and depositions over Europe.

The first 2 months of the model simulations are compared to satellite retrievals from OMI. The retrievals use an assumed plume height of 7 km. Averaging kernels from the satellite data are applied on the model data to compare the model data to the satellite. Because of the weighting, the satellite retrieved mass burden values are dependent on both vertical placement and amount of SO_2. Two sensitivity model simulations with different Holuhraun emission heights are compared to the satellite data together with the best-guess base simulation. After the kernel is applied, the results are more comparable to the satellite data. Constraining the SO_2 column burden with the satellite data while using the kernel along with the three simulated height distributions of SO_2, we estimate that the median of the daily burdens may have been between 13 and 40 kt in the North Atlantic area under investigation.

The model simulations are also compared to observed concentrations at stations over Europe for three different events with high concentrations measured due to the Holuhraun emissions. For all the events, the timing of the model peaks is compared to the observed peaks in concentration. There is a better timing in the two model simulations in which the emissions are injected lowest into the atmosphere than for the sensitivity run with the highest emission height. Due to

a special transport pattern of SO_2 during the first event, observed concentrations are higher here than during the later events, and the difference between models and observations is largest. $PM_{2.5}$ concentration during this first event is comparable to observations. Uncertainties in the model simulations increase by the length of transport, and some near misses of the narrow plumes can clearly explain differences between models and observation. To make a better assessment of model performance during the whole volcanic eruption, better quality checked station data are needed. Comparison between the model and wet deposition observations over Norway show significant and high contributions from the eruption, although the model overpredicts values at the stations studied and other stations to be found in the Supplement.

Studying the changes in pollution levels over Europe, increased SO_x wet deposition is most noticeable. In the 3-month base simulation there is 32 % more sulfate wet deposition found than in the model simulation with no Holuhraun emission, accounted for over the 28 European Union countries, Norway and Switzerland. The regions that have the highest increase, apart from Iceland, are northern Scandinavia and Scotland, regions that are among the least polluted in Europe. In particular, the coast of northern Norway, with a percent increase in total deposition of over 1000 %, shows levels equal to the most polluted regions in Europe Seen against the long-term record of observed levels of deposition since 1980 at the Tustervatn station in central Norway, the 2014 deposition values stand out and are only exceeded during the Grimsvötn eruption in 2011. We also find that high SO_x wet deposition values measured at the Kårvatn station in 2014 on the coast of western Norway are very likely due to the Holuhraun emissions.

The difference in SO_2 concentrations over Europe between the no_hol and model simulations with Holuhraun emission is around 13 % and increases occur as short peaks in concentration levels from a few hours to some days. Due to the underestimation seen at stations during September, the uncertainty of this number is large and the simulated volcanic contribution is possibly too small. For $PM_{2.5}$ concentration, the volcanic increase is 6 %, and the model shows better agreement with station observations. The biggest difference in percent increase is seen over Scandinavia and Scotland, however these regions are among the cleanest in Europe, also with the added sulfur caused by the Holuhraun emissions. The areas that show an increase in number of days with over 25 μgm^{-2} $PM_{2.5}$ concentrations are those that are already polluted. Even with high emissions from the volcanic fissure at Holuhraun, the increase in pollution levels over Europe was relatively small, with only transient episodes associated with high increases in SO_2 concentration.

The Supplement related to this article is available online at doi:10.5194/acp-16-9745-2016-supplement.

Acknowledgements. Most of the work done for this paper is funded by the Norwegian ash project financed by the Norwegian Ministry of Transport and Communications and AVINOR. Model and support is also appreciated through the Cooperative Programme for Monitoring and Evaluation of the Long-range Transmission of Air Pollutants in Europe (No: ECE/ENV/2001/003). The observations are made available through the EEA UTD database (http://www.eionet.europa.eu/aqportal) and the MACC project (MACC III project number 633080) obtained with the much appreciated help of Álvaro Valdebenito. Wenche Aas and Paul Eckhardt are thanked for provision of recent measurements of wet deposition measurements in northern Norway, included in the EBAS database. This work has also received support from the Research Council of Norway (Programme for Supercomputing) through CPU time granted at the super computers at NTNU in Trondheim.

Edited by: Y. Balkanski
Reviewed by: two anonymous referees

References

Barsotti, S.: 100 Days of Gas Release at Holuhraun, Vedur.is, http://en.vedur.is/pollution-and-radiation/volcanic-gas/measurements/ (last access: 26 March 2015), 2014.

Berge, E., Bartnicki, J., Olendrzynski, K., and Tsyro, S.: Long-term trends in emissions and transboundary transport of acidifying air pollution in Europe, J. Environ. Manage., 57, 31–50, 1999.

Brenot, H., Theys, N., Clarisse, L., van Geffen, J., van Gent, J., Van Roozendael, M., van der A, R., Hurtmans, D., Coheur, P.-F., Clerbaux, C., Valks, P., Hedelt, P., Prata, F., Rasson, O., Sievers, K., and Zehner, C.: Support to Aviation Control Service (SACS): an online service for near-real-time satellite monitoring of volcanic plumes, Nat. Hazards Earth Syst. Sci., 14, 1099–1123, doi:10.5194/nhess-14-1099-2014, 2014.

EMEP MSC-W: Transboundary acidification, eutrophication and ground level ozone in Europe 2013, EMEP Status Report 1/2015, 2015.

Gettelman, A., Schmidt, A., and Kristjansson, J. E.: Icelandic volcanic emissions and climate, Nat. Geosci, 8, 243–243, 2015.

Gíslason, S. R., Stefánsdóttir, G., Pfeffer, M. A., Barsotti, S., Jóhannsson, T., Galeczka, I., Bali, E., Sigmarsson, O., Stefánsson, A., Keller, N. S., Sigurdsson, Á., Bergsson, B., Galle, B., Jacobo, V. C., Arellano, S., Aiuppa, A., Jónasdóttir, E. B., Eiríksdóttir, E. S., Jakobsson, S., Guðfinnsson, G. H., Halldórsson, S. A., Gunnarsson, H., Haddadi, B., Jónsdóttir, I., Thordarson, T., Riishuus, M., Högnadóttir, T., Dürig, T., Pedersen, G. B. M., Höskuldsson, Á., and Gudmundsson, M. T.: Environmental pressure from the 2014–15 eruption of Bárðarbunga volcano, Iceland, Geochem. Persp. Lett., 1, 84–93, 2015.

Grattan, J., Durand, M., and Taylor, S.: Illness and elevated Human Mortality in Europe Coincident with the Laki Fissure eruption. Vocanic Degassing: Geol. Soc, SP 213, The Geological Society of London, 410–414, 2003.

Ialongo, I., Hakkarainen, J., Kivi, R., Anttila, P., Krotkov, N. A., Yang, K., Li, C., Tukiainen, S., Hassinen, S., and Tamminen, J.: Comparison of operational satellite SO_2 products with ground-based observations in northern Finland during the Icelandic

Holuhraun fissure eruption, Atmos. Meas. Tech., 8, 2279–2289, doi:10.5194/amt-8-2279-2015, 2015.

Levelt, P. F., van den Oord, G. H. J., Dobber, M. R., Mälkki, A., Visser, H., de Vries, J., Stammes, P., Lundell, J., and Saari H.: The Ozone Monitoring Instrument, IEEE T. Geosci. Remote, 44, 1093–1101, doi:10.1109/TGRS.2006.872333, 2006.

Kuenen, J. J. P., Visschedijk, A. J. H., Jozwicka, M., and Denier van der Gon, H. A. C.: TNO-MACC_II emission inventory; a multi-year (2003–2009) consistent high-resolution European emission inventory for air quality modelling, Atmos. Chem. Phys., 14, 10963–10976, doi:10.5194/acp-14-10963-2014, 2014.

Moxnes, E. D., Kristiansen, N. I., Stohl, A., Clarisse, L., Durant, A., Weber, K., and Vogel, A.: Separation of ash and sulphur dioxide during the 2011 Grimsvötn eruption, J. Geophy. Res.-Atmos., 119, 7477–7501, 2014.

Oberhuber, J. M., Herzog, M., Graf, H., and Schwanke, K.: Volcanic plume simulation on large scales, J. Volcanol. Geoth. Res., 87, 29–53, 1998.

Rodgers, C. D.: Inverse Methods for Atmospheric Sounding: Theory and Practice, World Sci., Singapore, 2000.

Schmidt, A., Ostro, B., Carslaw, K. S., Wilson, M., Thordarson, T., Mann, G. W., and Simmons, A. J.: Excess mortality in Europe following a future Laki-style Icelandic eruption, P. Natl. Acad. Sci. USA, 108, 15710–15715, 2011.

Schmidt, A., Leadbetter, S., Theys, N., Carboni, E., Witham, C. S., Stevenson, J. A., Birch, C. E, Thordarson, T., Turnock, S., Barsotti, S., Delaney, L., Feng, W., Grainger, R. G., Hort, M. C., Höskuldsson, Á., Ialongo, I., Ilyinskaya, E., Jóhannsson, T., Kenny, P., Mather, T. A., Richards, N. A. D., and Shepherd, J.: Satellite detection, long-range transport, and air quality impacts of volcanic sulphur dioxide from the 2014–2015 flood lava eruption at Bárðarbunga (Iceland), J. Geophys. Res.-Atmos., 120, 9739–9757, doi:10.1002/2015JD023638, 2015.

Sears, T. M., Thomas, G. E., Carboni, E., A Smith, A. J., and Grainger, R. G.: SO_2 as a possible proxy for volcanic ash in aviation hazard avoidance, J. Geophys. Res.-Atmos., 118, 5698–5709, 2013.

Sigmundsson, F., Hooper, A., Hreinsdottir, S., Vogfjord, K. S., Ofeigsson, B. G., Heimsson, E. R., Dumont, S., Parks, M., Spaans, K., Gudmindsson, G. B., Drouin, V., Arnadottir, T., Jonsdottir, K., Gudmundsson, M. T., Hognadottir, T., Fridriksdottir, H. M., Hensch, M., Einarsson, P., Magnusson, E., Samsonov, S., Brandsdottir, B., White, R. S., Agustdottir, T., Greenfield, T., Green, R. G., Hjartardottir, A. R., Pedersen, R., Bennet, R. A., Geirsson, H., La Femina, P. C., Bjornsson, H., Palsson, F., Sturkell, E., Bean, C. J., Mollhoff, M., Braiden, A. K., and Eibl, E. P. S.: Segmented lateral dyke growth in a rifting event at Barðarbunga volcanic system, Iceland, Nature, 517, 191–195, 2015.

Simpson, D., Benedictow, A., Berge, H., Bergström, R., Emberson, L. D., Fagerli, H., Flechard, C. R., Hayman, G. D., Gauss, M., Jonson, J. E., Jenkin, M. E., Nyíri, A., Richter, C., Semeena, V. S., Tsyro, S., Tuovinen, J.-P., Valdebenito, Á., and Wind, P.: The EMEP MSC-W chemical transport model – technical description, Atmos. Chem. Phys., 12, 7825–7865, doi:10.5194/acp-12-7825-2012, 2012.

Theys, N., De Smedt, I., van Gent, J., Danckaert, T., Wang, T., Hendrick, F., Stavrakou, T., Bauduin, S., Clarisse, L., Li, C., Krotkov, N., Yu, H., Brenot, H., and Van Roozendael, M.: Sulphur dioxide vertical column DOAS retrievals from the Ozone Monitoring Instrument: Global observations and comparison to ground-based and satellite data, J. Geophys. Res.-Atmos., 120, 2470–2491, doi:10.1002/2014JD022657, 2015.

Thomas, H. E. and Prata, A. J.: Sulphur dioxide as a volcanic ash proxy during the April–May 2010 eruption of Eyjafjallajökull Volcano, Iceland, Atmos. Chem. Phys., 11, 6871–6880, doi:10.5194/acp-11-6871-2011, 2011.

Thordarson, T. and Self, S.: The Laki (Skaftár Fires) and Grimsvötn eruptions in 1783–1785, B. Volcanol., 55, 233–263, 1993.

Thordarson, T. and Self, S.: Atmospheric and environmental effects of the 1783-1784 Laki eruption: A review and reassessment, J. Geophys. Res.-Atmos., 108, AAC 7-1–AAC 7-29, 2003.

Thordarson, T. and Hartley, M.: Atmospheric sulphur loading by the ongoing Nornahraun eruption, North Iceland, EGU General Assembly Conference Abstracts, 17, 2015EGUGA, 1710708T, 2015.

Tørseth, K., Aas, W., Breivik, K., Fjæraa, A. M., Fiebig, M., Hjellbrekke, A. G., Lund Myhre, C., Solberg, S., and Yttri, K. E.: Introduction to the European Monitoring and Evaluation Programme (EMEP) and observed atmospheric composition change during 1972–2009, Atmos. Chem. Phys., 12, 5447–5481, doi:10.5194/acp-12-5447-2012, 2012.

World Health Organisation (WHO): Air quality guidelines, Global update 2005, Particulate matter, ozone, nitrogen dioxide and sulphur dioxide, http://www.who.int/phe/health_topics/outdoorair/outdoorair_aqg/en/ (last access: 9 October 2015), World Health Organisation, European Centre for Environment and Health Bonn Office, ISBN 92 890 2192 2005.

Yang, K., Krotkov, N. A., Krueger, A. J., Carn, S. A., Bhartia, P. K., and Levelt, P. F.: Retrieval of large volcanic SO_2 columns from the Aura Ozone Monitoring Instrument: Comparison and limitations, J. Geophys. Res.-Atmos., 112, D24S43, doi:10.1029/2007JD008825, 2007.

II

Geosci. Model Dev. Discuss., doi:10.5194/gmd-2016-315, 2017
Manuscript under review for journal Geosci. Model Dev.
Published: 10 January 2017

Geoscientific Model Development Discussions

The operational eEMEP model for volcanic SO_2 and ash forecasting

Birthe M. Steensen, Michael Schulz, Peter Wind, Álvaro M. Valdebenito, Hilde Fagerli

Research department, Norwegian Meteorological Institute, Postbox 43 Blindern, 0313 Oslo, Norway

Correspondence to: Birthe M. Steensen (birthe.steensen@met.no)

Abstract.

This paper presents a new version of the EMEP MSC-W model called eEMEP developed for transportation and dispersion of volcanic emissions, both gases and ash. EMEP MSC-W is usually applied to study problems with air pollution and aerosol transport and requires some adaptation to treat volcanic eruption sources and effluent dispersion. The operational setup of model simulations in case of a volcanic eruption is described. Important choices have to be made to achieve CPU efficiency so that emergency situations can be tackled in time, answering relevant questions of ash advisory authorities. An efficient model needs to balance complexity of the model and resolution. We have investigated here a meteorological uncertainty component of the volcanic cloud forecast by using a consistent ensemble meteorological dataset (GLAMEPS forecast) in three resolutions for the case of SO_2 effusion from the 2014 Barðarbunga eruption. The low resolution (40x40km) ensemble members show larger agreement in plume position and intensity, suggesting that the ensemble here don't give much added value. For comparing the dispersion in different resolutions we compute the area where the column load of the volcanic tracer, here SO_2, is above a certain threshold, varied for testing purposed between 0.25-50 DU Dobson units. The increased numerical diffusion causes a larger area (+34%) to be covered by the volcanic tracer in the low resolution simulations than in the high resolution ones. The higher resolution (10x10km) ensemble members show higher concentrations farther away from the volcanic eruption site in more narrow plumes. Plume positions are more varied between the high resolution members, while the plume form resemble the observed plumes more than the low resolution ones. For a volcanic emergency case this means: To obtain quickly results of the transport of volcanic emissions an individual simulation with our low resolution is sufficient, however, to forecast peak concentrations with more certainty for forecast or scientific analysis purposes a finer resolution is needed. The model is further developed to simulate ash from highly explosive eruptions. A possibility to increase the number of vertical layers, achieving finer vertical resolution, as well as a higher model top is included in the eEMEP version. Ash size distributions may be altered for different volcanic eruptions and assumptions. Since ash particles are larger than typical particles in the standard model, gravitational settling across all vertical layers is included. We attempt finally a specific validation of the simulation of ash and its vertical distribution. Model simulations with and without gravitational settling for the 2010 Eyjafjallajökull eruption are compared to lidar observations over Central Europe. The results show that with gravitation the centre of ash mass can be 1km lower over central Europe than without gravitation. However the height variations in the ash layer caused by real weather situations are not captured perfectly well by either of the two simulations, playing down the role of gravitation parameterization imperfections. Both model simulations have on average ash centre of mass below the observed values. Correlation between the observed and corresponding model centre of

Geosci. Model Dev. Discuss., doi:10.5194/gmd-2016-315, 2017
Manuscript under review for journal Geosci. Model Dev.
Published: 10 January 2017

Geoscientific Model Development Discussions

mass are higher for the model simulation with gravitational settling for four of six stations studied here. The inclusion of gravitational settling is suggested to be required for a volcanic ash model.

1 Introduction

The European Monitoring and Evaluation Programme model developed at the Meteorological Synthesizing Centre - West (EMEP MSC-W) has been expanded to handle ash forecasting for the Norwegian Meteorological institute. Historically, the EMEP MSC-W Eulerian model has been used to deal with problems concerning acidifying substances deposition, and long-range transport of tropospheric ozone and particles (Simpson et al., 2012). The EMEP MSC-W model is already in use in a forecasting mode as one of the ensemble members of the MACC/CAMS daily ensemble production system for regional air quality forecasting (Marécal et al., 2015). This paper will present the developments of the EMEP MSC-W model that allow the model to describe transport of both gaseous and ash emissions from a volcanic eruption in both a forecast and hindcast setting; this version of the model is called the emergency EMEP (eEMEP) model.

The volcanic emission and transport of SO_2 can cause considerable air quality problems both close to a volcano and farther away. The preparation of the model for gaseous volcanic emissions is relatively simpler and we have documented the Holuhraun fissure eruption previously using the eEMEP model (Steensen et al., 2016). Volcanic eruptions that emit tephra into the atmosphere needs more consideration in the model compared to the standard setup of the model. Tephra are classified according to the particle diameter as blocks (< 64 mm) and lapilli (64 mm > d > 2 mm) that fall out quick and close to the volcano, the finer particles like coarse ash (2 mm > d > 64 µm) and especially fine ash (d < 64 µm) can stay in the atmosphere for days and be transported over large distances before settling to the ground. Exposed to fine ash, air traffic can experience both jet engine malfunction and damages to windshields (Casadevall, 1994). It is therefore of interest to study these smaller ash particles. The long-time closure of commercial air traffic during the 2010 Eyjafjallajökull volcanic eruption caused the European civil aviation authorities (CAAs) to step back from the previous zero-tolerance policy for air traffic in zones with observed or predicted ash and specific zones determined by ash concentrations with individual flight restrictions were introduced (UK Civil Aviation Authority, 2016). Currently there are three levels, low (< 2 mg m^{-3}) and medium (2 – 4 mg m^{-3}) ash concentration zones have lower restrictions and areas with high concentrations over 4 mg m^{-3} are usually avoided. This change in policy requires higher accuracy in ash dispersion modelling, which is part of the motivation for the development of the eEMEP model.

There are different approaches for volcanic ash transport and dispersion models (VATDMs). Eulerian models such as the eEMEP model are computationally more demanding compared to Lagrangian models, which most Volcanic Ash Advisory Centres (VAAC) use, e.g. NAME (Jones et al., 2007) at the London VAAC, or HYSPLIT (Draxler and Hess, 1997) at the Washington and Anchorage VAAC. Other well known Lagrangian models used for ash dispersion are FLEXPART (Stohl et al., 2005) and PUFF (Searcy et al., 1998), the latter is also used as backup by the Washington and Anchorage VAAC. Some Eulerian models used for ash dispersion are MOCAGE (Josse et al., 2004) used at VAAC Toulouse, Fall3d (Folch et al.,

Geosci. Model Dev. Discuss., doi:10.5194/gmd-2016-315, 2017
Manuscript under review for journal Geosci. Model Dev.
Published: 10 January 2017

2009) and Ash3d (Schwaiger et al., 2012). The Eulerian models calculate the advection of ash at every grid point, and emissions are instantaneously mixed within the grid box. In particular peak concentrations are dependent on the grid resolution. Lagrangian models release tracers and calculate their trajectories, the mass loadings and concentrations are calculated from the number density of multiple releases of these tracers. This can lead to an uncertainty in regions with low particle concentrations, but the output resolution for Lagrangian models is independent of the resolution of the input data and can therefore be indefinitely high.

For all models, in addition to uncertainties caused by numerical diffusion and advection, uncertainties in the ash dispersion forecasting can also be due to imperfections of the meteorological driver. Initial conditions can only be set with a certain degree of accuracy when starting a numerical weather prediction model. The initial errors may amplify during the forecast and can result in forecast inaccuracies. In addition to these initial condition errors, there are uncertainties due to how the dynamics and physics are represented in the numerical weather prediction model (NWP). Ensemble forecasting was established in weather forecasting to estimate associated uncertainties by producing probability forecasts on the state of the atmosphere on the basis of multiple similar forecast runs with perturbed initial conditions or different model parameterizations (Palmer 2000, Iversen et al., 2011). Since 1992 ensemble forecast have been operational at both the National Meteorological Centre (NMC) (Toth and Kalany, 1993) and the European Centre for Medium-Range Weather Forecasts (ECMWF) (Palmer, 1993). Ensemble modelling has undergone large developments in recent years. In this study the eEMEP model will be run on state-of-the-art ensemble meteorology data on three different resolutions to see the different spread in dispersion.

The aim of this paper is to present the new developments and applications of the eEMEP model for describing the dispersion of volcanic emissions in the atmosphere. Both volcanic eruption examples with SO_2 emissions and ash are presented. At the start of an eruption SO_2 can act as proxy for ash (Thomas and Prata et al., 2011; Sears et al., 2013), and proven capability of modelling both ash and SO_2 can give increased confidence for dispersion of future eruptions. Section two describes the additions made to the model to improve the capability to simulate volcanic eruptions and bigger ash particles. There are several sources of uncertainties connected to the transport of volcanic emissions in a dispersion model. CPU efficiency of forecasts, uncertainties connected to the meteorological driver and numerical diffusion effects caused by changing horizontal resolution are studied by running the model with ensemble members for the first days of the Barðarbunga eruption in September 2014 in section 3. The practicality of ensemble forecasts is also evaluated. A short ash model validation is presented in section 4 with comparison to lidar observations. Uncertainties for the description of gravitational settling are studied by comparing two model simulations with and without this effect included. Summary and conclusions are given in section 5.

Geosci. Model Dev. Discuss., doi:10.5194/gmd-2016-315, 2017
Manuscript under review for journal Geosci. Model Dev.
Published: 10 January 2017

2 Model description

The standard EMEP MSC-W model is described in Simpson et al. (2012) and updates are in addition presented in the yearly EMEP reports as well as the updated model code (EMEP Status Report, 2016). The most important aspects of the standard model for volcanic emission dispersion is shortly described while new added components for the eEMEP are presented in more detail, as well as how the model handles the source term and the operational setup.

2.1 Standard EMEP MSC-W model

Volcanic emissions are transported from the source by winds and lost due to several processes in the atmosphere. The advection scheme has a numerical solution based on the Bott's scheme (1989a,b), with the fourth order scheme in the horizontal directions and a second order version applied on the variable grid distances over the vertical resolutions. Time steps used in the advection scheme are dependent on grid resolution. Winds and other meteorological parameters needed are given as input and the EMEP MSC-W model is adapted to run with output from several numerical weather prediction models. Horizontal resolution follows the meteorological driver, and model simulations with resolutions from very fine (few km) to low resolutions of 1x1 degree are possible. Temporal resolution of the meteorology input fields is typically 3-hourly. The model may calculate some field if they are not included in the data (e.g. 3-D precipitation or vertical velocity). The chemical species, reactions as well as emissions included in the model have been developed over the history of the model, and the number of tracers is variable so the user can choose what to include. Deposition due to wet scavenging depends on precipitation fields given as input and specific removal efficiencies for the different gases and particle classes. Both in-cloud and sub-cloud removal are taken into account.

2.2 The eEMEP model

To improve the EMEP MSC-W model capabilities to model volcanic eruptions, the model was further developed in several components such that an efficient and flexible model framework was finally available for operations at the Norwegian Meteorological Institute. This emergency model is simplified in parts with respect to the original EMEP MSC-W model to be computational more efficient.

Meteorological driver

On a day to day basis the eEMEP model use ECMWF forecast meteorology, pre-processed for the CAMS 50 chemical weather forecasting at a resolution of 0.25 x 0.125 degrees latitude longitude. More details have already been provided in Steensen et al. (2016). For this study the eEMEP model has also been setup to run on ensemble weather forecast data as demonstrated in section 3. Ensemble forecast require considerable computational time. Explosive volcanic eruptions may in some cases inject ash and gases at heights well above the tropopause. This required that the eEMEP model, depending on actual eruption conditions, provides the possibility of introducing additional vertical levels to achieve increased vertical resolution as well as a higher model top. The standard EMEP MSC-W model has 20 vertical levels reaching up to 100 hPa,

Geosci. Model Dev. Discuss., doi:10.5194/gmd-2016-315, 2017
Manuscript under review for journal Geosci. Model Dev.
Published: 10 January 2017

Geoscientific Model Development Discussions

at around 16 km. For specific volcanic eruptions, where the ejection force places the emissions higher in the atmosphere, a more flexible version was developed with hybrid eta levels, where meteorological data from additional vertical levels, that are available in the eg. ECMWF driver model, can be used. Model simulations presented in this paper are done with 40 and 42 vertical levels. Vertical levels close to the surface where not altered because this would have changed the well characterized surface exchange processes in the EMEP model.

Volcanic source

A specific volcano source module reads in volcanic emission parameters from a file containing ash flux (kg s^{-1}), height interval in which emissions are injected along with a time line of release intensity. When only an emission top height is given the emissions are distributed uniformly down to the height of the top of the volcano. If more detailed information is provided the emissions are spread uniformly over the model vertical levels that are closest and within the height interval given in the input file. More sophisticated plume descriptions such as output from plume models that use atmospheric conditions like PLUMEIRA (Mastin, 2007) or emission profiles calculated through inversion techniques (Stohl et al., 2011) can therefore be used as input to the volcano source module. Fine-ash particle sizes and the distribution over the size bins can also be changed to what is provided by the source term. If the source term denotes all the tephra released from the volcanic eruptions, the largest sizes of tephra that quickly settles to the ground are excluded by using a fine-ash fraction either as given in Mastin et al. (2009) for the specific volcano or as provided based on more up-to-date case specific information.

Gas chemistry

To perform quick simulations of the spread of volcanic emissions, sophisticated chemistry and trace species emissions are computationally too demanding and the eEMEP model has been configured such that they are excluded. For volcanic eruptions with SO_2 emission the sulphate production is added. More detail can be found in Steensen et al. (2016).

Ash properties and removal processes

Apart form the wind advection of volcanic ash and wet scavenging as described in the standard EMEP MSC-W, an important process for the simulation of volcanic ash is the gravitational settling. In the standard EMEP MSC-W, sedimentation and dry depositions of the different pollutants are only calculated in the lowest model layer. Fine ash is large enough to have an effect from gravitational sedimentation and is emitted higher in the atmosphere compared to other coarse aerosol like sea salt and desert dust. A module that calculates gravitational settling in all vertical levels for ash particles is implemented. The assumed terminal fall speed v_s for the ash particles are set as

$$v_s = \sqrt{\frac{4g(\rho_p - \rho_a)d}{3C_d\rho_a}}, \quad (1)$$

where g is the gravitational constant, ρ_a and ρ_p are the densities for air and ash particle respectively. Default density for ash are assumed 2500 kg m^{-3}, however the density can range from 700 kg m^{-3} for the most porous part of tephra to 3300 kg m^{-3}

Geosci. Model Dev. Discuss., doi:10.5194/gmd-2016-315, 2017
Manuscript under review for journal Geosci. Model Dev.
Published: 10 January 2017

Geoscientific Model Development Discussions

for crystals (Wilson et al. 2011). d is the particle diameter and C_d is the drag coefficient. Wilson and Huang (1979) present a drag coefficient as a function of the particle shape found from fall velocity measurements of ash particles.

$$C_d = \frac{24}{R_e} F^{-0.828} + 2\sqrt{1.07 - F} \text{ , where } R_e = \frac{v_s \rho_a d}{\eta_a}, \quad (2)$$

R_e is the Reynolds number and η_a is the dynamic viscosity of air. $F = (a + b)/2c$ is a shape factor and $a < b < c$ are the three principal diameters of the particle. Although ash particles can vary in shapes the default value of F assumes that the ash particle is close to spherical at 0.8. The smallest fine ash particles can in some circumstances be of similar size as the mean free path length of an air molecule (λ_a), if this occurs the particle are in a slip-flow regime and non-continuum effects has to be taken into account. The vertical fall velocity is therefore modified with the Cunningham slip-factor and the Knutsen-Weber term (Jacobson, 1999, eq. 16.25). Fine ash is shown to fall faster than the Stokes Law calculates (Rose and Durant, 2009), therefore the more spherical shape (F=0.8) is set as default since slip flow corrections increase the fall speed for fine ash for more spherical fine ash particles (Schwaiger et al., 2012).

Operational set-up

The eEMEP model runs operationally every day at the Norwegian Meteorological Institute, for dispersion scenarios of volcanic emissions as defined in Mastin et al. (2009) for four selected volcanoes in the region of interest. If an increased risk for an eruption is given for any volcano, one or several of the default volcanoes are replaced with the volcano at risk of eruption. Meteorological input data are available every day before 08 30 UTC and 20 30 UTC and forecasts starting from 00 UTC and 12 UTC are run from these respectively. A standard eEMEP model simulation takes less than half an hour making forecasts from 00 UTC and 12 UTC available before 9 UTC and 21 UTC.

In case of a real volcanic eruption, several simulations are used and started as shown in Figure 1. The purpose of the every-day initial forecast with a default volcanic source is to provide a conservative first estimate of the dispersion. However, because of the high uncertainty in source intensity and vertical profile as well as ash size distribution the resulting concentrations are very uncertain. Thus, as soon as possible, source receptor model simulations, with a unit emission (1 kg s^{-1}) released every third hour over multiple emission heights, are started that are used as input data for a source inversion calculation (Stohl et al. 2011), shown in Figure 1 as thick arrows. The goal of applying the inversion algorithm is to create a source term that causes the model simulation to be more similar to observations. A very early timing of these model simulations is not as crucial since the inversion algorithm is dependent on good satellite observations to constrain the solution, meaning that enough satellite observations at some distance from the volcano are required. The source receptor simulations run for a 24 hour forecast to not include further uncertainties longer into the forecasts, and are restarted the next day for another 24 hour cycle. Model simulation with the inversion-derived emission estimate (dashed lines) are expected to be ready before a new forecast meteorology input dataset is available, since the inversion calculation is not computational demanding. More details on using the inversion method in a forecast setting are given in Steensen et al. (submitted to ACP, 2016). The length of the source receptor model simulations are set here as an example of three days as the inversion study

Geosci. Model Dev. Discuss., doi:10.5194/gmd-2016-315, 2017
Manuscript under review for journal Geosci. Model Dev.
Published: 10 January 2017

found that additional satellite observations are seen to have little effect on the emission term after 48 hours. The ash may however stay in the domain for a longer time so the model simulations with the optimized emission term have to be started from an earlier time.

3 Meteorological predictability of volcanic plumes, example SO_2 from Barðarbunga

The EMEP MSC-W model results have been compared to model results from other dispersion models and observations in several studies. In particular Steensen et al. (2016) compares model simulations for the Barðarbunga eruption to satellite and ground observations of SO_2 and SO_X wet deposition. A simplified emissions term is used where SO_2 is released with a constant rate, uniformly distributed over three emissions heights, to see which height produces a simulation that matches better with observations. With some discrepancies caused by the description of the planetary boundary layer also found in Schmidt et al. (2015) with the Lagrangian NAME model and in Boichu et al. (2016) with the Eulerian CHIMERE model, the EMEP MSC-W model matches well the observed surface SO_2 timing and concentration levels. Compared to SO_2 column satellite observations from the Ozone Monitoring Instrument (OMI) similar mass loadings and dispersions patterns are found. However, it remains a question how much the uncertainty in the meteorological fields determines the quality of the volcanic plume predictability.

Ensemble forecasts consist of several almost identical simulations to quantify the uncertainty of a forecast. Large spread between the ensemble members caused by a large difference between possible future scenarios indicates a high uncertainty in the forecast. Combining the eEMEP model with ensemble forecasts would create an opportunity for quantifying the uncertainty in the eEMEP ash/SO_2 forecasting related to the uncertainty in the meteorology. However, running the eEMEP model on several (tens of) ensemble forecast members (on a relatively high resolution) is computationally a very expensive task. At the same time, the volcanic emission forecasting system is required to deliver results very fast and several times a day. One might think at first, that this leaves us with the choice between a low resolution ensemble forecast and a high resolution deterministic forecast for the operational volcanic emission forecasting system.

Here we investigate how the different resolutions of the ensemble forecasts affect the spread of the volcanic plume for SO_2 for three days in the beginning of the Barðarbunga eruption, including the probability of the resulting SO_2 concentrations in the different members to be over different thresholds. Although this part focuses on volcanic emissions of SO_2, similar results may be expected for spread of the fine-grained long-range transported volcanic ash.

3.1 Model setup

The eEMEP model is run on meteorological ensemble forecast data from the Grand Limited Area Ensemble Prediction Systems (GLAMEPS) for the Barðarbunga eruption case. The starting dates, 3 to 5 September 2014 - from which respective 48 hour forecast are launched - , correspond to the first phase of the Barðarbunga volcanic eruption.

Geosci. Model Dev. Discuss., doi:10.5194/gmd-2016-315, 2017
Manuscript under review for journal Geosci. Model Dev.
Published: 10 January 2017

Geoscientific Model Development Discussions

Significant amounts of SO_2 were ejected into the atmosphere during the Barðarbunga eruption, but little ash. Schmidt et al. (2015) studied the emission term during September by comparing model simulations to satellite data, and found that a SO_2 emission estimate with a 120 kt d^{-1} flux over an eruption column between 1500 m to 3000 m matched best for the first days of September. This emission term is also supported by Thordarson and Hartley (2015) and used here.

GLAMEPS meteorological data

GLAMEPS aims to account for all the major sources of weather forecast inaccuracy by looking at both the differences due to model parameter uncertainty and initial state perturbations (Iversen et al., 2011). GLAMEPS ensemble forecast is produced at ECMWF, and in 2014 the ensemble consisted of 50 members from both the HIRLAM (High Resolution Limited Area Model) and ALADIN (Aire Limitée Adaptation Dynamique Développement International) model. To include the uncertainty in the forecast, members are perturbed both in the initial field and on the model domain border. The perturbations are from the EuroTEPS (European Targeted Ensemble Prediction system), a version of the global ECMWF EPS, with higher resolution on a smaller European domain (Frogner and Iversen, 2010).

This study will only use the 24 HIRLAM (High Resolution Limited Area Model) perturbation members of the ensemble, (not the control member). The 24 HIRLAM members are split between two different cloud physics parameterisations. HirEPS_S members use the STRACO scheme (Sass et al., 1999; Undén et al., 2002) for stratiform, convective cloud, and precipitation, HirEPS_K members uses the Kain-Fritsch schemes for deep cumulus (Kain and Frisch, 1990; Kain, 2004; Calvo, 2007) and Rasch and Kristjansson (1998) for stratiform clouds and precipitation (Ivarsson, 2007). To also include the uncertainty in the forecast caused by the start time of the forecast, members are divided in two groups with two different forecast start times. Six members of the HirEPS_S and six of the HirEPS_K start the forecast at 00 UTC and 12 UTC, and the remaining 12 of the ensemble members start the forecast at 06 UTC and 18 UTC. Each member has a forecast time of 72 hours. The original resolution is 10x10 km. Such a fine resolution is computationally very demanding.

The GLAMEPS data have been downloaded from ECMWF for the period from 3 to 5 September 2014, corresponding to the first phase of the Barðarbunga volcanic eruption. Each member is used as input data for the eEMEP model to run 48 hour forecasts starting from 00 UTC from each of the three days by using the 18 UTC and 00 UTC meteorological forecasts. That means that for half of the members, the forecast is six hours old (the forecasted started 18 UTC). The relatively short forecast of 48 hours is chosen due to the large uncertainties related to the emission term when running a forecast of volcanic emission (VAAC London only issues a maximum 24 hour forecast). Furthermore, running the full 72 hour forecast is not feasible due to the different start times of the forecasts (18 UTC and 00 UTC). In contrast to what is possibly done for a real case, all the forecasts are started from an SO_2 free state and not restarted from the previous forecast simulation. This is done to investigate only the difference in spread due to the different weather situation over the three days studied, and not take into account possible differences in the initial SO_2 field.

Three different horizontal resolutions are generated as input, the original high resolution of 10x10 km, a medium resolution of 20x20 km and a low resolution of 40x40 km, referenced hereafter as high_res, mid_res and low_res. High resolution NWP is desired as more processes in the atmosphere can be resolved. A simple reduction in resolution of the meteorological

Geosci. Model Dev. Discuss., doi:10.5194/gmd-2016-315, 2017
Manuscript under review for journal Geosci. Model Dev.
Published: 10 January 2017

input data is obtained here by letting every other and every fourth original grid value represent a twice and four times bigger grid point respectively. Alternatively, one could have aggregated 10x10 km grid cells into 20x20 km and 40xkm grid cells. This would lead to a smoother field, but the largest values/variations would have been lost. The GLAMEPS domain covers an area from 16 to 81 degrees north and 67 degrees west to 83 degrees east which means that Europe and the North Atlantic are well covered including some parts of Sahara and Newfoundland. There are 40 vertical levels for all the three horizontal resolutions. Table 1 lists all simulations in this paper.

3.2 Results

The spread in the ensemble forecast of SO_2 is presented here by calculating the possibility of an ensemble member to be over certain threshold values. Figure 2 and 3 show the frequency of ensemble members over a low 5 DU (Dobson Unit) threshold and a high 50 DU threshold after 48 hours forecast, respectively. A high and low threshold is chosen as increased dilution will lead to a larger area with lower concentrations and a smaller area with higher concentrations. For the first forecast starting 3 September 00 UTC, the SO_2 emitted from the volcano is caught in a low pressure system and transported over Northern Scandinavia and Russia. In the forecast simulations starting 24 and 48 hours later, the transport of volcanic emissions is southward over Great Britain by a high pressure system placed more southerly compared to the first system.
Compared to the two higher resolution forecasts, the low_res forecasts have a large area where 20 or more members agree and have column loads over the 5 DU threshold after 48 hours of dispersion. The mid_res and high_res simulations show however a larger spread between the members with a bigger area with only one or a few members above the low threshold. This larger spread among the higher resolution forecast is also shown in the Figure 3. The high_res forecast have members that exceed the 50 DU threshold far away from the source, as seen over the coast of Northern Russia in the first forecast (0309 00 UTC + 48 hours) and also further down in the high pressure system appearing during the two later forecasts. Due to increased numerical diffusion in the low_res forecasts, the area where the members are over the higher threshold is much smaller and mostly confined to an area close to the source.
The difference in the spread is also seen to be weather dependent especially when using a low threshold. For the first forecast the volcanic SO_2 is transported over longer distances and the small low pressure system is positioned differently in the ensemble members. The two forecasts started later experience weaker northerly winds and smaller plume position differences appear in between the members.
To further investigate the differences in the three resolutions, Table 2 shows the area summed up at time step +48 hours for all the three forecasts where simulated SO_2 column loads exceed the given threshold values. There is a 34% larger area with column burdens above 0.25 DU in the low resolution forecasts compared to the high resolution forecasts, due to the increased diffusion. At 10 DU, the difference in area between the three resolutions is minimal, while for the thresholds above the 10 DU the high resolution forecast exhibits a larger area.
Figure 4 shows the frequency above 10 DU of low and high resolution averaged over the hours from 8 to 16 UTC on 5 September, for the forecast starting 4 September 00 UTC. The model results are compared to OMI (Ozone Monitoring

Geosci. Model Dev. Discuss., doi:10.5194/gmd-2016-315, 2017
Manuscript under review for journal Geosci. Model Dev.
Published: 10 January 2017

Instrument) satellite observations from overpasses during the same time. Retrievals are described in Theys et al. (2015) and have an assumed plume height of 7 km, which is higher than the actual plume height and as a consequence the retrievals have too low values. Even though the column burdens from OMI and the model results are not easily comparable (see discussion in Steensen et al., 2016), the patterns should be similar. The satellite has high concentrations going south from Iceland in a thin filament. Even though the total amount of area, where ensemble members show SO_2 column loads above the 10 DU threshold, is found equal for the three resolutions, the high_res ensemble forecasts have members exhibiting further south loads over the threshold. An area in the southwest is not captured by either of the forecasts. Since forecast starts with no SO_2 emitted before 00 UTC 4 September, we believe this area is affected by older emissions and thus not apparent in our model calculations.

The higher resolution ensemble members show higher concentrations further away from the volcanic eruption site in more narrow plumes that resemble the observed plumes more. However, the location of the plumes varies more between the high resolution ensemble members, e.g. a larger spread between the ensemble members indicates a higher uncertainty. Although a lower uncertainty in a forecast is appreciated as it indicates that the weather situation is stable, less spread in low resolution also indicates that information in the meteorology is lost when reducing the resolution. This suggests that running ensemble forecasts with low resolution for transport of volcanic emissions is less meaningful as it would not show the actual uncertainty in the forecast.

Even though a high resolution is desirable, the computational efficiency is important in an emergency forecast environment. For this study, the highest resolution runs use over 13 times more computational time than the lowest resolution runs, while the mid_res simulations use only five times more. To run a total ensemble forecast with high resolution for volcanic eruptions may therefore not be feasible. From a pragmatic point of view, ensemble forecasts for volcanic emissions are most valuable in situations where the weather forecast is uncertain. Thus an alternative would be to launch ensemble forecasts only in unstable weather situations (as predicted by the ensemble weather prediction models). This study indicates that less information is lost between the high_res and mid_res than going from the mid_res to the low_res resolution, suggesting that resolutions around 20x20 km could be a reasonable choice for ensemble (and deterministic) forecasts when needed.

4 Ash model testing and validation

4.1 Model setup

The eEMEP model with improved ash modelling capabilities as described above is tested here for the Eyjafjallajökull eruption in 2010. For this purpose the model is run with the emission term from Stohl et al. (2011), an emission term constrained by satellite observations through an inversion routine. The ash is distributed over nine size bins from 4 µm to 25 µm and the density is set by default to 2500 kg m^{-3}. Our eEMEP model uses here meteorological data from ECMWF, namely the IFS (Integrated Forecasting System) model with a 0.25 x 0.25 degree latitude longitude resolution, selecting 42 of the

Geosci. Model Dev. Discuss., doi:10.5194/gmd-2016-315, 2017
Manuscript under review for journal Geosci. Model Dev.
Published: 10 January 2017

lower levels from the original IFS 60 vertical levels, setting the eEMEP model top to around 30 km. The simulations are performed for the main volcanic ash eruption episode from 13 April.-25 May 2010.

4.2 Comparison with other ash models

Part of the validation has been done in the scope of the Norwegian ash project and shall not be repeated here in all detail. We compared initially ash dispersion from this eruption calculated with eEMEP and FLEXPART model results as well as the Norwegian Meteorological Institute version of the NAME model SNAP (Saltbones et al., 1994), and found very similar ash plumes in all three models (Norwegian ash project, 2014). Figure 5 shows results where all three model results are compared to satellite ash retrievals from SEVIRI (Spinning Enhanced Visible and Infrared Imager) and IASI (Infrared Atmospheric Sounding Interferometer) available from vast.nilu.no. The FLEXPART model is used in several studies and validated towards observations for several volcanic eruptions with ash emission (Stohl et al. 2011; Kristiansen et al. 2012; Moxnes et al 2014). All models use the same wind fields from ECMWF, and the conclusion for this eruption case was that neither the Eulerian nor the Lagrangian models showed particular better performance. The structure and intensity of the plumes was rather similar, reproducing the observations fairly well when it comes to the ash fields.

4.3. Validation with lidar observations

Apart from the horizontal dispersion, the vertical placement of the transported ash may have important consequences for impact assessments, both for air quality and air traffic perturbations. Meteorological processes such as subsidence and frontal lifting may alter the initial vertical distribution of ash. In addition ash removal and settling may alter the vertical distribution. Although several observational sets are available for the Eyjafjallajökull eruption, to test here the treatment of gravitational settling for ash particles in the eEMEP model, model results with and without gravitational settling of ash included are compared to lidar observations of the ash layer.

Lidar observations provide a vertical location of aerosol. The European Aerosol Research Lidar Network (EARLINET) consisted at the time of the Eyjafjallajökull eruption of 27 aerosol stations over Europe. On 15 April, an alert was given to start continuous measurements providing, if weather conditions permitted, an hourly vertical coverage of the ash cloud over Europe (Pappalardo et al. 2013), documented as a consolidated dataset which we use here. Ash is detected as significant aerosol backscatter signal, linked to the Iceland eruption through backward trajectory analysis. Only backscatter profiles with a relative statistical error from signal detection less than 50 % are used to retain a reliable aerosol mask. The vertical resolution in the dataset ranges between 60 and 180 m for the different stations. The dataset includes the identified top and bottom of the ash layer, as well as the centre of mass, the altitude where most of the aerosol load is located. Identified ash layers where other aerosol sources are also found from e.g. continental aerosol are classified as mixed layers. These mixed layers are also given with the maximum and minimum observed height and centre of mass. Observed planetary boundary layer (PBL) height is also included in the database. The six lidar stations used here are situated in Central Europe (see Figure 6), covering coastal stations, inland and mountain regions. Weather conditions at the lidar stations, and sometimes technical

Geosci. Model Dev. Discuss., doi:10.5194/gmd-2016-315, 2017
Manuscript under review for journal Geosci. Model Dev.
Published: 10 January 2017

issues, made it difficult to continuously produce observations. For example, frequent low clouds over Cabauw prevented most lidar retrievals there. Observations at Neuchatel are also limited to the first episode in April. Altogether, the ash layer was observed over a long period over central Europe during the Eyjfjallajökull eruption and as the ash has been transported over a long distance the effect of gravitational settling may be visible, making this dataset the best available at the time for our purpose.

Figure 7 shows the model concentrations for the simulation with gravitational settling over the entire Eyjafjallajökull period along with observed height of the ash layer and height of the mixed aerosol layer at the EARLINET stations. Although the mixed layers may be weighted with the other aerosol they are plotted here also. Figure 8 concentrates on the centre of mass comparison (without the mixed layers).

Ash was first detected at the Hamburg station during the morning of 16 April, 48 hours after the start of the eruption. Ash was also observed early at the other stations, and while the timing of the observations match well at Hamburg and Leipzig, at Neuchatel ash is observed before the model has transported ash to this station. At Cabauw, the first part of the ash plume is not detected by the lidar, while the second part shows similar simulated and observed level of maximum concentrations. A descent in the ash plume is observed at several of the stations, at Hamburg between 05 UTC to 17 UTC 16 April and at Palaiseau, Munich and Neuchatel stations from 16 UTC 16 April to 00 UTC 17 April (Pappalardo et al. 2013). This decent is due to the high pressure system that transported the ash over Central Europe. The model shows this shift in model height from the higher first part of the plume to the lower second part of the plume for all the stations. At Leipzig, Hamburg, Palaiseau and Munich much of the simulated ash is even below the observed PBL in the night of 17/18 April. As the ash layer in EARLINET is calculated above the observed PBL, observed centre of mass is at higher altitudes than the model ash. The ash cloud persisted over Central Europe until 26 April, model and observed ash layer are mostly at similar heights for this later April period. There are some discrepancies: for Cabauw the observations vary in height over short time periods indicating uncertainties for these measurements, and in Munich, the maximum heights of the observed ash layer are at higher altitudes than the model maximum ash height, while the observed centres of mass are close to the observed lowest layer of ash, indicating that most of the ash mass indeed is lower in the atmosphere and more comparable to model heights. In Leipzig a few observations of centre of mass on 16 and 18 April are much higher than the model centre of mass heights and the corresponding heights at the other stations at this time, signifying that there may be uncertainty in these observations.

From May 2 the model results show small ash concentrations at the lidar stations, due to small ash emissions after 29 April. On May 5-6 ash is observed lower down in the atmosphere compared to simulated ash at Hamburg, however a layer where ash is mixed with other aerosol is detected at higher altitudes more similar to where the model has ash. More ash was then emitted on 5 May (Stohl et al 2011), but southerly winds transported the ash over Spain and the Atlantic Ocean. Not until the night 16/17 May are weather conditions favourable again for transport of ash to central Europe. No measurements are available for this time at Neuchatel. The other stations have observations of the ash layer at similar altitudes as the model.

To show more broadly the impact of the gravitational settling processes on the vertical profile of ash, Figure 8 shows all calculated centres of mass for ash in the model simulation with and without gravitational settling. The rather small

Geosci. Model Dev. Discuss., doi:10.5194/gmd-2016-315, 2017
Manuscript under review for journal Geosci. Model Dev.
Published: 10 January 2017

displacement between the two model simulations implies that not gravitation but rather weather and emission height are the main driver for the ash layer height. This is especially visible in the simultaneous rapid decrease in centre of mass height for the first plume (17-18 April) in both simulations. On some occasions there are larger differences between the two model simulations, specifically in the beginning of May during a period with smaller concentrations. Unstable north-westerly winds at this time can cause the small differences in height distribution of ash to grow over time due to different wind directions in the column.

In order to compare to the observed values more properly, a centre of mass above the observed PBL is calculated for the two model simulations (only for the cases when an observed height is available), see Figure 8. Model centre of mass are generally lower than observed altitudes for both model simulations, indicating that the model simulations have too much descent of the ash layer eg. around 18 April, independent of inclusion or not of gravitational settling. Figure 9 show scatterplots where the observed ash centre of mass height (not including the mixed layers) is plotted against model with and without gravitational settling at the stations. As discussed above some measured and modelled values are unrealistic high, therefore only values below 8 km are taken into account for correlation calculations. The scatterplot confirms that observed heights are generally higher than model calculations. At Palaiseau and Hamburg, model height descends faster than observed on 20 April causing the low correlation at these stations. Neuchatel generally exhibits higher observed centre of mass, explaining possibly a slightly higher correlation for the model simulation with no gravitational settling. Except for Neuchatel and Hamburg however, the model simulation with gravitational settling exhibits a slightly higher correlation to lidar retrieved height data compared to the model simulation without gravitation.

5 Summary and conclusions

A new model version of the standard EMEP MSC-W model has been developed, aimed at modelling dispersion of volcanic emission, called the eEMEP model. Changes with respect to the standard model are: a simplified gas chemistry; a modification of the aerosol part to handle ash particles in different size classes; the description of gravitational settling of ash particles; a volcanic source module which has a default source term and can be altered to include improved source estimates; an increase in vertical levels to increase the model top and vertical resolution; the possibility to run as an ensemble model based on ensemble meteorological forecasts; a formal procedure for an operational use of the model in an emergency case and an inversion algorithm coupled to the model, using satellite data to retrieve an improved source estimate (see Steensen et al. 2016, submitted to ACPD). With this model version we document here selected important aspects of the volcanic gas and ash dispersion simulation.

We have first studied the impact of ensemble meteorological input fields of different resolution on the dispersion of volcanic emissions from Iceland. Compared to Lagrangian VATDMs, Eulerian models such as the eEMEP model have inherent numerical diffusion dependent on the grid size. eEMEP model simulations thus have to have a sufficiently high resolution, especially when peak concentrations shall be predicted, for example for the purpose of establishing flight restriction zones.

Geosci. Model Dev. Discuss., doi:10.5194/gmd-2016-315, 2017
Manuscript under review for journal Geosci. Model Dev.
Published: 10 January 2017

High resolution simulations are however computationally demanding while obtaining results quickly is critical in situations with volcanic eruptions. How to best use CPU resources for transport of volcanic emission is studied here by looking at the change in spread between ensemble model simulations on three different resolutions. The eEMEP model is run for a 48 hour forecast from three start dates for the Barðarbunga eruption period with meteorological fields from 24 HIRLAM ensemble members originally produced for the GLAMEPS forecast. The original 10x10 km resolution is degraded to lower resolutions of 20x20 km and 40x40 km.

The increased numerical diffusion causes a larger area (+34%) to be covered by the volcanic tracer in the low resolution simulations than in the high resolution ones. For the higher resolution forecast simulations, the members show more spread between them and there are members with higher concentrations further away from the source. Therefore there is also a greater possibility for a member to exceed a high threshold concentration. For all three simulations, the spread between members is seen to be weather dependent and a measure for how uncertain the forecast is. The increased agreement between low resolution ensembles due to increased numerical diffusion limits the importance of the ensemble forecast. Ensemble forecasts have to be done with sufficient high resolution to show the real uncertainty of the weather situation. Compared to satellite observations, the high resolution model simulations also match better the transport of a narrow volcanic SO_2 cloud. High resolution ensemble forecast may nevertheless not be possible due to the computational cost. The study shows that there is a bigger change in transport when going from 40x40 km to 20x20 km resolution compared to 20x20km to 10x10km, indicating that the increased cost to run a high resolution simulation at 10x10km may not give the same increase in quality of the result. The study also shows that low resolution simulations are sufficient for quick results to predict the most likely transport of volcanic emission, while high resolution model simulations are needed to estimate possible occurrence of high peak concentrations.

The vertical dispersion of ash transport was studied. Gravitational settling for ash tracers is added in the model over the entire vertical column. This addition is evaluated by comparing a model simulation with and without gravitational settling to observations during the 2010 Eyjafjallajökull eruption. EARLINET ground stations measured the vertical location of the volcanic ash layer over the eruption providing hourly observations of the height and centre of mass for the ash layer when the weather allowed it. Centre of mass calculated for the two model simulations show that gravitational settling displaces the centre of mass closer to the ground by up to 1km. Besides emission height the weather situation is found to be a more important factor than gravitation for the height of the ash layer as most of the vertical displacement is caused by subsidence in high pressure systems and is similar in both model simulations. An example is a rapid descent in ash plume height on 16 April caused by an anti-cyclone seen in both observation and model. However the descent in the model is quicker and puts the ash closer to ground compared to observations, especially at Hamburg and Leipzig lidar stations. A second descent in the ash layer at the stations is seen 20 April, and this subsidence occurs later in the observational data at Hamburg and Palaiseau compared to the model data. The model has a centre of ash mass height on average below the observed one, independent on gravitational settling. Calculated correlation between observed centres of mass height and corresponding model heights are higher in the model simulation with gravitational settling for four of the six stations studied here, suggesting improved

Geosci. Model Dev. Discuss., doi:10.5194/gmd-2016-315, 2017
Manuscript under review for journal Geosci. Model Dev.
Published: 10 January 2017

quality of model when including the gravitation process. The addition of gravitational settling is found to have a relatively small influence on the vertical placement of the ash layer and thus is responsible only for a small improvement in model results.

Even with the included gravitational settling in the EMEP model, the assumed density, shape and size distribution of the ash particles bring along large uncertainties during a forecast situation. Ash properties show large differences in between volcanic eruptions (Vogel et al. submitted to JGR 2016). The Eyjafjallajökull model results presented here are initiated with a time and height resolved emission estimate calculated by inversion with FLEXPART model results, constrained with satellite observations (Stohl et al. 2011), to be used with the eEMEP model for a new volcanic eruption in an operational setup. Uncertainties in satellite retrievals due to meteorological clouds that obscure ash clouds and a 0.2 g m^{-2} ash cloud detection limit (Prata and Prata, 2012) need to be explored further. Low concentrations in satellite and model data are in particular uncertain, as shown during the intermediate period (end of April and beginning of May) where only small emissions were released and then observed at the lidar stations as almost insignificant ash clouds. Another factor of uncertainty is the variability in ash particle sizes, which changed between the first eruption period in April and the second in May (Dellino et al. 2012). Both model and satellite retrievals used as input to the inversion, operate today with assumed equal ash characteristics during the whole eruption period. Other processes, such as fine ash aggregation that increases the gravitational settling speed and reduces the atmospheric residence time (Brown et al. 2011), were also observed during the Eyjafjallajökull eruption (Taddeucci et al., 2011), but are not included in the model at this time.

Although a correct model description of bulk volcanic emissions is useful, other factors such as model resolution, details of the source term and the model set-up are seen as important for safety assessments. The developed model is capable to guide near real time emergency assessments of the spread of high volcanic gas and aerosol concentrations.

6 Code availability

The model code to the standard EMEP MSC-W model is available on gitbub: https://github.com/metno/emep-ctm. The eEMEP model with reduced chemistry and gravitational settling for ash is available from here: https://github.com/metno/emep-ctm/releases/tag/rv4_10_eEMEP_ASH

Acknowledgement

The authors would like to thank Fred Prata and Lieven Clarisse for SEVIRI and IASI satellite data for the model comparison and Nina I. Kristainsen for numerous inspiring discussions and technical help. We also thank Inger-Lise Frogner for the valuable help with obtaining GLAMEPS data. We thankfully acknowledged the EARLINET lidar data providers for assembling a very useful lidar dataset. This work has also received funding under the ACTRIS project from the European Union's Horizon 2020 research and innovation programme under grant agreement No 654109. The work done for this paper

is funded by the Norwegian ash project financed by the Norwegian Ministry of Transport and Communications and AVINOR. Model and support is also appreciated through the Cooperative Programme for Monitoring and Evaluation of the Long-range Transmission of Air Pollutants in Europe (No: ECE/ENV/2001/003). This work has also received support from the Research Council of Norway (Programme for Supercomputing) through CPU time granted at the super computers at NTNU in Trondheim.

References

Boichu, M., Chiapello, I., Brogniez, C., Péré, J.-C., Thieuleux, F., Torres, B., Blarel, L., Mortier, A., Podvin, T., Goloub, P., Söhne, N., Clarisse, L., Bauduin, S., Hendrick, F., Theys, N., Van Roozendael, M., and Tanré, D.: Current challenges in modelling far-range air pollution induced by the 2014–2015 Bárðarbunga fissure eruption (Iceland), Atmos. Chem. Phys., 16, 10831-10845, doi:10.5194/acp-16-10831-2016, 2016.

Bott, A.: A positive definite advection scheme obtained by nonlinear re-normalization of the advection fluxes, Mon. Weather Rev., 117, 1006–1015, 1989a.

Bott, A.: Reply, Mon. Weather Rev., 117, 2633–2636, 1989b.

Brown, R.J., Bonadonna, C. and Durant, A.J: A review of volcanic ash aggregation. Phys. Chem. Earth 45-46. 65-78, 2011.

Calvo, J.: Kain-Fritsch convection in HIRLAM. Present status and prospects. HIRLAM Newslett. 52, 57–64. Available at: http://hirlam.org/index.php?option = com_content&view = article&id = 64&Itemid = 101, 2007.

Casadevall, T.J.: Volcanic ash and aviation safety: Prodeedings of the First International Symposium on Volcanic Ash and Aviation Safety, U.S. Geol. Surv. Bull., 2047, 450 pp., 1994.

Dellino, P., Gudmundsson, M.T., Larsen, G., Mele, D., Stevenson, J.A., Thordarson, T. and Zimanowski B.: Ash from the Eyjafjallajökull eruption (Iceland): Fragmentation processes and aerodynamic behavior, J. Geophys. Res., 117, B00C04, doi:10.1029/2011JB008726, 2012.

Draxler, R.R. and Hess, G.: Description of the HYSPLIT_4 modeling system NOAA Tech. Memo. ERL ARL-224, NOAA Air Resources Laboratory, Silver Spring, MD 24 pp, 1997.

EMEP Status Report 1/2016: Transboundary particulate matter, photo-axidants, acidifying and eutrophying components, EMEP MSC-W & CCC & CEIP, Norwegian Meteorlogical Institute (EMEP MSC-W), Oslo, Norway, 2016.

Folch, A., Costa, A., Macedonio, G.: FALL3D: A computational model for transport and deposition of volcanic ash, Comput. Geosci, 35(6) 1334-1342, doi:10.1016/j.cageo.2008.08.008, 2009.

Frogner, I-L., and Iversen, T. EuroTEPS—a targeted version of ECMWF EPS for the European area. Tellus A 63.3 415-428, 2011.

Geosci. Model Dev. Discuss., doi:10.5194/gmd-2016-315, 2017
Manuscript under review for journal Geosci. Model Dev.
Published: 10 January 2017

Ivarsson, K. I.: The Rasch Kristjansson large scale condensation. Present status and prospects. HIRLAM Newslett. 52, 50–56. Available at: http://hirlam.org/index.php?option = com_content&view =article&id = 64&Itemid = 101, 2007.

Iversen, T., Deckmyn, A., Santos, C., Sattler, K., Bremnes, J. B., Feddersen, H. and Frogner, I.-L.: Evaluation of 'GLAMEPS'—a proposed multimodel EPS for short range forecasting. Tellus A, 63: 513–530. doi: 10.1111/j.1600-0870.2010.00507.x, 2011.

Jacobson, M. Z.: Fundamentals of atmospheric modeling. Cambridge university press, 1991.

Jones, A., Thomson, D., Hort, M. and Devenish, B.: The UK Met Office's next generation atmospheric dispersion model, NAME III, in Air Pollution Modelling and its Application XVII, edited by C. Borrego and A.-L. Norman, pp. 580–589, Springer, New York, 2007.

Josse, B., Simon, P. and Peuch, V.-H.: Radon global simulationswith the multiscale chemistry and transport model MOCAGE, Tellus,Ser. B, 56(4), 339–356, doi:10.1111/j.1600-0889.2004.00112.x, 2004.

Kain, J. S. The Kain-Fritsch Convective Parameterization. Anupdate. J. Appl. Meteorol. 43, 170–181, 2004.

Kain, J. S. and Fritsch, J. M.: A one-dimensional entraining/detraining plume model and its application in convective parameterization. J. Atmos. Sci., 47, 2784–2802, 1990.

Kristiansen, N. I., et al., Performance assessment of a volcanic ash transport model mini-ensemble used for inverse modeling of the2010 Eyjafjallajök ull eruption, J. Geophys. Res., 117, D00U11, doi:10.1029/2011JD016844, 2012.

Marécal, V., Peuch, V.-H. Andersson, C., Andersson, S., Arteta, J., Beekmann, M., Benedictow, A., Bergström, R., Bessagnet, B., Cansado, A., Chéroux, F., Colette, A., Coman, A., Curier, R. L., Denier van der Gon, H. A. C., Drouin, A., Elbern, H., Emili, E., Engelen, R. J., Eskes, H. J., Foret, G., Friese, E., Gauss, M., Giannaros, C., Guth, J., Joly, M., Jaumouillé, E., Josse, B., Kadygrov, N., Kaiser, J. W., Krajsek, K., Kuenen, J., Kumar, U., Liora, N., Lopez, E., Malherbe, L., Martinez, I., Melas, D., Meleux, F., Menut, L., Moinat, P., Morales, T., Parmentier, J., Piacentini, A., Plu, M., Poupkou, A., Queguiner, S., Robertson, L., Rouïl, L., Schaap, M., Segers, A., Sofiev, M., Tarasson, L., Thomas, M., Timmermans, R., Valdebenito, Á., van Velthoven, P., van Versendaal, R., Vira, J. and Ung, A. A regional air quality forecasting system over Europe: the MACC-II dayly ensemble production, Geosci. Model Dev., 8, 2777–2813, doi:10.5194/gmd-8-2777-2015, 2015

Mastin, Larry G. "A user-friendly one-dimensional model for wet volcanic plumes." Geochemistry, Geophysics, Geosystems 8.3. 2007.

Mastin, L. G., Guffanti, M., Servranckx, R., Webley, P., Barsotti, S., Dean, K., Durant, A., Ewert, J.W., Neri, A., Rose, W.I., Schneider, D., Siebert, L., Stunderj, B., Swansonk, G., Tupperl, A. Volentikm, A and Waythomash, G.F.: A multidisciplinary effort to assign realistic source parameters to models of volcanic ash-cloud transport and dispersion during eruptions. Journal of Volcanology and Geothermal Research, 1(186), 10-21, 2009.

Moxnes, E. D., Kristiansen, N.I., Stohl, A., Clarisse, L., Durant, A., Weber, K., and Vogel, A.: Separation of ash and sulfur dioxide during the 2011Grímsvötn eruption, J. Geophys. Res.Atmos., 119, 7477–7501, doi:10.1002/2013JD021129, 2014.

Palmer, T. N., Molteni, F., Mureau, R., Buizza, R., Chapelet, P., & Tribbia, J.: Ensemble prediction. In Proceedings of the ECMWF Seminar on Validation of models over Europe (Vol. 1), 1993.

Norwegian ash Project, Kristiansen N.I., Steensen B.M., Klein, H., Fagerli,. H. and Bartnicki, J.: 2.3.1. Norwegain ash project report 2.3.1, internal report, available at request.2014

Palmer, T. N:. Predicting uncertainty in forecasts of weather and climate. Rep. Prog. Phys. 63, 71–116, 2000.

Pappalardo, G., Mona, L., D'Amico, G., Wandinger, U., Adam, M., Amodeo, A., Ansmann, A., Apituley, A., Alados Arboledas, L., Balis, D., Boselli, A., Bravo-Aranda, J. A., Chaikovsky, A., Comeron, A., Cuesta, J., De Tomasi, F., Freudenthaler, V., Gausa, M., Giannakaki, E., Giehl, H., Giunta, A., Grigorov, I., Groß, S., Haeffelin, M., Hiebsch, A., Iarlori, M., Lange, D., Linné, H., Madonna, F., Mattis, I., Mamouri, R.-E., McAuliffe, M. A. P., Mitev, V., Molero, F., Navas-Guzman, F., Nicolae, D., Papayannis, A., Perrone, M. R., Pietras, C., Pietruczuk, A., Pisani, G., Preißler, J., Pujadas, M., Rizi, V., Ruth, A. A., Schmidt, J., Schnell, F., Seifert, P., Serikov, I., Sicard, M., Simeonov, V., Spinelli, N., Stebel, K., Tesche, M., Trickl, T., Wang, X., Wagner, F., Wiegner, M., and Wilson, K. M. (2013) Four-dimensional distribution of the 2010 Eyjafjallajökull volcanic cloud over Europe observed by EARLINET, Atmos. Chem. Phys., 13, 4429-4450, doi:10.5194/acp-13-4429-2013.

Rasch, P. J. and Kristjánsson, J. E. A comparison of the CCM3 model climate using diagnosed and predicted condensate parameterizations. J. Clim. 11, 1587–1614. 1998

Rose, W. I., and A. J. Durant. "Fine ash content of explosive eruptions." Journal of Volcanology and Geothermal Research 186.1, 32-39, 2009.

Prata, A. J., and A. T. Prata.: Eyjafjallajökull volcanic ash concentrations determined using Spin EnhancedVisible and Infrared Imager measurements, J. Geophys. Res., 117, D00U23, doi:10.1029/2011JD016800, 2012.

Sass, B. H., Nielsen, N.W., Jørgensen, J. U. and Amstrup, B.: The Operational HIRLAM System at DMI. DMI Tech Rep. no 99–21. Danmarks Meteorologiske Institutt, Lyngby v. 100, Copenhagen, Denmark, 1999.

Saltbones, J., Foss, A. and Bartnicki, J.: 1994: SNAP: Severe Nuclear Accient Program. Technical Description. Research Report No. 15. Norwegian Meteorological Office, Oslo, Norway.

Schmidt, A., Leadbetter, S., Theys, N., Carboni, E., Witham, C. S., Stevenson, J. A., Birch, C. E., Thordarson, T., Turnock, S., Barsotti, S., Delaney, L., Feng, W., Grainger, R.G., Hort, M.C., Höskuldsson, Á., Ialongo, I., Ilyinskaya, E., Jóhannsson, T., Kenny, P., Mather, T.A., Richards, N.A.D. and Shepherd, J.: Satellite detection, long-range transport, and air quality impacts of volcanic sulfur dioxide from the 2014–2015 flood lava eruption at Bárðarbunga (Iceland), J. Geophys. Res. Atmos., 120, 9739–9757, doi:10.1002/2015JD023638, 2015.

Schwaiger, H. F., R. P. Denlinger, and L. G. Mastin.: Ash3d: A finite-volume, conservative numerical model for ash transport and tephra deposition, J. Geophys. Res., 117, B04204, doi:10.1029/2011JB008968, 2012.

Scott, B. C.: Parameterization of sulphate removal by precipitation, J. Appl. Met., 17, 11375–11389, 1979.

Searcy, C., Dean, K., and Stringer, W.: PUFF: A high-resolution volcanic ash tracking model, Journal of Volcanology and Geothermal Research, 80, 1-16, 1998.

Sears, T. M., Thomas, G. E., Carboni, E., A Smith, A. J., and Grainger, R. G.: SO2 as a possible proxy for volcanic ash in aviation hazard avoidance, J. Geophys. Res.-Atmos., 118, 5698–5709, 2013.

Simpson, D., Benedictow, A., Berge, H., Bergstrøm, R., Emberson, L. D., FagerliI, H., Flechard, C. R., Hayman, G. D., Gauss, M., Jonson, J. E., Jenkin, M. E., Nyiri, A., Richter, C., Semeena, V. S., Tsyro, S., Tuovinen, J., Valdebenito, A. & Wind, P.: The EMEP MSC-W chemical transport model: technical description. Atmospheric Chemistry and Physics, 12, 7825-7865, 2012.

Steensen, B. M., Schulz, M., Theys, N., and Fagerli, H,: A model study of the pollution effects of the first 3 months of the Holuhraun volcanic fissure: comparison with observations and air pollution effects, Atmos. Chem. Phys., 16, 9745-9760, doi:10.5194/acp-16-9745-2016, 2016.

Steensen, B. M., Kylling, A, Kristiansen, N.I and Schulz, M.: Uncertainty assessment and applicability of an inversion method for volcanic ash forecasting, submitted to ACPD 2016.

Stohl, A., Forster, C., Frank, A., Seibert, P. and Wotawa, G..: Technical note: The Lagrangian particle dispersion model FLEXPART version 6.2, Atmos. Chem. Phys., 5(9), 2461–2474, doi:10.5194/acp-5- 2461-2005, 2005.

Stohl, A., Prata, A. J., Eckhardt, S., Clarisse, L., Durant, A., Henne, S., Kristiansen, N. I., Minikin, A., Schumann, U., Seibert, P., Stebel, K., Thomas, H. E., Thorsteinsson, T., Tørseth, K., and Weinzierl, B.: Determination of time- and height-resolved volcanic ash emissions and their use for quantitative ash dispersion modeling: the 2010 Eyjafjallajökull eruption, Atmos. Chem. Phys., 11, 4333-4351, doi:10.5194/acp-11-4333-2011, 2011.

Taddeucci, J., Scarlato, P., Montanaro, C., Cimarelli, C., Del Bello, E., Freda, C., Andronico, D., Gudmundsson, M. T.and Dingwell, D. B.: Aggregation-dominated ash settling from the Eyjafjallajökull volcanic cloud illuminated by field and laboratory high-speed imaging, Geology, 39, 891–894, doi:10.1130/G32016.1, 2011.

Theys, N., De Smedt, I., van Gent, J., Danckaert, T.,Wang, T., Hendrick, F., Stavrakou, T., Bauduin, S., Clarisse, L., Li, C., Krotkov, N., Yu, H., Brenot, H., and Van Roozendael, M.: Sulphur dioxide vertical column DOAS retrievals from the Ozone Monitoring Instrument: Global observations and comparison to groundbased and satellite data, J. Geophys. Res.-Atmos., 120, 2470–2491, doi:10.1002/2014JD022657, 2015.

Thomas, H. E. and Prata, A. J.: Sulphur dioxide as a volcanic ash proxy during the April–May 2010 eruption of Eyjafjallajökull Volcano, Iceland, Atmos. Chem. Phys., 11, 6871–6880, doi:10.5194/acp-11-6871-2011, 2011.

Thordarson, T. and Hartley, M.: Atmospheric sulphur loading by the ongoing Nornahraun eruption, North Iceland, EGU General Assembly Conference Abstracts, 17, 2015EGUGA, 1710708T, 2015.

Toth, Z., & Kalnay, E.: nsemble forecasting at NMC: The generation of perturbations. Bulletin of the american meteorological society, 74(12), 2317-2330, 1993.

Wilson, L. and Huang, T.C.: The influence of shape on the atmospheric settling velocity of volcanic ash particles, Earth and Planetary Sci. Lett., 44,311-324, 1979.

Wilson, T.M., Stewart, C., Sword-Daniels, V, Leanard, G.S., Johnston, D.M., Cole, J.W., Wardman, J., Wilson, G. and Barnard, S.T. Volcanic ash impacts on critical infrastructure. J. Phys. Chem. Earth, doi:10.1016/j.pce.2011.06.006. 2011

Winker, D. M., W. H. Hunt, and M. J. McGill.: Initial performance assessment of CALIOP, Geophys. Res. Lett., 34, L19803, doi:10.1029/2007GL030135, 2007.

Geosci. Model Dev. Discuss., doi:10.5194/gmd-2016-315, 2017
Manuscript under review for journal Geosci. Model Dev.
Published: 10 January 2017

Winker, D. M., Z. Liu, A. Omar, J. Tackett, and D. Fairlie.: CALIOP observations of the transport of ash from the Eyjafjallajökull volcano in April 2010, J. Geophys. Res., 117, D00U15, doi:10.1029/2011JD016499, 2012.

UK Civil Aviation Authority (2016). A history of ash and aviation [online] Available at: https://www.caa.co.uk/Safety-initiatives-and-resources/Safety-projects/Volcanic-ash/A-history-of-ash-and-aviation/ [Accessed 12 Dec.. 2016].

Undén, P., Rontu, L., Järvinen, H., Lynch, P., Calvo, J. and co-authors. (2002): HIRLAM-5 Scientific Documentation HIRLAM-5 Project. Available from SMHI, S-601767 Norrköping, Sweden.

Table 1: List and names of model simulations used in this paper.

Name	Period	Meteorology	Resolution	Emission
Low	03.08.2014 00UTC + 48 UTC 04.08.2014 00UTC + 48 UTC 05.08.2014 00UTC + 48 UTC	GLAMEPS 24 perturbed ensemble members	40 km x 40 km	Schmidt et al. (2015)
Mid	03.08.2014 00UTC + 48 UTC 04.08.2014 00UTC + 48 UTC 05.08.2014 00UTC + 48 UTC	GLAMEPS 24 perturbed ensemble members	20 km x 20 km	Schmidt et al. (2015)
High	03.08.2014 00UTC + 48 UTC 04.08.2014 00UTC + 48 UTC 05.08.2014 00UTC + 48 UTC	GLAMEPS 24 perturbed ensemble members	10 km x 10 km	Schmidt et al. (2015)
Eyja_grav	13.04.2010 – 25.05.2010	ECMWF IFS	0.25 x 0.25 degree	Stohl et al. (2011)
Eyja_no_grav	13.04.2010 – 25.05.2010	ECMWF IFS	0.25 x 0.25 degree	Stohl et al. (2011)

Table 2: Total area A where SO_2 loads are above a given threshold, found on average in members of the low, mid and high resolution ensembles (see table 1). Areas are accumulated at the end of a 48 hour forecast, corresponding to Fig. 1 and 2.

SO_2 load threshold [DU]	A_{Low} [$1e^6$ km^2]	A_{Mid} [$1e^6$ km^2]	A_{High} [$1e^6$ km^2]
0.25	69.7	58.3	52.1
5	25.0	23.1	21.3
10	14.9	14.8	14.3
20	7.4	8.0	8.1
50	1.9	2.4	2.2

Geosci. Model Dev. Discuss., doi:10.5194/gmd-2016-315, 2017
Manuscript under review for journal Geosci. Model Dev.
Published: 10 January 2017

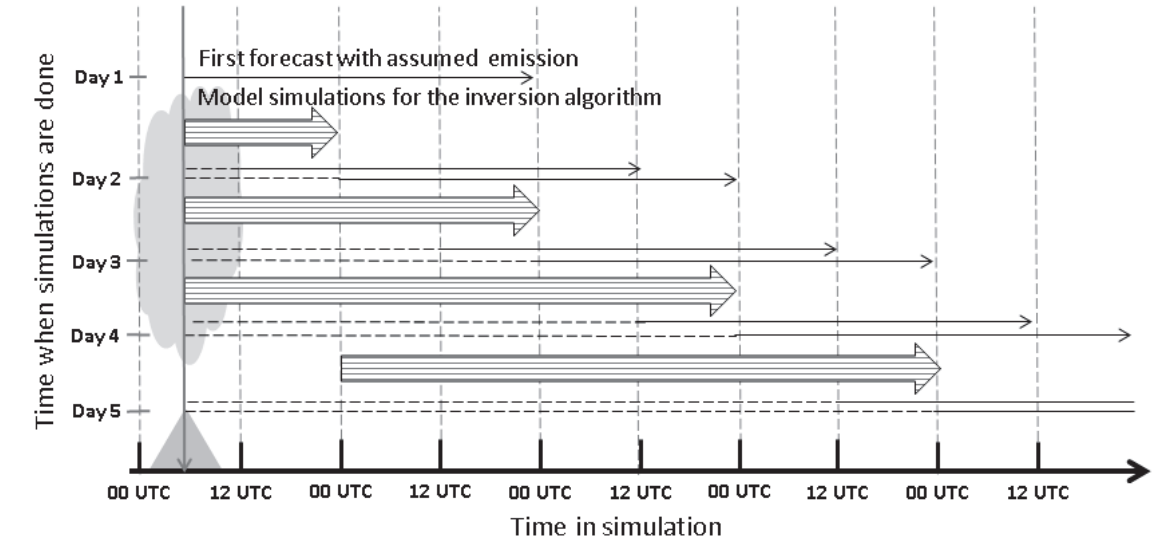

Figure 1: Sequence of model simulations started at the Norwegian Meteorological Institute in the case of a volcanic eruption. The single black arrows indicate a 48 hour forecast simulations. The thick striped arrows represent the multiple model simulations started for the inversion algorithm to retrieve an improved emission estimate using satellite data. Dashed lines represent spin-up model simulations with emission estimate found by the inversion algorithm. These model simulations are continued as forecasts (single black arrows). The chronological order of simulations starts from the top, so new forecast results are available every 12 hour. The inversion simulations are restarted every 24 hour.

Geosci. Model Dev. Discuss., doi:10.5194/gmd-2016-315, 2017
Manuscript under review for journal Geosci. Model Dev.
Published: 10 January 2017

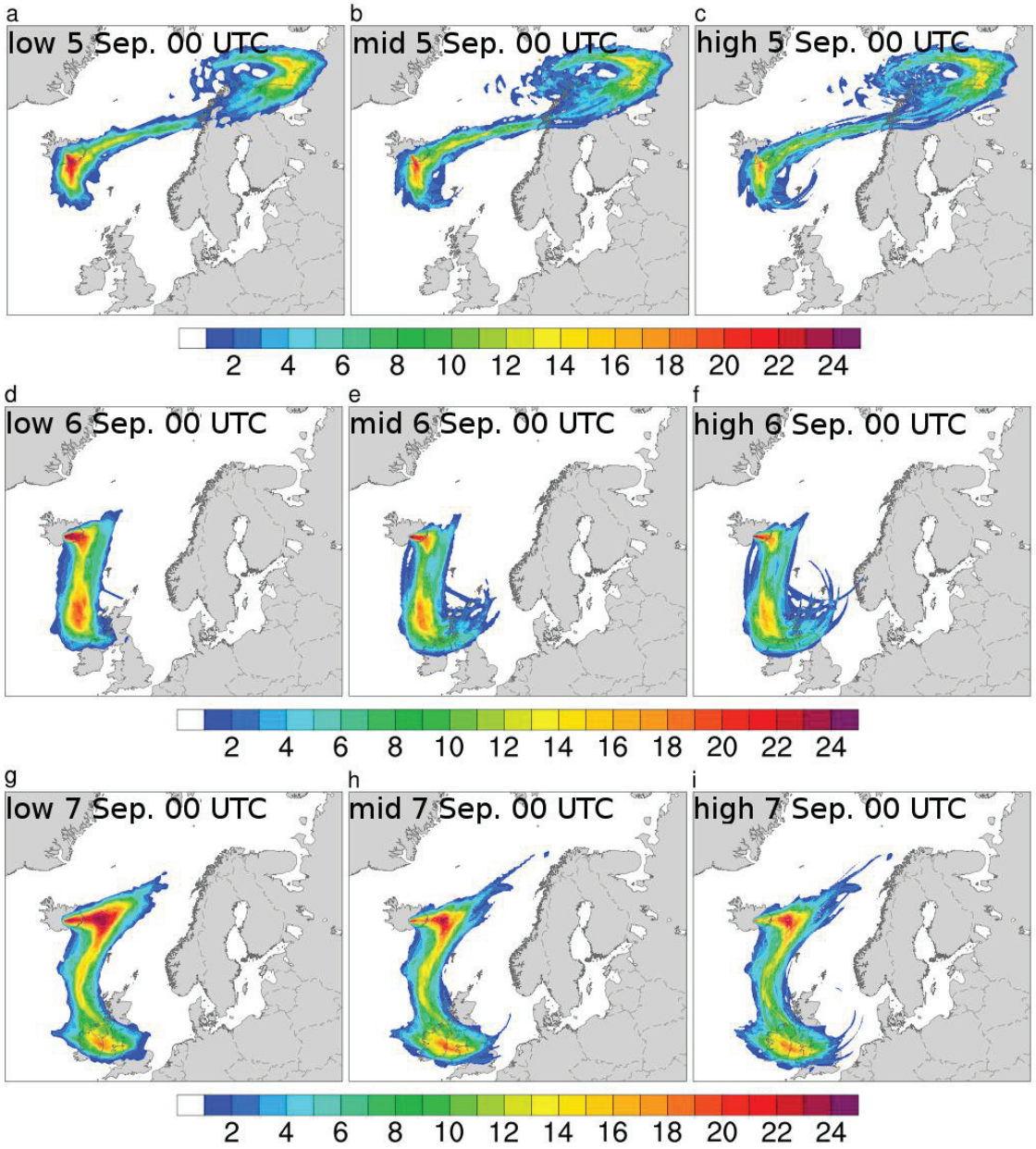

Figure 2: Map of number of ensemble members that is locally exceeding a 5 DU SO_2 limit. Counted after 48 hours in the low, mid and high resolution ensembles, in the left, middle and right column respectively, for start time 00 UTC 3. September (panels a,b,c), 00 UTC 4. September (panels d,e,f) and 00 UTC 5 September (panels g,h,i).

Geosci. Model Dev. Discuss., doi:10.5194/gmd-2016-315, 2017
Manuscript under review for journal Geosci. Model Dev.
Published: 10 January 2017

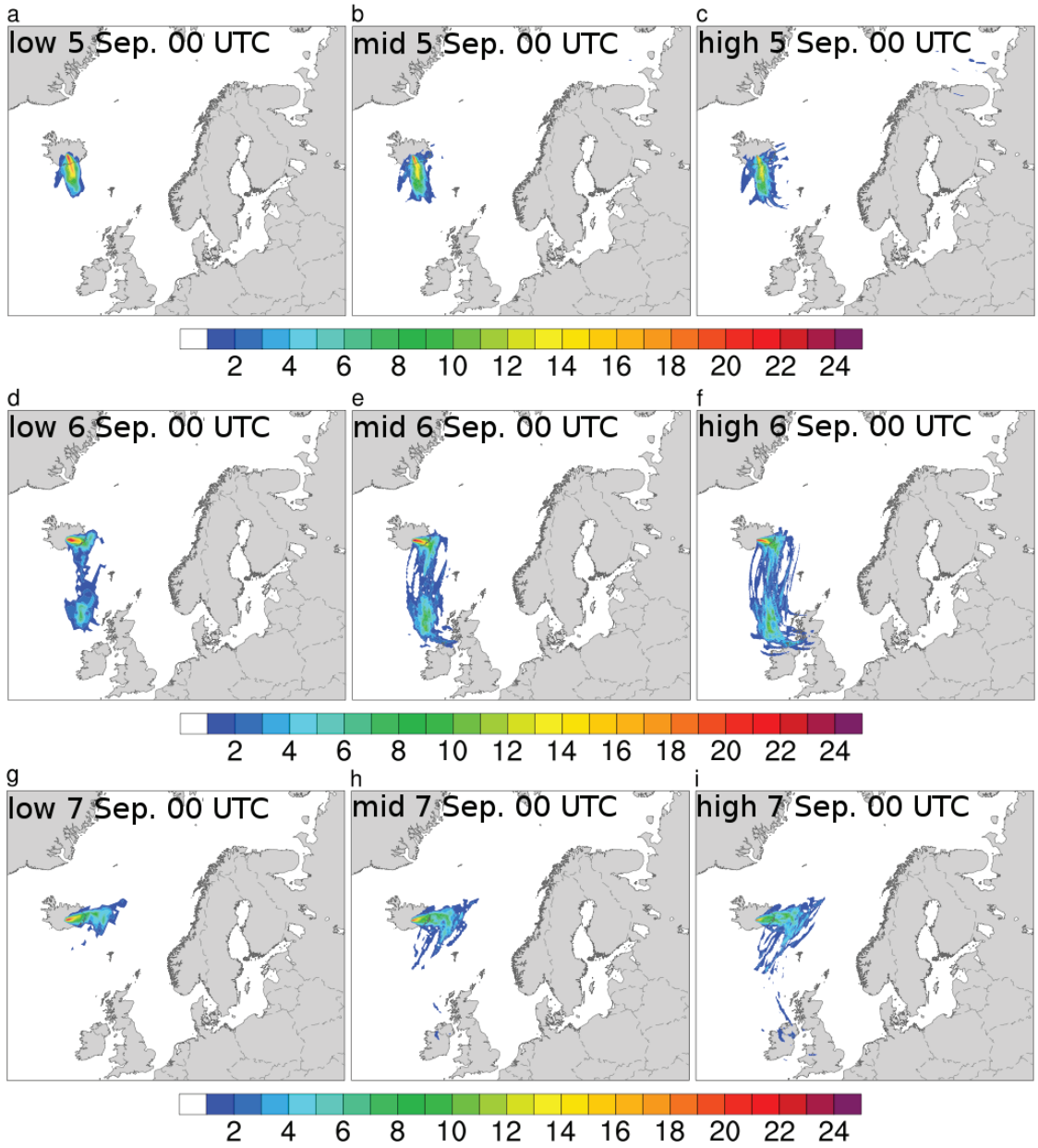

Figure 3; The same as Figure 2, counting ensemble members locally exceeding a 50 DU limit.

Geosci. Model Dev. Discuss., doi:10.5194/gmd-2016-315, 2017
Manuscript under review for journal Geosci. Model Dev.
Published: 10 January 2017

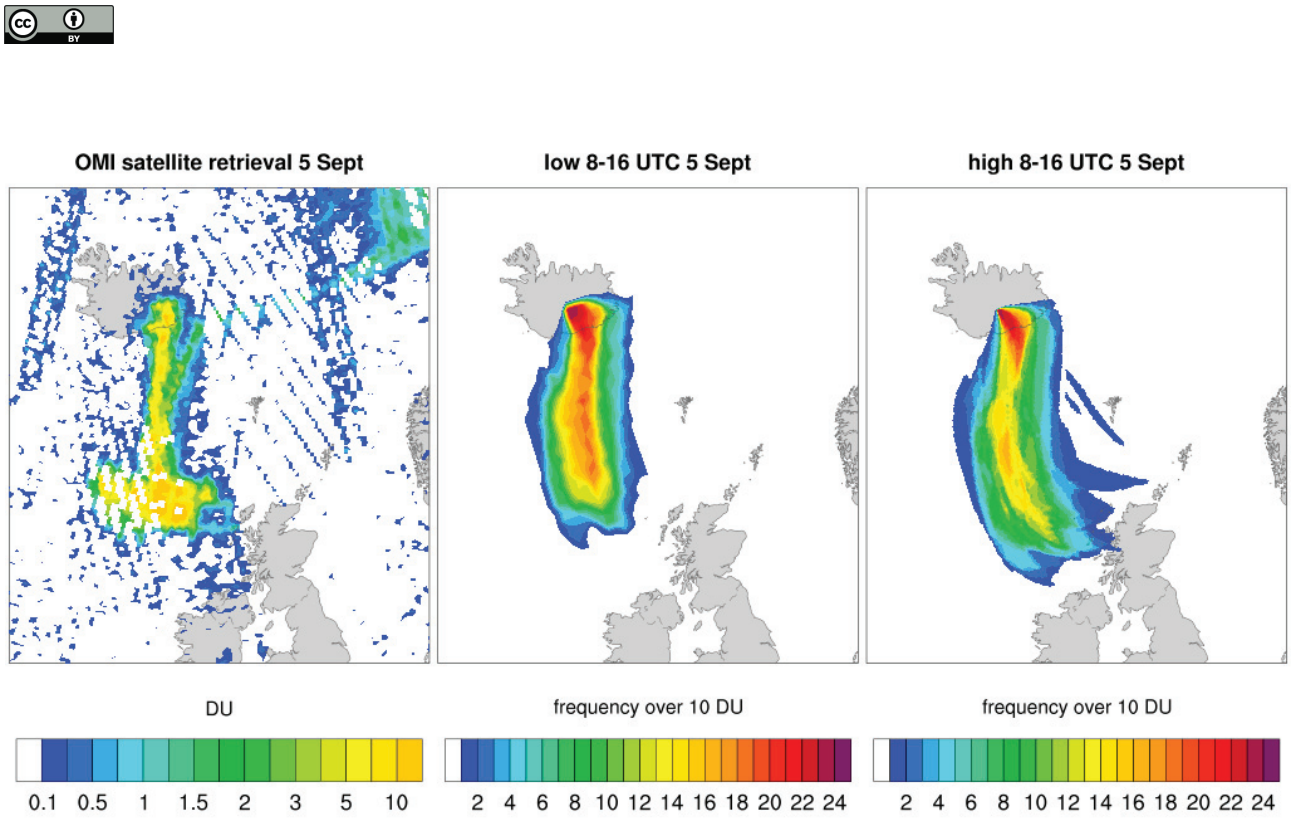

Figure 4; OMI retrieval of SO_2 (left) for the satellite overpasses between 8 UTC and 16 UTC 5 Sept. Frequency of ensemble members over 10 DU for the low (middle) and high (right) resolution runs. Frequencies are computed every hour and averaged over the same time period, using the forecast runs started 4 September 00 UTC.

Geosci. Model Dev. Discuss., doi:10.5194/gmd-2016-315, 2017
Manuscript under review for journal Geosci. Model Dev.
Published: 10 January 2017

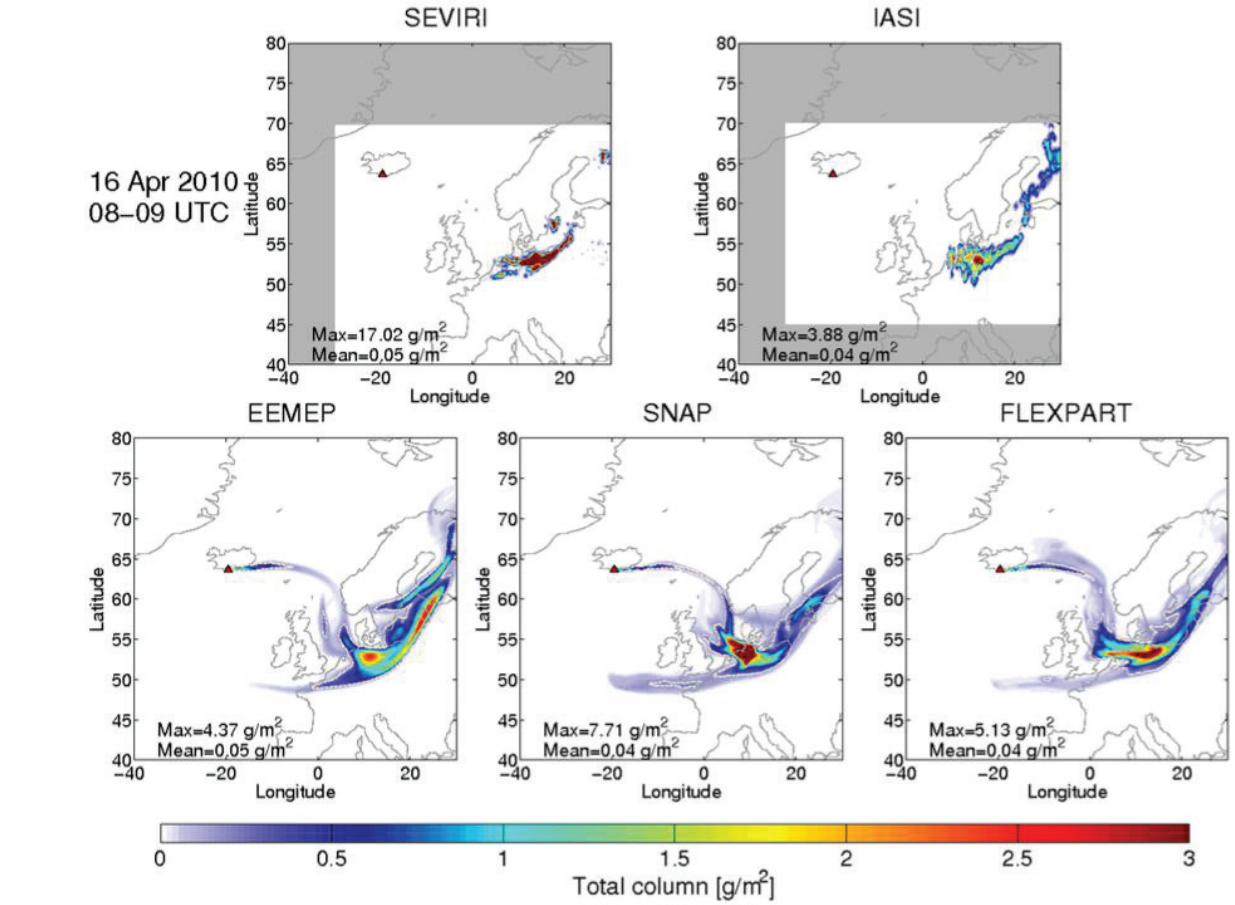

Figure 5: Mean ash column burdens from 8 to 9 UTC 16 April for SEVIRI and IASI satellite ash retrievals, and eEMEP, SNAP and FLEXPART model simulations.

Geosci. Model Dev. Discuss., doi:10.5194/gmd-2016-315, 2017
Manuscript under review for journal Geosci. Model Dev.
Published: 10 January 2017

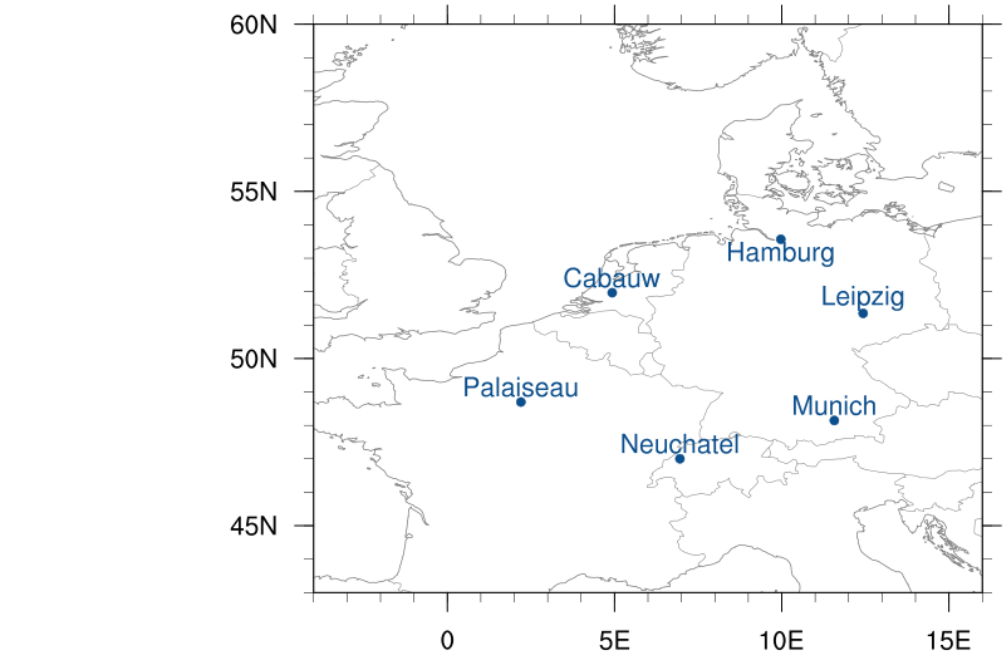

Figure 6: Map of EARLINET lidar measurement sites used in the study.

Geosci. Model Dev. Discuss., doi:10.5194/gmd-2016-315, 2017
Manuscript under review for journal Geosci. Model Dev.
Published: 10 January 2017

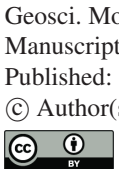

Geoscientific Model Development Discussions
Open Access
EGU

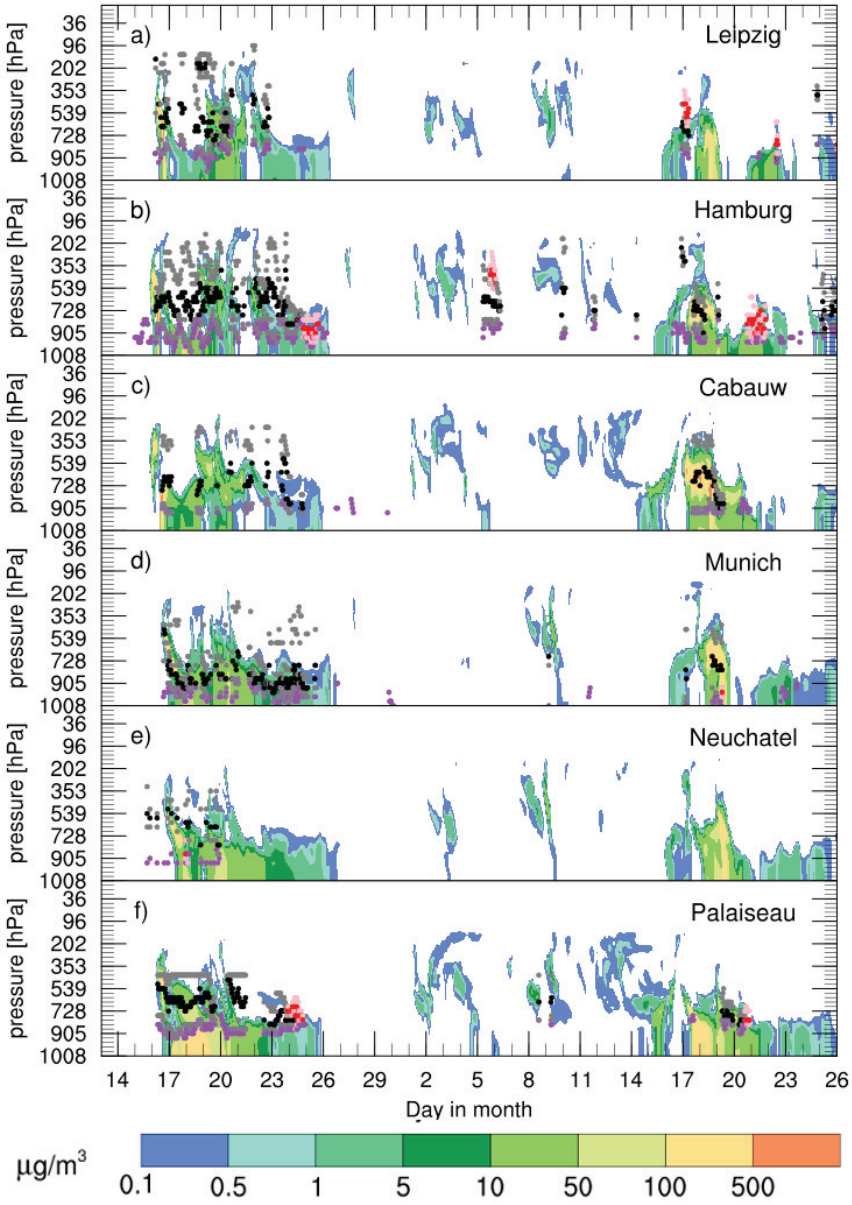

Figure 7; Height-time profiles of ash concentrations from eEMEP model, including gravitational settling, at the six EARLINET lidar stations (see figure 6) in April-May 2010 episode (contour graph in background). Lidar-detected upper and lower height of ash layer is presented as grey dots. The lidar retrieved centre of mass for ash is plotted as black dots. For mixed layers where ash is identified with continental aerosol, the height of the layer is presented as light pink dots, and centre of mass are red dots. The height of the planetary boundary layer is shown in violet. Due to weather conditions and technical difficulties the lidar measurements are not a continuous series.

Geosci. Model Dev. Discuss., doi:10.5194/gmd-2016-315, 2017
Manuscript under review for journal Geosci. Model Dev.
Published: 10 January 2017

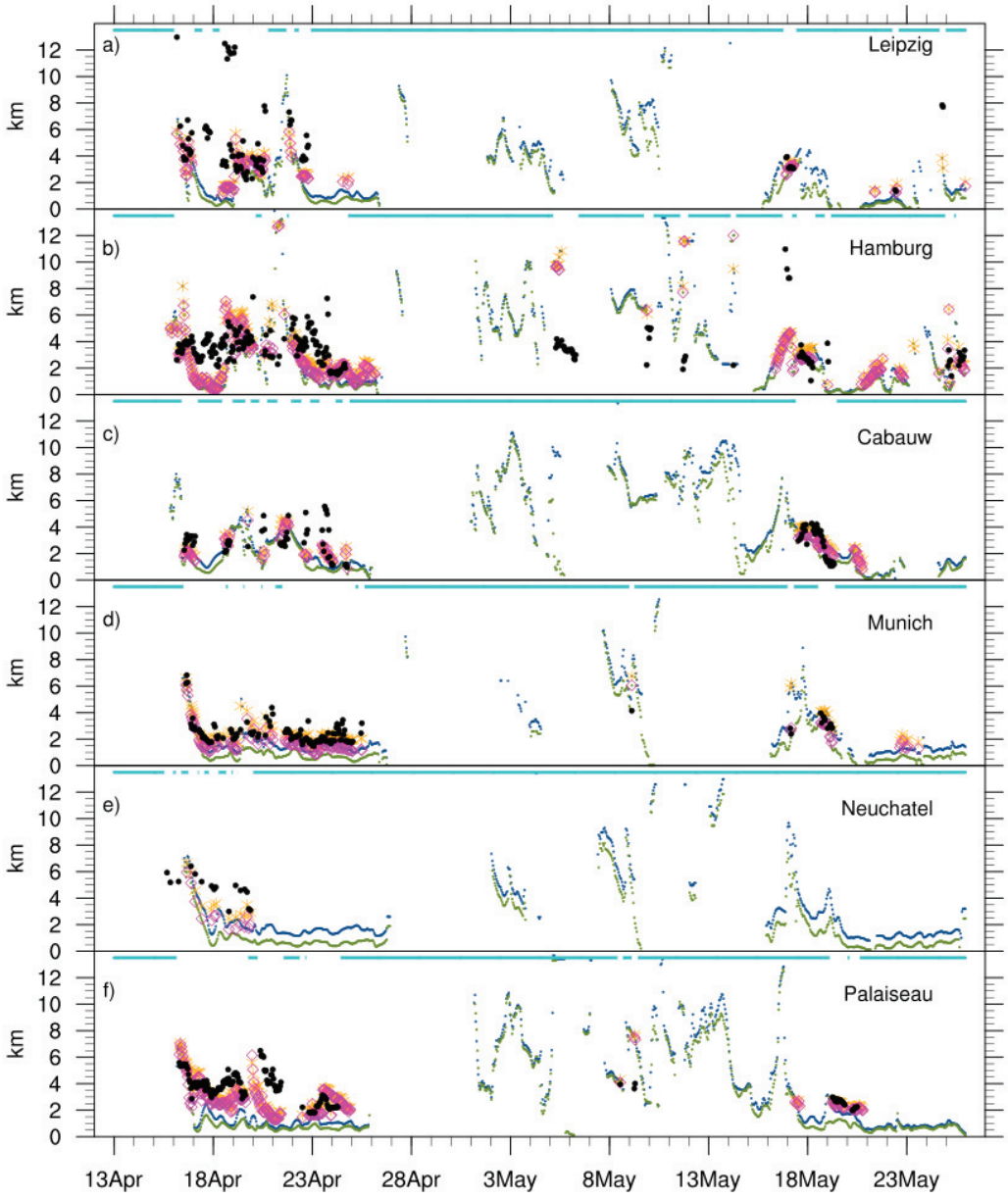

Figure 8; Modelled and observed centre of mass for ash at the lidar stations. Green and blue dots represent centre of ash mass, computed from the entire model column, for simulations with and without gravitational settling, shown where ash concentrations were larger than 0.1 μg m^{-3}. Magenta and orange represents model centre of ash, calculated above the observed planetary boundary layer (PBL) with and without gravitational settling, respectively. Black dots are corresponding lidar retrieved centre of mass for ash above the PBL (same as Figure 7). Light blue line above indicates where observations are missing.

Geosci. Model Dev. Discuss., doi:10.5194/gmd-2016-315, 2017
Manuscript under review for journal Geosci. Model Dev.
Published: 10 January 2017

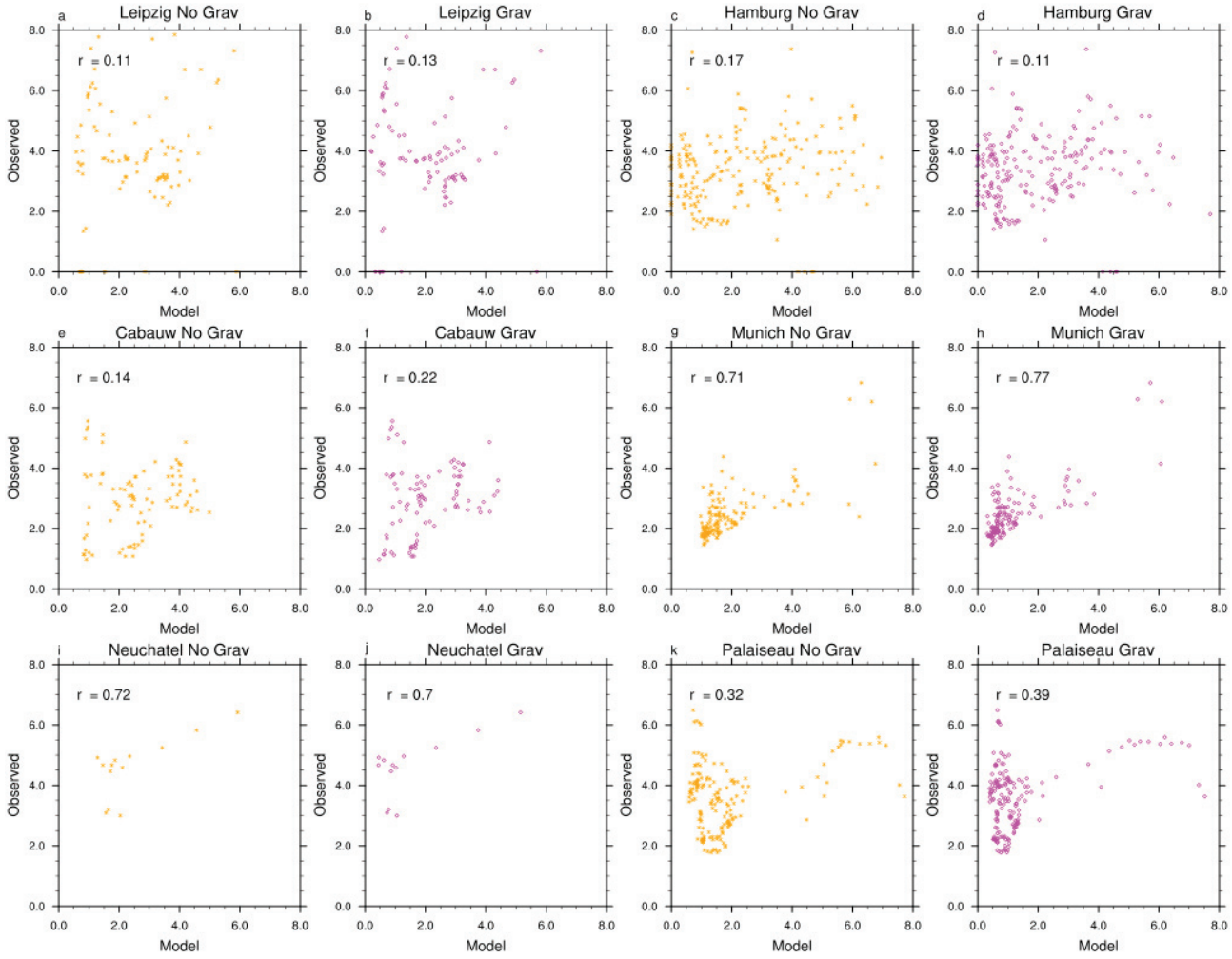

Figure 9: Scatterplots for observed versus simulated centre of ash mass with (magenta) and without gravitational settling (orange). Data correspond to Fig. 8 using model and observed values under 8 km but above the PBL. Correlation between observed and model values is given in the upper left corner.

III

Atmos. Chem. Phys. Discuss., doi:10.5194/acp-2016-1075, 2017
Manuscript under review for journal Atmos. Chem. Phys.
Published: 27 January 2017

Atmospheric Chemistry and Physics Discussions

Uncertainty assessment and applicability of an inversion method for volcanic ash forecasting

Birthe Marie Steensen[1], Arve Kylling[2], Nina Iren Kristiansen[2], Michael Schulz[1]

[1]Research department, Norwegian Meteorological Institute, Oslo, 0131, Norway
[2]Atmosphere and Climate Department, Norwegian Institute for Air Research (NILU), Kjeller, 2007, Norway

Correspondence to: Birthe Marie Steensen (birthe.steensen@met.no)

Abstract. Significant improvements in the way we can observe and model volcanic ash clouds have been obtained since the 2010 Eyjafjallajökull eruption. One major development has been data assimilation techniques, which aim to bring models in closer agreement to satellite observations and reducing the uncertainties for the ash emission estimate. Still, questions remains to which degree the forecasting capabilities are improved by inclusion of such techniques are and how these improvements depend on the data input. This study exploits how different satellite data and different uncertainty assumptions of the satellite and a priori emissions affect the calculated volcanic ash emission estimate, which is computed by an inversion method that couples the satellite and a priori emissions with dispersion model data. Two major ash episodes over four days in April and May of the 2010 Eyjafjallajökull eruption are studied. Specifically, inversion calculations are done for four different satellite data sets with different size distribution assumptions in the retrieval. A reference satellite data set is chosen and the range between the minimum and maximum 4 day average load of hourly retrieved ash is 121 % in April and 148 % in May, compared to the reference. The corresponding a posteriori maximum and minimum emission sum found for these four satellite retrievals range from 26 % and 47 % of the a posteriori reference estimate for the same two periods. Varying the assumptions made in the satellite retrieval therefore translates into uncertainties in the calculated emissions and the modelled ash column loads. By further exploring the weighting of uncertainties connected to a priori emissions and the other-than-size uncertainties in the satellite data, the uncertainty in the a priori estimate is found to have an order of magnitude more impact on the a posteriori solution compared to the other-than-size uncertainties in the satellite. Part of this is explained by a too high a priori estimate used in this study that is reduced by around half in the a posteriori reference estimate. Setting large uncertainties connected to both a priori and satellite input data is shown to compensate each other. Because of this an inversion based emission estimate in a forecasting setting needs well tested and considered assumptions on uncertainties for the a priori emission and satellite data. The quality of using the inversion in a forecasting environment is tested by adding gradually, with time, more observations to improve the estimated height versus time evolution of Eyjafjallajökull ash emissions. We show that the initially too high a priori emissions are reduced effectively when using just 12 hours of satellite observations. More satellite observations (>12h), in the Eyjafjallajökull case, place the volcanic injection at higher altitudes. Adding additional satellite observations (>36h) changes the a posteriori emissions to only a small extent for May and minimal for the April period, because the ash is dispersed and transported effectively out of the

Atmos. Chem. Phys. Discuss., doi:10.5194/acp-2016-1075, 2017
Manuscript under review for journal Atmos. Chem. Phys.
Published: 27 January 2017

Atmospheric Chemistry and Physics Discussions

domain after 1-2 days. A best-guess emission estimate for the forecasting period was constructed by averaging the last 12 hours of the a posteriori emission. Using this emission for a forecast simulation performs better especially compared to model simulations with no further emissions over the forecast period in the case of a continued volcanic eruption activity. Because of undetected ash in the satellite retrieval and diffusion in the model, the forecast simulations generally contain more ash than the observed fields and the model ash is more spread out. Overall, using the a posteriori emissions in our model reduces the uncertainties connected to both the satellite observations and the a priori estimate to perform a more confident forecast in both amount of ash released and emission heights.

1 Introduction

The fine ash fraction (ash particles with diameter < 64 μm) of tephra from volcanic eruptions can be transported over large distances and cause jet engine malfunction and damages to windshields (Casadevall, 1994). Both the 2010 April and May Eyjafjallajökull eruption and the May 2011 Grimsvötn eruption caused flight delays and cancellations leading to economical loss (European Commission, 2011). Although satellite observations can show snapshots of the current horizontal extension of ash, volcanic ash transport and dispersion models (VATDMs) are needed to forecast the dispersion of the volcanic clouds. The source term needed to run these forecasts can be highly uncertain. Stohl et al. (2011) presents an inversion method to calculate a source term constrained by satellite observations, using a priori emission estimates and model simulations. This inversion technique has been successfully applied to calculate ash emissions from the Eyjafjallajökull and Grimsvötn eruptions as well the 2014 Kelut eruption (Stohl et al., 2011; Kristiansen et al., 2012; Moxnes et al., 2014; Kristiansen et al., 2015). The method has also been applied to volcanic eruptions with SO_2 emissions (Kristiansen et al. 2010; Eckhardt et al. 2008).

The satellite data, a priori and model input data required by the inversion algorithm all have assumed uncertainties connected to them that weight the inversion calculations. Both the assumed a priori and satellite uncertainties used in the studies mentioned above varies from around 100% of the input data values and downwards to zero or a minimum value based on the confidence of the a priori emission and satellite data available for the three eruption cases. For the Kelut eruption however, where the eruption reached the stratosphere, the a priori emission estimate was highly unreliable so the uncertainty was set to 1000% of the assumed a priori emission values to make the result be almost exclusively driven by the satellite data. Eckhardt et al (2008) found that using a zero and constant a priori estimate gave similar a posteriori estimates for the Jebel at Tair 2007 eruption. This highlights that uncertainty settings in the inversion are case dependent. In this study, inversion calculations with different assumed uncertainties are presented to increase understanding of the effects on the a posteriori emissions.

Boichu et al. (2013) investigated the SO_2 emissions of the 2010 Eyjafjallajökull eruption in early May by a similar inversion method and found that SO_2 emission estimate calculations by only a single satellite image gave consistent results for young plumes, but showed increased uncertainty as the plume evolved over time. A more accurate emission term are found by

Atmos. Chem. Phys. Discuss., doi:10.5194/acp-2016-1075, 2017
Manuscript under review for journal Atmos. Chem. Phys.
Published: 27 January 2017

Atmospheric Chemistry and Physics Discussions

assimilating more satellite observations further into the period and therefore reducing the forecasting time. Wilkins et al. (2016a) used an insertion method for ash forecasting by initializing a dispersion model with ash layers derived from SEVIRI (Meteosat Second Generation Spinning Enhanced Visible and Infrared Imager) satellite retrievals. The study found that the model field calculated by including up to six satellite observations gave a broader and more extensive ash cloud, which compared worse to the 8 May 9 UTC satellite observation, than a single satellite retrieval inserted six hours before the observation time. The ash cloud found by several retrievals is considered a more conservative choice for giving commercial air traffic advice however as it includes ash that may not be captured by a single observation.

In the previous studies using the inversion method by Stohl et al. (2011), the a posteriori emission estimates were calculated after the eruption had ceased and using all satellite data available for the entire eruption period. However, in this study more satellite observations will be added gradually to the inversion algorithm to simulate a real forecast scenario. The purpose of using the inversion method is to make the model simulated ash with the inversion derived a posteriori source emission term more alike the observed ash column loads, as compared to model simulations with source terms calculated by empirical plume height relationships like the one given in Mastin et al. (2009) (used here as a priori emission). The inversion algorithm only calculates a constrained source term up until the start of the forecast, as it requires satellite observations. For emissions during the forecast period one has to use other methods 1) assume no further emissions 2) use the latest a priori emission from Mastin et al. (2009), or 3) average of the last hours of the a posteriori from the inversion. As the latter option includes some information from the satellite observations that limits the uncertainty, a 12 hours average will be tested here as opposed to zero forecast emission.

Meteorological clouds that contain ice, super-cooled droplets or unfrozen cloud droplets decrease the ability to identify ash in satellite retrievals, or retrieve higher concentrations than what is the truth (Prata and Prata, 2012, Kylling et al., 2015). Retrieval of ash from one single satellite image of the cloud is therefore more uncertain than a series of retrievals covering a longer time period. Hourly SEVIRI satellite retrievals are used in this study, and weaknesses in the satellite retrievals are explored further by differentiating pixels where no ash is detected and unclassified pixels where it is uncertain if the pixels contain ash.

The aim of this study is to use the inversion method by Stohl et al. (2011) in a forecasting setting and investigate how changes in input influence emission estimate results. Two four days periods in April and May of the 2010 Eyjafjallajökull eruption are studied. During the first period from 14 to 18 April, an ash cloud is transported over Central Europe originating from ash emitted on 14 and 15 April, while a smaller amount is released on 17 April. The second period studied covers 5 to 9 May when more ash was emitted again after a period with low emissions. The ash was transported south and entrained in a high pressure system causing the ash cloud to persist over the North Atlantic and stay in the domain over the whole period. More satellite observations are therefore available for this episode.

The paper is structured as follows: section two gives a short description of the inversion method, the model and satellite data used in this study, as well as the structure, amplitude and location (SAL) scoring method (Wernli et al., 2008), a performance metric that also was used in Wilkins et al. (2016a). Results are presented in section three: First the sensitivity of inversion

Atmos. Chem. Phys. Discuss., doi:10.5194/acp-2016-1075, 2017
Manuscript under review for journal Atmos. Chem. Phys.
Published: 27 January 2017

Atmospheric Chemistry and Physics Discussions

calculations on input data uncertainty is demonstrated; secondly, the robustness of the calculated source term is tested by simulating a real case, where increasing amounts of satellite data are used, and modelled ash clouds are compared to observed ones. Discussion and conclusions are given in section four and five respectively.

2 Methods

2.1 Source estimate calculations

Assimilated volcanic source estimates are calculated in this study by an inversion algorithm, based on the work given in Seibert (2000), and further developed to calculate the vertical distribution of volcanic emissions by Eckhardt et al. (2008) and Kristiansen et al. (2010). Stohl et al. (2011) presents modifications to the method to also produce time resolved emission estimates of ash for the 2010 Eyjafjallajökull eruption. Since the inversion method for volcanic ash emission estimates has been extensively described in previous studies, further detailed description of the inversion method will not be given here, but some aspects are presented for the use in a forecasting setup.

The algorithm calculates an assimilated emission estimate using input data from a dispersion model and satellite retrievals, as well as a priori emission estimates. First, source receptor model data, representing all possible dispersion scenarios of the ash cloud, are matched with satellite data. For each grid point in the considered domain, modelled column loadings over every hour of the assimilation time that exceed a certain threshold (here 10^{-12} gm^{-2}) emitted from a unit ash emission (1 kg s^{-1} m^{-1}) released from one particular emission time and height are matched with the corresponding assimilation time and grid point of the satellite ash mass loading retrieval. Using a threshold exceedance criterion for the model data helps reduce the data volume and inversion cpu time. Model source receptor calculations are done by using an unit emission that are later scaled by the a priori emissions in the algorithm, making it possible to change the a priori estimate without performing new model calculations. Model simulations used for the inversion are further described in section 2.2. Since grid boxes are used only where model results have ash loads above the threshold, the chance of the result being influenced by possible false positive ash retrievals in the satellite data, described in section 2.3, is reduced. On the other side, grid points which are unclassified, meaning it is uncertain whether they contain ash or not, are excluded from the inversion calculations. To reduce the amount of data and computational time, a randomly selected 70 % of the gridded data points, which hold satellite data with definitely no ash, are discarded, similar to Stohl et al. (2011).

2.2 Model Simulations

Volcanic ash dispersion calculations are done with the EMEP (The European Monitoring and Evaluation Programme) MSC-W (Meteorological Synthesizing Centre - West) model described in Simpson et al. (2012), updates are in addition presented in the yearly EMEP reports (EMEP MSC-W, 2016). Model modifications to improve the description of ash dispersion such as gravitational settling in all model layers, are described in Steensen et al. (2017). This new version of the model is called the emergency EMEP (eEMEP) model. Simulations are done with 3 hourly meteorological input from the ECMWF

Atmos. Chem. Phys. Discuss., doi:10.5194/acp-2016-1075, 2017
Manuscript under review for journal Atmos. Chem. Phys.
Published: 27 January 2017

(European Centre for Medium-Range Weather Forecast) IFS (Integrated Forecasting System) model with a horizontal resolution of 0.25 x 0.25 degrees in latitude and longitude, with 42 layers in the vertical. The model domain spans from 40 degrees to 80 degrees north, and 40 degrees west to 30 degrees east. The ash emissions are distributed over nine ash particle size bins from 4 µm to 25 µm particle diameter with an ash density of 2500 kg m^{-3}.

To produce source receptor model input for the inversion calculations, a unit amount of ash is released from 19 height intervals above the volcano as a pulse over a period of three hours. The three hourly ash emissions are distributed over the appropriate model layers given by the height intervals in the source emissions. Simulations are started every three hours until the whole period of interest is covered. With the current setup, ash is assumed to have a maximum residence time in the domain of 6 days before it is transported out of the domain or settled to the ground. The simulations therefore last for 6 days after the pulse emission is released.

There are uncertainties connected to the model simulation caused by uncertainties in the meteorological input and assumptions about ash in the model. Stohl et al. (2011) tested the sensitivity of different model ash size distributions on the inversion calculations and found that, as the satellite observations only see a small range of ash size classes, changing the distribution over the size bins gave a negligible difference. The model simulations used as input to the inversion are also done for an early part of the forecasted meteorological data when numerical weather prediction model uncertainties are still small. Errors caused by uncertainty in the meteorology and modelled size distribution are assumed minimal in our set-up, compared to the uncertainties connected to a priori emissions and satellite data and will not be studied here.

Figure 1 shows the timeline of the inversion calculation and the forecast via the eEMEP model simulation, both as used in this study and in the case of a real volcanic eruption. The a posteriori emission estimate calculated from the inversion routine is used as the emission source term in the model simulations and can reach back up to six days counted from the forecast start time. An emission estimate for the forecast period is normally calculated as the average of the last 12 hours of the a posteriori source term. For practical reasons, the two model simulations (inversion method and forecast) are run separately from each other.

2.3 Satellite data

Ash satellite detection and retrievals are made using infrared measurements by SEVIRI on board the Meteosat Second Generation (MSG-2) satellite. MSG-2 is geostationary, centred at approximately 0 degrees latitude and has a 70 degrees view coverage (Schmetz et al., 2002). Pixel resolution is 3 x 3 km at nadir, while at the edge of the coverage it increases to 10 x 10 km. Observations are available every 15 minutes. Pixels are identified as containing ash if the brightness temperature difference (BTD) between the SEVIRI 10.8 µm and 12.0 µm channels (Prata, 1989) is below a certain threshold value, here -0.5 K. The BTDs have been adjusted for water vapour absorption using the approach of Yu et al. (2002). Ash clouds give negative BTDs, ice give positive BTDs, while BTDs of water clouds are closer to zero.

For the inversion, satellite observations for every hour are used as input and interpolated by forward mean to the 0.25 x 0.25 degree model domain, two examples for April and May are shown in Figure 2. Grey areas in the plots represent unclassified

Atmos. Chem. Phys. Discuss., doi:10.5194/acp-2016-1075, 2017
Manuscript under review for journal Atmos. Chem. Phys.
Published: 27 January 2017

Atmospheric Chemistry and Physics Discussions

pixels where the satellite ash detection cannot determine if ash is present or not, that is, the BTD is around zero and pixels can therefore contain water, ice and ash. The ash detection can falsely classify ash in regions where there is no ash over land due to spectral land surface emissivity and for pixels with large viewing angles close to the edge of the SEVIRI coverage (Prata and Prata 2012). For the first date shown at the beginning of the eruption (15 April 2010 12 UTC, left plot Figure 2), stationary ash clouds are detected both to the north and west of Iceland, while the main ash emission is transported east towards Norway, indicating that these ash clouds to the north and west are likely false positives. Other false positives are observed over Great Britain and in the North Atlantic Ocean for this time. For the second retrieval shown (7 May 12 UTC, right plot Figure 2), a large ash cloud is detected to the south west of Iceland that probably does not originate from volcanic emissions according to our understanding of the transport conditions. Because of the different thresholds and method used to detect ash this cloud is not detected in the Francis et al (2012) and Wilkins et al (2016a) studies. False positives may be included in the inversion calculation because in a forecasting environment manual adjustments to the satellite data for these pixels can be difficult to accomplish, however, since model data where no ash is transported is disregarded, the chances of false positives being used in the inversion calculations are minimal.

The ash mass loading and effective ash particle radius are retrieved as described in Kylling et al. (2015). The retrieval is based on a modification of the Bayesian optimal estimation technique used by Francis et al. (2012). There are several factors that affect the ash retrieval causing uncertainties in the calculated column loadings. Corradini et al (2008) studied uncertainties due to ± 2 K surface temperature and ± 2 % surface emissivity changes and found total mass retrieval errors of 30 % and 10 %, respectively. The same study also estimated a retrieval error of 10 % caused by variations in ash plume altitude and cloud thickness, and shows an almost approximately proportional uncertainty retrieval error due to water vapour. Changing the ash type (e.g from andesite to the ash type from Volz (1973)) also give uncertainties in the total mass (Corradini et al., 2008, Francis et al., 2012, Wen and Rose, 1994). Wen and Rose (1994) studied the volcanic eruption at Crater Peak, Alaska in 1992 and found that total mass is doubled due to changes in ash particle size distribution. Kylling et al. (2014) found 30 % difference in total mass due to the assumed ash particle shape. The effect of meteorological clouds is seen to both increase and decrease the retrieved ash-mass loading (Kylling et al., 2015).

We assume andesite ash with refractive index from Pollack et al. (1973), spherical ash particles and a lognormal size distribution. The lognormal size distribution is described by the geometric mean radius and the geometric standard deviation. The geometric mean radius is related to the effective radius which is retrieved. To test the sensitivity to the shape of the size distribution the geometric standard deviation was varied between 1.5, 1.75, 2.0 and 2.25, which is a subset of the values used by Francis et al. (2012). The four satellite retrievals with different geometric standard deviations are henceforth referenced as sat 1.5, sat 1.75, sat 2.0 and sat 2.25. Figure 3 shows the total ash mass in the domain for every hour during the Eyjafjallajökull eruption from the four satellite data sets. A larger geometric standard deviation gives a wider size distribution that includes more of the larger ash particles and therefore increased retrieved ash mass loading. The difference between the four satellite sets (fig. 3) show the effect the size distribution shape has on the observed ash loads. For the inversion algorithm an additional uncertainty is assigned to the ash loads in the grid cell. To see the effect of these other than

Atmos. Chem. Phys. Discuss., doi:10.5194/acp-2016-1075, 2017
Manuscript under review for journal Atmos. Chem. Phys.
Published: 27 January 2017

Atmospheric Chemistry and Physics Discussions

size dependent uncertainties on the inversion calculations, four uncertainties are assigned to the satellite data in separate inversion calculations; 0 %, 50 %, 100 % and 200% as a percent of the retrieved column load in each grid cell.

2.4 A priori emissions

Mastin et al. (2009) presents an empirical relationship between observed height and mass emission rate (MER) based on historic volcanic emissions.

$$MER = \left(\frac{H}{2.0}\right)^{?468\ 5} \quad H\ \emptyset$$

The observed plume heights (H) used in this study are given in Arason et al. (2011) with a three hour temporal resolution, density (ρ) for ash is equal as in the model simulations (2500 kg m^{-3}). A priori MER over the eruption period is shown in Figure 3. The a priori emission is distributed uniformly over the total emission column. Mastin et al. (2009) also gave a fine ash fraction for classified volcanoes over the globe based on previous eruptions. Larger tephra are assumed to fall close to the volcano and this tephra associated fraction of the total MER is not available for long range transport and is not included in our simulations. Large tephra is also not observed by the infrared satellite instruments using the BTD technique. Fine ash fraction for the Eyjafjallajökull volcano, classified as a silicic standard case is 0.4 which is higher than the 0.1 fine ash fraction used in Stohl et al. (2011) and Kristiansen et al. (2012). However, 0.4 are chosen to simulate a real case forecasting mode, where this fraction must be assumed as it is likely to be the only information available in the first phase of an emergency. Note this higher fraction involves significantly higher a priori emissions than used by Stohl et al. (2011) and Kristiansen et al. (2012). Note also that the observed heights used to calculate the a priori emissions here are on some occasions lower compared to the more uncertain heights used in the previous mentioned studies as the Arason et al. (2011) heights were not available at the time of these studies. Since a rather conservative a priori method is used here that does not favour any release height over another, the uncertainty range, within which the a priori estimate may fall, is chosen to be for four test cases 25%, 50%, 75% and 100%. We assume that this is informative to understand how uncertainty in the a priori emitted mass weights into the inversion calculations.

2.5 SAL metric

To measure the performance of the model as more observations are added to the inversion algorithm for the source term calculations as well as its forecast ability, the SAL (Structure Amplitude Location) scores (Wernli et al., 2008) are computed and evaluated. The SAL method is an object based quality measure originally developed to evaluate quantitative precipitation forecast with observations, and later applied to air quality forecasts (Dacre, 2011). The same satellite retrieval as used in the inversion assimilation is used as the observation field. This gives the opportunity to study how the model simulations in the analysis and forecast period become more similar to the assimilated data. Objects are identified in the forecast and observations field where parameter values exceed a certain threshold. The equations used to calculate the S, A

Atmos. Chem. Phys. Discuss., doi:10.5194/acp-2016-1075, 2017
Manuscript under review for journal Atmos. Chem. Phys.
Published: 27 January 2017

Atmospheric Chemistry and Physics Discussions

and L components of the method are described in Wernli et al. (2008) and Wilkins et al. (2016a), only a short description will be given here.

As in Wilkins et al. (2016) a more conservative ash threshold value of 0.5 g m^{-2} is chosen to identify objects for the satellite and model fields, even though the satellite detection threshold is considered to be about 0.2 gm^{-2} (Prata and Prata 2012).

For the amplitude component, the average ash mass over the domain are calculated for the modelles and observed fields. A is the normalized difference between these two averages, and ranges between -2 to +2, with 0 being the perfect forecast. An A value of +1 indicates a model overestimation by a factor of 3, and values of 0.4 and 0.67 represent model overestimations of 1.5 and 2 respectively.

The structure component compares the normalized volume objects by scaling the ash loading with the maximum ash loading within each object. Forecast and observed objects are then weighted proportionally to the ash mass of the objects. S is the normalized difference between these weighted modelled and observed volumes. S also ranges between -2 to +2. S is positive when the model ash field is too spread out and flat, while a negative value correspond to a model field that is peaked and/or too small.

The first part of the L component measures the normalized distance between the centres of mass for the modelled and observed fields. Different ash clouds can have the same centre of mass, and the second part of L considers the averaged distance between the centre of mass of the total field and individual objects. Both parts of L ranges between 0 and 1, a maximum of L is +2. The definition of L is however insensitive to the rotation around the centre.

The combined SAL score is given by (|S|+|A|+L), a perfect forecast is given by 0, while the maximum score is 6. The possibility of a perfect score forecast for modelled fields with a posteriori emissions and satellite retrievals is minimal because of the difficulties detecting ash in the satellite data, however the tendencies of a possible improvement in the forecast can be analysed by the use of this method.

The SAL scores are calculated for every 12 and 00 UTC time step after the start of the eruption in the April and May period for all the forecast and assimilation period. Two 48 hour forecast experiments are characterized, one with average and zero emissions estimate included in the forecast period. To only compare the ash clouds that are in areas where the model calculations show ash levels above a (very low) threshold value (see above), false positives in the satellite data are not included. In addition areas with unclassified pixels in the satellite data are excluded for both the observed and modelled fields.

3 Results

3.1 Emission estimate uncertainties

Multiple inversion calculations are performed using the four satellite data sets with the different size distribution shape (sat 1.5, sat 1.75, sat 2.0 and sat 2.25) in combination with varying the uncertainties connected to the a priori source estimate (25%, 50%, 75% and 100%) and satellite retrieval uncertainty due to other factors than size distribution (0 %, 50 %, 100 %

Atmos. Chem. Phys. Discuss., doi:10.5194/acp-2016-1075, 2017
Manuscript under review for journal Atmos. Chem. Phys.
Published: 27 January 2017

Atmospheric Chemistry and Physics Discussions

and 200%.). Figure 4 shows the a priori emission estimate over time during the two periods in April and May, as well as the total range in the a posteriori emission resulting from the multiple inversion calculations. As the amount of ash emitted in the a priori is a function of the observed emission height at the volcano, more ash reflects a higher observed emission column. All our a posteriori estimates reduce the emissions from the a priori, suggesting that the default parameter value for the fine ash fraction of 0.4, as taken from Mastin et al. (2009) is indeed too high as discussed in section 2.4. Other parameters such as density and plume height may also result in too much a priori emission.

In April, a high emission column at the start of the period is followed by reduced column height observations before more ash is emitted again from 16 April 9 UTC. The a posteriori show a large range of solutions for the first plume released. During the low emission period in April all the a posteriori follow the a priori as the inversion can not constraint the a posteriori solution without any satellite observations. On 17 April when the satellite detected more ash, the a posteriori emissions are strongly reduced compared to the a priori estimate, similar to what is found in previous inversion studies using model input data from FLEXPART and NAME (Stohl et al., 2011; Kristiansen et al., 2012). The May period also starts with a high a priori emission estimate, followed by a period with almost constant lower a priori emissions. The a posteriori estimate is strongly reduced for the whole period.

Figure 5 shows the average vertical distribution in the emissions over the April period for the a priori and all inversions performed, grouped into eight ensembles. In Figure 5a) the a priori uncertainty is set to 75 %, and for each of the four different satellite data sets the other-than-size uncertainty of the satellite data is varied from 0 to 200%, giving the shown spread in the vertical emission distribution estimate. In figure 5b) the other-than-size satellite data uncertainty is set to 100% and the a priori emission uncertainty is varied from 25 to 100%. The resulting spread in vertical emission distribution for the different satellite data sets represent the a priori uncertainty.

All a posteriori estimates are strongly reduced compared to the a priori especially at altitudes below 4 km. The reduction of ash in the resulting emission estimate is proportional to the reduction in amount of ash in the satellite retrievals. A posteriori for the satellite data set with most ash (sat 2.25) have higher emissions than the other satellite data set with less ash. As the other-than-size satellite uncertainty is a percentage of the retrieved ash for each grid point, the satellite set with the highest column loads also shows the largest spread (Fig 5a). Comparing figures 5a) and 5b) this spread is however much smaller than that caused by varying the a priori uncertainty (Fig 5b).

Another feature can be found in these plots of the vertical distribution of the emissions and the spread in different heights. Since the inversion redistributes ash emissions to the heights where trough transport processes the best match to satellite observations, the vertical distribution is changed from a priori. The emission close to ground is reduced and the largest spread due to a priori uncertainty is at this altitude (below 4 km) (Fig 5b). More trust in the a priori estimate (low uncertainty) causes the a posteriori estimate to deviate less from the a priori emission profiles (right part of the result envelopes in Fig 5b). The most left profile representing the lowest emission term is attained with high uncertainty for the a priori emissions and little ash mass retrieved by the satellite (sat 1.5). Therefore the a posteriori estimates for this satellite

Atmos. Chem. Phys. Discuss., doi:10.5194/acp-2016-1075, 2017
Manuscript under review for journal Atmos. Chem. Phys.
Published: 27 January 2017

data set have the largest spread as a function of variation in a priori uncertainty. The corresponding vertical emission distribution plots for the May period show similar results (not shown).

The spread in a posteriori estimates caused by varying the inversion input, both with regards to the column loads in the satellite retrieval and uncertainties connected to them and the a priori emission uncertainty represent the ambiguity in the a posteriori. Ideally, uncertainties should be set at values that are representative of the real uncertainties connected to the data, however these uncertainties are often not well known at the start of an eruption. Using a range of uncertainty values provides insight into the confidence of the results and should ideally be performed during real case operational setting. This is unfortunately computationally demanding and practically not feasible. The spread of a posteriori estimates presented here can however contribute to further interpretation of the a posteriori results in the case of future volcanic eruptions dealt with in an operational setting.

For the remainder of the results presented in this study, an other-than-size satellite uncertainty of 100 % and an a priori uncertainty of 75 % will be used on the 1.75 satellite retrieval data that are termed “the reference a posteriori”, shown as magenta line in Figure 4. The inversion result and associated simulation is typical for our ensemble. Table 1 shows for instance that the total emitted fine ash for the a priori emission estimate is reduced by around 45 % for April and 65 % for May in the reference a posteriori seen against the a priori emission estimate. The different ranges of the total a posteriori ash emission for the different satellite retrievals, the other-than-size satellite uncertainties and the a priori uncertainties input are also calculated by fixing the other two parameters as the reference. For both periods, the largest spread is caused by the four different satellite retrievals while changing the other-than-size satellite uncertainty produces the smallest spread. Since this smaller spread is seen to depend on the amount of ash in the satellite retrieval, forecast simulations are therefore also done for the 2.25 satellite retrieval with the same uncertainty estimates as for the reference (orange line in Figure 4).

3.2 Inversion in forecasting-mode

In a real volcanic alert case, more and more information will become available while the event is enfolding. To test and investigate the change in the a posteriori estimate as more observations become available, new inversion calculations are made every 12 hours of the 4 day periods in April and May. The first inversion calculations become available on 00 UTC 15 April and 00 UTC 6 May with observations accumulated up until that time (24 hours of satellite observations). It would have been possible to do the first inversion calculations before this first time step, the satellite observations often have problems detecting the ash close to Iceland due to the high optical thickness of the ash cloud close to the volcano so only a few satellite observations are available. Figure 6 and 7 show the a priori as well as a subset of the consecutive a posteriori vertical distribution emission estimates at three-hourly resolution, calculated with observations that would have been available up until 00 UTC for each day of interest in April and May, respectively. Comparing multiple consecutive estimates illustrates how robust the a posteriori emission is, especially for the first high ash emissions in the periods.

The first a posteriori estimate calculated with satellite data up until 15 April 00 UTC shows a strong reduction in the emissions compared to the a priori over the 9 UTC to 18 UTC 14 April emission columns (figure 6). Adding another 24

Atmos. Chem. Phys. Discuss., doi:10.5194/acp-2016-1075, 2017
Manuscript under review for journal Atmos. Chem. Phys.
Published: 27 January 2017

Atmospheric Chemistry and Physics Discussions

hours of satellite observations increases the emissions at 8 km height, while reducing the emissions closer to ground. This redistribution is caused by the transport patterns seen in the satellite ash images, which imply that transport happened at high altitudes and not at low altitudes. Even more observations including days 3 and 4 only change the 14-15 April emission estimate slightly. Figure 4 shows that the a posteriori estimates have minimal differences compared to the a priori between 15 April 12 UTC and 17 April 00 UTC. The larger impact of the inversion on emission estimates altering the a priori to rather low values for the second part of the emissions on 17 April is caused by only a few hours of satellite observations.

Figure 7 shows that the high emission estimates during the first 24 hours of the May period overall are also reduced early on in the first inversion result. The first nine hours show agreement between a priori and a posteriori. For the 15 UTC to 21 UTC period on 5 May, there are numerous height levels where emissions are zero. This is caused by how the inversion algorithm handles unphysical negative inversion calculations that are caused by inaccuracies in model and data. The standard error for these negative source vector elements are reduced and inversion calculations are repeated until the sum of all negative emissions is less than 1 % of the sum of positive emissions (Eckhardt et al. 2008). Small negative emissions that are still present in the estimate are set to zero. By adding more observations, these artefacts are reduced and the negative values are replaced by very low emissions, indicating a more confident estimate. Another noticeable factor is the number of observations needed to reduce the emission released between 21 UTC 6 May and 00 UTC 7 May. The first estimate calculated at 8 May 00 UTC shows little reduction, only when more observations up to 8 May 12 UTC are included (not shown, but visible in the 9 May 00 UTC inversion) these emissions become small. Similar difficulties to correct the night-time emission are seen for the 21 UTC 7 May to 00 UTC 8 May emission as well as during the April period. The reason for this is beyond the scope of this study however the results indicate that there is an increased uncertainty connected to the inversion method attempting to derive night-time emissions.

Figure 8 shows where the differences in vertical emission distribution are located when two satellite data sets are fed into the inversion calculation for the two periods. Although more ash in the satellite retrieval sat 2.25 causes the source emission to have higher emission fluxes, the change in a posteriori emissions when adding more observations are similar for the 1.75 and 2.25 satellite retrievals for both the April and May period. Although the biggest differences are seen for the same emission time as the maximum flux of the emission estimate during the two periods, the largest differences are closer to ground. The increase of the maximum emission fluxes at the higher levels between the two satellite retrieval is minimal. During April, the highest emission level is transported quickly out of the domain while lower levels are transported over Europe with larger differences between the satellite retrievals. For the May period, the large difference below 4 km are caused by the satellite retrieval in sat 2.25 having an increase over time in column loading for the southerly part of the plume that is not present in the sat 1.75. This different increase is ash loading over time between the different satellite retrievals is because the size distribution enters the radiative transfer equation non-linearly. The emissions released at higher levels have been transported further north and are not affected by this.

Atmos. Chem. Phys. Discuss., doi:10.5194/acp-2016-1075, 2017
Manuscript under review for journal Atmos. Chem. Phys.
Published: 27 January 2017

Atmospheric Chemistry and Physics Discussions

3.3 Forecast model results compared to satellite observations

Figure 9 show the ash distribution satellite retrievals (sat 1.75) every 12 hour from 16 April 12 UTC to 17 April 12 UTC. It also shows corresponding model results for a simulation with an emission estimate calculated up to the satellite observation and corresponding results including a 36 hour forecast period, applying a mean forecasted emission term established for the 12h preceding to the start of the forecast. All the model results have more extensive ash clouds compared to the observed ash clouds. Maximum concentrations are however high in the observed data (10.5 g m^{-2}, 9.5 g m^{-2} and 6 g m^{-2} on 16 April 12 UTC, 17 April 00 UTC and 17 April 12 UTC respectively). Disregarding areas close to the volcano, Figure 9b shows that initially simulated ash concentrations, right after the assimilation period, have the highest concentrations of ash in the area of observed ash, but with a maximum of 5.1 g m^{-2} the modelled ash column values are lower compared to the maximum values in the observations. The forecast started using the first emission estimate, covering emissions released before 15 April 00 UTC (Fig. 9c), have high a posteriori emissions and therefore also high forecast emissions causing a large amount of ash to be released into the atmosphere, and have maximum column load of 19.5 g m^{-2} in the area where the satellite retrieve ash. The model simulation does not manage to transport narrow ash clouds with high concentrations due to numerical diffusion and the optimized field (Fig 9b) therefore have smaller maximum values. For the next forecasts starting 12 hours later (Fig. 9f), the emissions are already reduced. Differences between the forecast starting on 17 April 00 UTC (Fig. 9e) and the 36 hour forecast (fig. 9f) are minimal due to low emissions during this time, both have maximums over central Europe at 4.0 g $m^{-2}$and 5.1 g m^{-2} for the initial and forecast respectively. In both model simulations there is an area with higher column loads to the south of Iceland due to more emissions being accumulated by weak northerly winds. No ash is retrieved in the satellite observation. For the satellite plot in Fig. 9g retrieved 12 hours later, ash is detected to the east of Iceland that is released before 12 hours prior demonstrating the difficulty of retrieving the opaque ash clouds close to Iceland. For this retrieval, there is also no ash detected over Europe, even though ash was observed over Europe at this time (Pappalardo et al. 2013).

The exemplary results in Figure 9 show that for a 36 hour forecast, being a long forecast including an unknown emission estimate, rapid changes in the mass eruption rate may lead to significant error.

While the ash observations during the April episode are characterized by small observed ash clouds with high ash concentrations, the observations of the ash during the May period show larger ash clouds with lower column loadings. Figure 10a and 10b show retrieved satellite ash on 8 May 12 UTC for the 1.75 and 2.25 size distributions. Model results with emission estimate calculated with the respective satellite retrieval calculated up to 8 May 12 UTC and a 36 hour forecast from 7 May 00 UTC is also shown. Because of small ash emission estimated from 6 May 00 UTC onwards the differences between the forecast emission estimate and the assimilated estimate is minor, except for more ash south of Iceland for both satellite retrievals for the initial simulation. As discussed in the previous section, for the most southerly ash cloud in the 2.25 satellite retrieval the ash column loads increase over time and cause the cloud in the model results in Figure 10e to have more ash than in the forecast simulation (Fig. 10f) even though this emission is already inverted from previously

Atmos. Chem. Phys. Discuss., doi:10.5194/acp-2016-1075, 2017
Manuscript under review for journal Atmos. Chem. Phys.
Published: 27 January 2017

observations of the ash cloud. This change in the emission estimate for distant, early emissions caused by more satellite observations demonstrates the ability to improve ash simulations, if ash was obscured by clouds in earlier retrievals.

3.4 Performance quantification forecasts

The SAL score and its components (see section 2.5) are calculated every 12 hours during the simulation periods including the assimilation period plus a 48 hour forecast to quantify the performance of the model as more and more observations are added. SAL scores are also calculated for a simulation using the a priori estimate to estimate how the assimilated source term improves over the a priori.

For the April period, the retrieved satellite ash clouds are small compared to model clouds and consequently the S and A scores become very high. An exception is for the 17 April 00 UTC retrieval where the areas with unclassified retrievals are large over Europe (Fig. 9d). This large unidentified area is due to high emissivity over land during night time that disrupts the brightness temperature retrieval quality. Removal of these areas in the model data causes the fields to be more comparable. Even though the model ash clouds are indeed larger and more spread than the observed ash for the period, comparing the observed and modelled fields for this time provides some information about how the amount of ash are changed by adding more observations. Table 2 shows the SAL scores for the two satellite retrievals (sat 1.75 and sat 2.25) and the corresponding model stimulations with the emission estimates constrained by the satellite retrievals. For the simulations where the assimilation period and inversion estimate ends before the comparison time (15 April 00 UTC to 16 April 12 UTC) the 12h averaged forecast emission estimate is added, while for the rest of the model simulations (17 April 00 UTC to 18 April 00 UTC) the observation is included in the assimilation calcualtions. Compared to the a priori estimate, all forecast model results are worse for the structure (S) component because of the too spread out model fields. The amplitude (A) scores that measures the amount of ash in the domain is however improved for the second assimilation with forecast estimate (0415 12 UTC + 36 hours) and the preceding simulations.. The structure score does not improve until the 17 April 00 UTC satellite observation is included in the assimilation (three lasts lines in Table 2). This improvement is due to a smaller area over the 0.5 threshold over Europe in these simulations.

Figure 11 shows all the SAL scores in the May period for satellite observations and the model simulations for the sat 1.75 (a) and the sat 2.25 (b) size assumptions. SAL score calculations are in addition done for a 48 hours forecast with the last 12 hours average emission estimate (dashed lines) and zero emission (solid lines) over the forecast period. Because of the optical thick ash cloud close to the volcano there is no ash originating from the Eyjafjallajökull eruption in the 5 May 12 UTC satellite retrieval, it is not possible to calculate the location (L) and structure (S) scores for these times and the amplitude (A) gives the worst score (2) due to infinitely more model ash than satellite. SAL scores generally are better during the May period because of the increased amount and areas with retrieved ash for the observation field compared to the April period. The first emissions in the May a posteriori estimate are not reduced enough in the inversion calculations causing the A score to be high for the May 6 00 UTC comparison in all the model comparisons. Transport later in the period aligns this model ash released early with ash released later in the period forming the southern ash cloud (Fig. 10). For the 7

Atmos. Chem. Phys. Discuss., doi:10.5194/acp-2016-1075, 2017
Manuscript under review for journal Atmos. Chem. Phys.
Published: 27 January 2017

May 00 UTC comparison time, the two forecast estimates show good results for the S score, while the model simulations with this observation time late in the assimilation period performs worse. Further into the period as the observations time becomes earlier in the assimilation period the model performs better for both A and S. The two model simulations with assimilation period up to 9 May 00 UTC score better for the A and S than all the other model simulations for most of the comparison times, even though the emission estimate did not change much during this time.

The A and S scores are positive for most comparison times showing that the model fields have more ash and the fields are more spread out than the satellite observations. This can be explained by the difficulty of retrieving ash close to the volcano and ash that are obscured by meteorological clouds.

Ash locations score (L) between satellite and model data is low, both because of the centre of mass is close to each other in the domain, and in addition the L score for the idealized fields shown in Wernli et al. (2008) are lower than the S and A values. Low L values also indicate that the transport of ash in the model compare well to observations which also indicate that the ash emissions are placed in the right layer.

Although the emission estimates are calculated by using different satellite retrievals and compared to their respective satellite data, the scores for the two satellite data sets do not show large differences. The difference in the S score on 17 April 00 UTC is caused by less ash in the small objects for the 1.75 observed fields. For the May period, the S scores are similar to each other however more ash in the 2.25 satellite retrievals compare better to the amount of ash in the model simulations leading to a better A score for the 2.25 satellite retrievals.

4 Discussion

Emission fluxes in the a posteriori estimates depend on the amount of ash in the satellite retrieval and the weighting of uncertainties connected to the input data to the inversion. Giving the a priori estimate a high uncertainty causes the a posteriori estimate to deviate from the a priori while assigning a high uncertainty to the satellite data forces an inversion solution closer to the a priori emission term. It is therefore important that the a priori and satellite uncertainties connected to these values represent reasonable assumptions. Default settings for an operational setup can ignore some aspects of a volcanic eruption for tephra size distribution and amount in emission.

Of major importance is the uncertainty in the satellite data input to the inversion, and especially the change in ash loads by using different assumptions about the shape of the ash size distribution. The results in this study show that the spread in a posteriori estimates due to other-than-size satellite uncertainties are much smaller compared to the spread when using the four different satellite sets with different size distributions. For the a posteriori estimate it is therefore important to use the best available assumptions in the satellite retrieval rather than correct other-than-size uncertainty assumptions.

Satellite retrievals from other satellites instruments with better spatial resolution such as for example MODIS (Moderate Resolution Imaging Spectroradiometer), IASI (Infrared Atmospheric Sounding Interferometer) and VIIRS (Visible Infrared Imaging Radiometer Suite) may provide more confidence in the extent of the ash clouds (Clarisse et al., 2010). Such

Atmos. Chem. Phys. Discuss., doi:10.5194/acp-2016-1075, 2017
Manuscript under review for journal Atmos. Chem. Phys.
Published: 27 January 2017

retrievals may carry similar uncertainty for finding ash mass, but may bring additional size info and separation of ash from cloud. Satellite information can also give information about the height of the ash layer. This may be obtained from dual view instruments such as SLSTR (The Sea and Land Surface Temperature Radiometer), and space borne lidars such as CALIOP (Cloud-Aerosol Lidar with Orthogonal Polarization) also provide valuable information if their narrow footprint match the ash cloud (Winker et al., 2012).

The SEVIRI satellite observations have high temporal resolution as a new retrieval is available every 15 minutes for the whole domain. Polar-orbiting satellites on the other hand, may only observe a small part of the domain during an overpass. Stohl et al. (2011) show that performing inversion with only IASI retrievals may provide a too small sampling size to constrain the solution. Ash mass loadings from other satellite retrievals with better aerosol detection capability are nevertheless useful for comparisons with the amount of ash in the SEVIRI retrieval and a possible combination of the satellite retrievals with the SEVIRI retrieval for the inversion.

The a posteriori solution is found to only use the a priori estimate in the absence of ash in the satellite retrievals, this solution is independent on the uncertainty settings for a priori and satellite data. A good a priori estimate is therefore important for these cases. Observed heights from Arason et al. (2011) obtained by weather radars are used in this study, and the heights show a good match with the maximum a posteriori heights. However the fine ash fraction is found to be too large causing too much ash to be released during the April period. Observations and more information are needed to produce a good a priori estimate. At the time of the Eyjafjallajökull eruption, Iceland had only one operational weather radar to observe the plume height, situated at Keflavik International Airport, 155 km to the west of the volcano (Arason et al. 2011). Another permanent weather radar is now situated on the eastern part of Iceland, and two mobile radars are prepared (Jordan et al. 2013). Monitoring of activity on Iceland is also improved by the FUTUREVOLC project (http://futurevolc.hi.is), and will increase the amount of observations available in the case of future volcanic eruption.

Even when using higher a priori emission heights for the estimate for the Eyjafjallajökull eruption as in Stohl et al. (2011) and Kristiansen et al. (2012), their results show that the inversion algorithm places ash at equal heights as found in this study. The fine ash fraction of 0.1 used in Stohl et al (2011) and Kristiansen et al. (2012) gives however a better match than the too high 0.4 used in this study for the periods where the satellite observations are too few to constrain the a posteriori (and a posteriori therefore only use the a priori estimate). Eckhardt et al. (2008) showed that a posteriori estimates calculated with no emission in the a priori emission gave similar results to a posteriori estimates calculated with estimated emissions in the a priori. A posteriori estimates are also calculated with low ash emissions in the a priori estimates in the Moxnes et al. (2014) and Kristiansen et al. (2015) studies. Ash can however be obscured by meteorological clouds and optical thick ash clouds may not be detected, so an a priori emission with ash is therefore considered more conservative. A parallel sensitivity calculation with no or little ash in the a priori estimation is possible in case of a volcanic eruption but not done in this study.

The insertion method presented in Wilkins et al. (2016a) and a refined method in Wilkins et al. (2016b) only takes into account the ash in the satellite retrievals and adds no additional emissions from the volcano in the forecast, eliminating the concerns with the a priori emissions for periods with no ash detected. By inserting several ash retrievals in the model field

Atmos. Chem. Phys. Discuss., doi:10.5194/acp-2016-1075, 2017
Manuscript under review for journal Atmos. Chem. Phys.
Published: 27 January 2017

Atmospheric Chemistry and Physics Discussions

over several times, possible undetected ash can be included in the calculations as it may become visible in later satellite retrievals. Comparing the insertion and the inversion methods for 16 April 2010 12 UTC show that the insertion method have ash clouds only at similar location as the observations while the results presented here have too extensive ash clouds. Wilkins et al. (2016a) also present SAL metric results from 8 May 2010 9 UTC. Although not calculated at the same satellite retrieval time, the SAL metric results in this study for May are better for a long forecast period. The amplitude score for the insertion method show that the averaged mass in the model results is less than retrieved ash, while in this study model simulations have more ash than in the retrieval. Some of these differences are caused by the inversion calculations using only the a priori estimate in the absence of satellite observations, for the April period, and how the observations field are defined for the SAL score calculations. In Wilkins et al. (2016a) the observed satellite data is represented by the maximum values retrieved over the previous hour, while in this study, the observations are strictly the ash loading retrieved at the time studied. Another reason is caused by the difficulty the satellite retrievals have detecting high density ash close to the volcano leading both to too much ash in this study that includes these ash clouds in the forecast and possibly too little ash in the insertion method that does not use emissions over the forecast period.

5 Summary and conclusions

In this paper the inversion method is tested in an operational forecasting setting over two short periods of four days during the Eyjafjallajökull eruption. Both of these periods started with high ash emissions during the first day and while the observations of ash during the April period indicated small clouds with high column loadings, the retrieved ash clouds during the May periods were larger in extent with lower column loads. This provides an opportunity to explore the feasibility of using an inversion method to constrain emission in an operational setting where the impact of volcanic eruptions on air traffic shall be assessed. The observed ash cloud during the April period are shown difficult to simulate in the model due to diffusion and the model results with the a posteriori therefore have ash clouds that are more spread out and ash column loads that are lower compared to satellite. The ash clouds observed in the May period are better simulated by the model.

A posteriori emission estimates are calculated with the inversion algorithm for four different satellite data sets with different spread in size assumptions that affect the retrieved ash column loadings. Note that the satellite data also contain areas with unclassified pixels where the satellite retrieval is not able to decide whether ash is present or not. These areas are ignored by the inversion algorithm. The effect of different uncertainties connected to the input satellite data and a priori estimate in the inversion are studied and multiple inversion calculations are documented. Because of the high fine ash fraction (0.4) assumed for Eyjafjallajökull as a silicic standard volcano (Mastin et al. 2009), the a priori estimate has too emission and all the calculated a posteriori emissions are reduced by the inversion. Inversion calculations for the four satellite retrievals with the least ash have the highest deviation from the a priori, and changing the uncertainties connected to the a priori term leads to large spread in the a posteriori estimates. Other-than-size uncertainties connected to the satellite retrieval are found to have lower effect.

Atmos. Chem. Phys. Discuss., doi:10.5194/acp-2016-1075, 2017
Manuscript under review for journal Atmos. Chem. Phys.
Published: 27 January 2017

Atmospheric Chemistry and Physics Discussions

As the inversion routine forces the source term and the model simulations to be more similar to the observed ash values, ultimately better quality data are needed for the retrieved column load values. Combining and comparing the SEVIRI satellite data with ash retrieval from other satellite instruments with different spatial and temporal resolution and different viewing angles are therefore necessary.

In a forecasting mode, the change in a posteriori estimates by adding more observations every 12 hours show, that although the a priori emissions are too high they are reduced early on with only a small amount of satellite observations. Adding more observations at later times of the ash cloud, further away from Iceland, causes the inversion to redistribute the ash emissions to higher altitudes in the Eyjafjallajökull case. The redistribution is caused by ash originating from these upper level emission heights witch are found to match better with the location of the observed ash. The results show that the change in a posteriori estimate by adding more observations are minimal after 36 to 48 hours, in particular for those times where high ash occur. Emission times with no significant ash emissions are reduced after only a few satellite observations, exceptions are found for the night-time emission estimate between 21 and 00 UTC. During the April period, large ash emissions were followed by a period of no or insignificant ash emissions, where no ash is detected in the satellite retrieval. As the a posteriori estimate uses only the a priori for emission times that are not matched with satellite observations, more information about the source term are necessary. For future Icelandic volcanic emissions such information will be available due to the increase in radar coverage in Iceland since the Eyjafjallajökull eruption.

The SAL scores show that the model at most times have more ash that is more spread out than the observations. Discrepancies between the observations and model results are explained by too much ash in the a priori, and undetected ash in the satellite retrieval close to the volcano or obscured by meteorological clouds. Model results with a posteriori emissions decreases the ambiguity to both the forecast and the satellite observations by obtaining model ash loads more comparable to satellite values, and improving confidence in the satellite data by identifying areas with false positives and possible undetected ash.

Acknowledgements

The work done for this paper is funded by the Norwegian ash project financed by the Norwegian Ministry of Transport and Communications and AVINOR. Model and support is also appreciated through the Cooperative Programme for Monitoring and Evaluation of the Long-range Transmission of Air Pollutants in Europe (No: ECE/ENV/2001/003). This work has also received support from the Research Council of Norway (Programme for Supercomputing) through CPU time granted at the super computers at NTNU in Trondheim.

Atmos. Chem. Phys. Discuss., doi:10.5194/acp-2016-1075, 2017
Manuscript under review for journal Atmos. Chem. Phys.
Published: 27 January 2017

References

Arason, P et al. (2011): Plume-top altitude time-series during 2010 volcanic eruption of Eyjafjallajökull. Icelandic Meteorological Office, Reykjavik, doi:10.1594/PANGAEA.760690

Boichu, M., Menut, L., Khvorostyanov, D., Clarisse, L., Clerbaux, C., Turquety, S., and Coheur, P.-F.: Inverting for volcanic SO2 flux at high temporal resolution using spaceborne plume imagery and chemistry-transport modelling: the 2010 Eyjafjallajökull eruption case study, Atmos. Chem. Phys., 13, 8569-8584, doi:10.5194/acp-13-8569-2013, 2013.

Casadevall, T., The 1989–1990 eruption of Redoubt Volcano, Alaska: Impacts on aircraft operations, J. Volcanol. Geotherm. Res.,62(1–4), 301–316, doi:10.1016/0377-0273(94)90038-8, 1994

Clarisse, L., Prata, F., Lacour, J. L., Hurtmans, D., Clerbaux, C., and Coheur, P. F.. A correlation method for volcanic ash detection using hyperspectral infrared measurements. Geophysical research letters, 37(19), 2010.

Corradini, S., Spinette, C., Carboni, E., Tirelli, C., Buongiorno, M. F., Pugnaghi, S., and Gangale, G.: Mt. Etna tropospheric ash retrieval and sensitivity analysis using Moderate Resolution Imaging Spectroradiometer Measurements, J. of Applied Remote Sensing, 2, doi:10.1117/1.3046 674, 2008.

Eckhardt, S., Prata, A. J., Seibert, P., Stebel, K., and Stohl, A.: Estimation of the vertical profile of sulfur dioxide injection into the atmosphere by a volcanic eruption using satellite column measurements and inverse transport modeling, Atmos. Chem. Phys., 8, 3881-3897, doi:10.5194/acp-8-3881-2008, 2008.

European Commission (2011) Volcano Grimsvötn: how is the European response different to the Eyjafjallajökull eruption last year? Frequently Asked Questions, 26 May 211, Available at http://europa.eu/rapid/press-release_MEMO-11-346_en.htm

EMEP MSC-W: Transboundary acidification, eutrophication and ground level ozone in Europe 2014, EMEP Status Report 1/2016, 2016.

Francis, P. N., Cooke, M. C., and Saunders, R.W.: Retrieval of physical properties of volcanic ash using Meteosat: A case study from the 2010 Eyjafjallajökull eruption, Journal of Geophysical Research: Atmospheres, 117, doi:10.1029/2011JD016788, URL http://dx.doi.org/10.1029/2011JD016788, 2012.

Jordan, C., Sigmundsson, F., Vogfjord, K., Gudmundsson, M. T., Kristinsson, I., Loughlin, S., Ilyinskaya, E., Hooper, A., Kylling, A,. Witham, C.; Bean, C.; Braiden, A.; Ripepe, M.; Prata, F. Futurevolc: a European volcanological supersite observatory in Iceland, a monitoring system and network for the future. In: IEEE International Geoscience and Remote Sensing Symposium 2013, Melbourne, Australia, 21-26 Jul 2013. 286-289, 2013.

Kylling, A., Kahnert, M., Lindqvist, H., and Nousiainen, T.: Volcanic ash infrared signature: porous non-spherical ash particle shapes compared to homogeneous spherical ash particles, Atmos. Meas. Tech., 7, 919-929, doi:10.5194/amt-7-919-2014, 2014

Atmos. Chem. Phys. Discuss., doi:10.5194/acp-2016-1075, 2017
Manuscript under review for journal Atmos. Chem. Phys.
Published: 27 January 2017

Kylling, A., Kristiansen, N., Stohl, A., Buras-Schnell, R., Emde, C., and Gasteiger, J.: A model sensitivity study of the impact of clouds on satellite detection and retrieval of volcanic ash, Atmos. Meas. Tech., 8, 1935-1949, doi:10.5194/amt-8-1935-2015, 2015.

Kristiansen, N. I., Stohl, A., Prata, A. J., Richter, A., Eckhardt, S., Seibert, P., Hoffmann, A., Ritter, C., Bitar, L., Duck, T. J. and Stebel K. Remote sensing and inverse transport modeling of the Kasatochi eruption sulfur dioxide cloud, J. Geophys. Res., 115, D00L16, doi:10.1029/2009JD013286, 2010

Kristiansen, N. I., A. Stohl, Prata, A. J., Bukowiecki, N., Dacre, H., Eckhardt, S., Henne, S., Hort, M. C., Johnson, B. T., Marenco, F., Neininger, B., Reitebuch, O., Seibert, P., Thomson, D. J., Webster, H. N. and Weinzierl, B. "Performance assessment of a volcanic ash transport model mini-ensemble used for inverse modeling of the 2010 Eyjafjallajökull eruption." Journal of Geophysical Research: Atmospheres 117.D20, 2012.

Kristiansen, N. I., A. J. Prata, A. Stohl, and S. A. Carn, Stratospheric volcanic ash emissions from the 13 February 2014 Kelut eruption, Geophys. Res. Lett., 42, 588–596, doi:10.1002/2014GL062307, 2015.

Mastin, L. G., et al. "A multidisciplinary effort to assign realistic source parameters to models of volcanic ash-cloud transport and dispersion during eruptions." Journal of Volcanology and Geothermal Research 186.1: 10-21, 2009.

Moxnes, E. D., N. I. Kristiansen, A. Stohl, L. Clarisse, A. Durant, K. Weber, and A. Vogel, Separation of ash and sulfur dioxide during the 2011 Grímsvötn eruption, J. Geophys. Res. Atmos., 119, 7477–7501, doi:10.1002/2013JD021129, 2014

Prata, A. J. "Observations of volcanic ash clouds in the 10-12 μm window using AVHRR/2 data." International Journal of Remote Sensing 10.4-5: 751-761, 1989.

Pappalardo, G., Mona, L., D'Amico, G., Wandinger, U., Adam, M., Amodeo, A., Ansmann, A., Apituley, A., Alados Arboledas, L., Balis, D., Boselli, A., Bravo-Aranda, J. A., Chaikovsky, A., Comeron, A., Cuesta, J., De Tomasi, F., Freudenthaler, V., Gausa, M., Giannakaki, E., Giehl, H., Giunta, A., Grigorov, I., Groß, S., Haeffelin, M., Hiebsch, A., Iarlori, M., Lange, D., Linné, H., Madonna, F., Mattis, I., Mamouri, R.-E., McAuliffe, M. A. P., Mitev, V., Molero, F., Navas-Guzman, F., Nicolae, D., Papayannis, A., Perrone, M. R., Pietras, C., Pietruczuk, A., Pisani, G., Preißler, J., Pujadas, M., Rizi, V., Ruth, A. A., Schmidt, J., Schnell, F., Seifert, P., Serikov, I., Sicard, M., Simeonov, V., Spinelli, N., Stebel, K., Tesche, M., Trickl, T., Wang, X., Wagner, F., Wiegner, M., and Wilson, K. M.: Four-dimensional distribution of the 2010 Eyjafjallajökull volcanic cloud over Europe observed by EARLINET, Atmos. Chem. Phys., 13, 4429-4450, doi:10.5194/acp-13-4429-2013, 2013

Pollack, J. B., O. B. Toon, and B. N. Khare (1973), Optical properties of some terrestrial rocks and glasses, Icarus, 19, 372–389, doi:10.1016/0019-1035(73)90115-2.

Prata, A. J., and A. T. Prata (2012), Eyjafjallajökull volcanic ash concentrations determined using Spin Enhanced Visible and Infrared Imager measurements, J. Geophys. Res., 117, D00U23, doi:10.1029/2011JD016800.

Schmetz, J., Pili, P., Tjemkes, S., & Just, D. (2002). An introduction to Meteosat second generation (MSG). Bulletin of the American Meteorological Society,83(7), 977.

Atmos. Chem. Phys. Discuss., doi:10.5194/acp-2016-1075, 2017
Manuscript under review for journal Atmos. Chem. Phys.
Published: 27 January 2017

Seibert, P.: Inverse modelling of sulfur emissions in Europe based on trajectories, In: Inverse Methods in Global Biogeochemical Cycles, edited by: Kasibhatla, P., Heimann, M., Rayner, P., Mahowald, N., Prinn, R. G., and Hartley, D. E., Geophysical Monograph 114, American Geophysical Union, ISBN 0-87590-097-6, Washington, DC, USA, 147–154, 2000.

Simpson, D., Benedictow, A., Berge, H., Bergström, R., Emberson, L. D., Fagerli, H., Flechard, C. R., Hayman, G. D., Gauss, M., Jonson, J. E., Jenkin, , M. E., Nyíri, A., Richter, C., Semeena, V. S., Tsyro, S., Tuovinen, J.-P., Valdebenito, A. and Wind, P. The EMEP MSC-W chemical transport model–technical description. Atmospheric Chemistry and Physics, 12(16), 7825-7865, 2012.

Steensen, B. M., Schulz, M., Wind, P., Valdebenito, Á., and Fagerli, H.: The operational eEMEP model for volcanic SO2 and ash forecasting, Geosci. Model Dev. Discuss., doi:10.5194/gmd-2016-315, in review, 2017.

Stohl, A., Prata, A. J., Eckhardt, S., Clarisse, L., Durant, A., Henne, S., Kristiansen, N. I., Minikin, A., Schumann, U., Seibert, P., Stebel, K., Thomas, H. E., Thorsteinsson, T., Tørseth, K., and Weinzierl, B.: Determination of time- and height-resolved volcanic ash emissions and their use for quantitative ash dispersion modeling: the 2010 Eyjafjallajökull eruption, Atmos. Chem. Phys., 11, 4333-4351, doi:10.5194/acp-11-4333-2011, 2011.

Wen, S. and Rose, W. I.: Retrieval of sizes and total masses of particles in volcanic clouds using AVHRR bands 4 and 5, J. Geophys. Res., 99, 5421–5431, 1994.

Wernli, Heini, et al. SAL-A novel quality measure for the verification of quantitative precipitation forecasts. Monthly Weather Review 136.11, 4470-4487, 2008.

Wilkins, K. L., et al. "Using data insertion with the NAME model to simulate the 8 May 2010 Eyjafjallajökull volcanic ash cloud." Journal of Geophysical Research: Atmospheres 121.1, 306-323, 2016a.

Wilkins, K. L., L. M. Western, and I. M. Watson. Simulating atmospheric transport of the 2011 Grímsvötn ash cloud using a data insertion update scheme. Atmospheric Environment 141 , 48-59. 2016b

Winker, D. M., Z. Liu, A. Omar, J. Tackett, and D. Fairlie, CALIOP observations of the transport of ash from the Eyjafjallajökull volcano in April 2010, J. Geophys. Res., 117, D00U15, doi:10.1029/2011JD016499, 2012.

Yu, Tianxu, William I. Rose, and A. J. Prata. Atmospheric correction for satellite-based volcanic ash mapping and retrievals using “split window” IR data from GOES and AVHRR. Journal of Geophysical Research: Atmospheres 107.D16, 2002.

Atmos. Chem. Phys. Discuss., doi:10.5194/acp-2016-1075, 2017
Manuscript under review for journal Atmos. Chem. Phys.
Published: 27 January 2017

Atmospheric Chemistry and Physics Discussions

Table 1: Total fine ash emissions in Tg over the April and May period for the a priori estimate and the reference a posteriori with the satellite retrieval with 1.75 geometric standard deviation, 100 % uncertainty in the satellite data and 75 % uncertainty of the a priori emission. The minimum and maximum a posteriori emission with varying the satellite input data with different retrieval assumptions, uncertainty connected to the satellite retrieval and a priori uncertainty while keeping the other uncertainties equal to the reference. The percent the sensitivity spreads are on the reference are also calculated for the two periods.

	April	May	% of reference April	% of reference May
A priori	17.4	13.3		
Reference a posteriori	9.5	4.7		
Sat ret. (min/max)	9.4/11.0.	4.2/6.4	26%	47%
Sat uncert (min/max)	9.4/9.5	4.7/4.8	1%	2%
A pri uncert (min/max)	9.0/11.4	4.7/5.8	25%	23%

.

Table 2: Structure Amplitude Location (SAL) scores (ranging from -2 to 2 for structure and amplitude, and 0 to 2 for location, best is 0 for all) for different model simulations for comparison on the 17 April 00 UTC using satellite retrievals (sat 1.75 and sat 2.25, see text). The model simulations that end the assimilation window before the comparison, and then use assumed forecast emission are marked as +hh hours. The last three lines correspond to simulations where the forecast starts after the observation comparison time.

Model forecast	Structure		Amplitude		Location	
	sat 1.75	sat 2.25	sat 1.75	sat 2.25	sat 1.75	sat 2.25
A priori	0.20	0.37	1.82	1.69	0.26	0.22
Forecast starting before 17 April 00 UTC						
0415 00 UTC + 48 hours	0.92	1.05	1.90	1.83	0.18	0.13
0415 12 UTC + 36 hours	0.57	0.77	1.75	1.62	0.20	0.16
0416 00 UTC + 24 hours	1.00	1.23	1.21	0.91	0.32	0.25
0416 12 UTC + 12 hours	0.36	0.75	1.66	1.47	0.24	0.22
Simulations with observation included in the assimilation to the inversions						
0417 00 UTC	-0.21	0.32	1.79	1.66	0.23	0.21
0417 12 UTC	-0.18	0.35	1.78	1.65	0.23	0.21
0218 00 UTC	-0.15	0.42	1.78	1.65	0.24	0.21

Atmos. Chem. Phys. Discuss., doi:10.5194/acp-2016-1075, 2017
Manuscript under review for journal Atmos. Chem. Phys.
Published: 27 January 2017

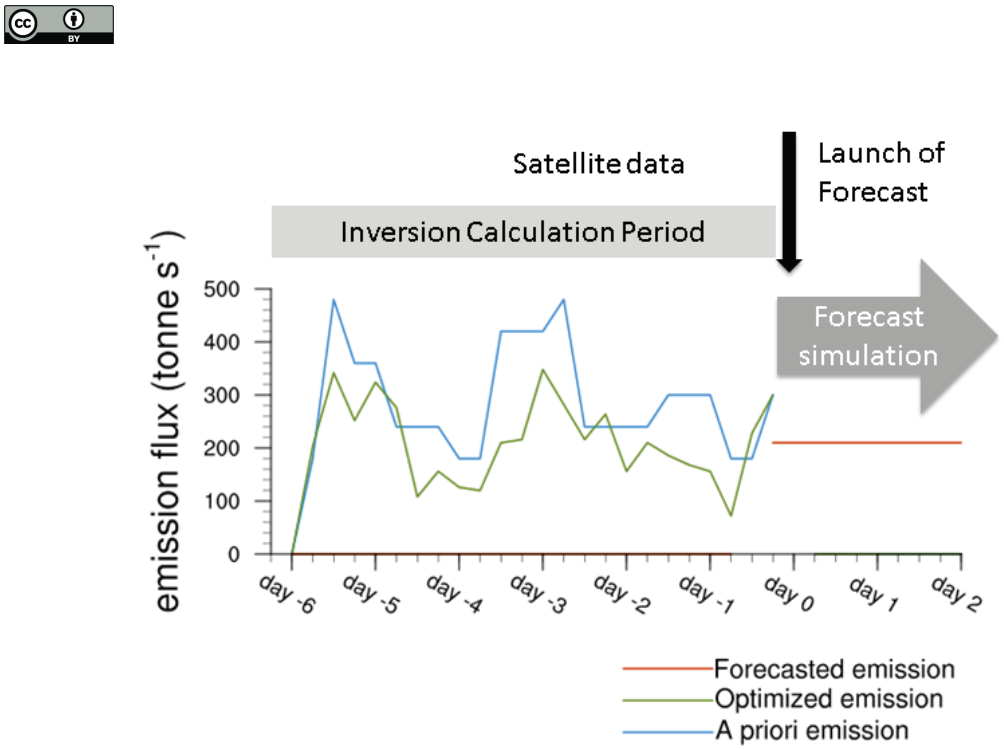

Figure 1: Scheme of how the evolution of ash emissions used in the eEMEP model simulations may look like, with an a priori emission estimate, the calculated a posterior (optimized) emission estimate and a forecast emission estimate.

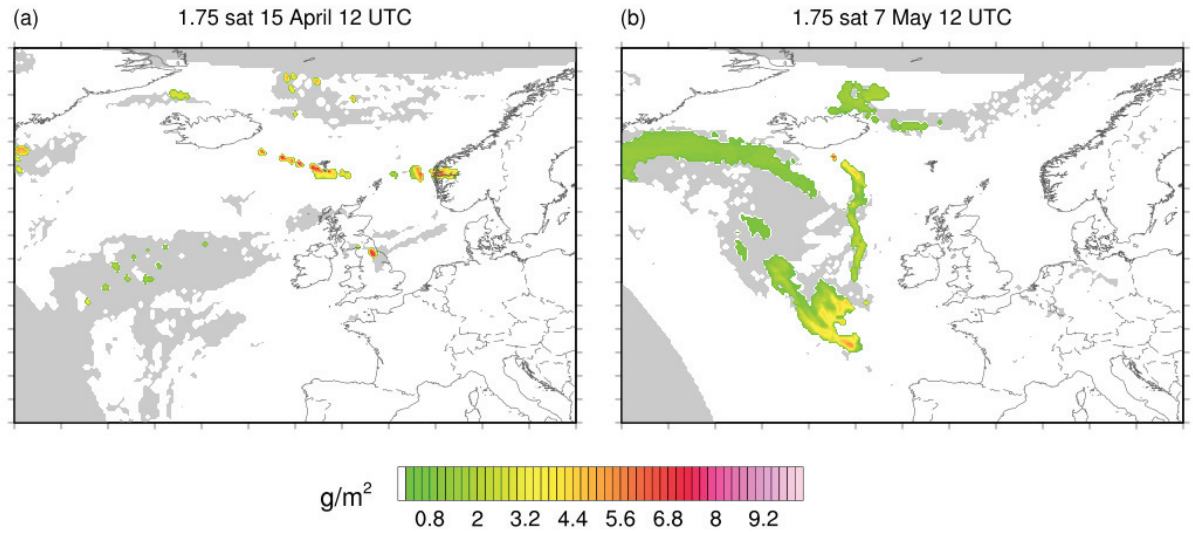

Figure 2: SEVIRI satellite ash mass loading with a 1.75 lognormal size distribution on 15 April 12 UTC and 7 May 12 UTC 2010. The grey areas show the unidentified pixels, where the ash retrieval can not distinguish if contain ash or not.

Atmos. Chem. Phys. Discuss., doi:10.5194/acp-2016-1075, 2017
Manuscript under review for journal Atmos. Chem. Phys.
Published: 27 January 2017

Atmospheric Chemistry and Physics Discussions

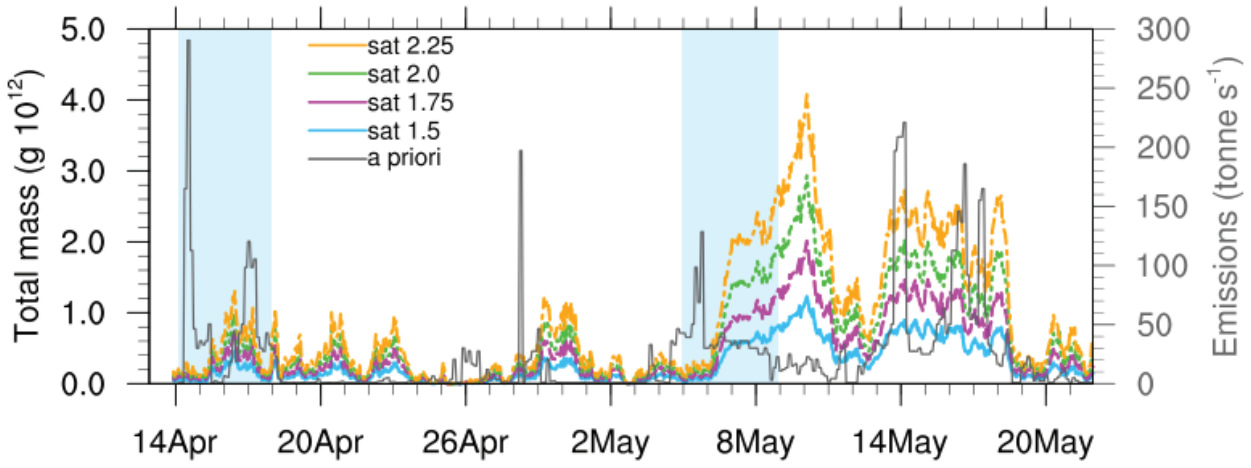

Figure 3: Left axis, the total mass of ash in the domain for the four satellite retrievals with different size distribution assumptions (sat 1.5 – 2.25), for every hour over the entire Eyjafjallajökull eruption period. Right axis shows the emissions in the a priori estimate calculated from observed plume height at the volcano. The blue shaded areas indicate the periods studied in the paper.

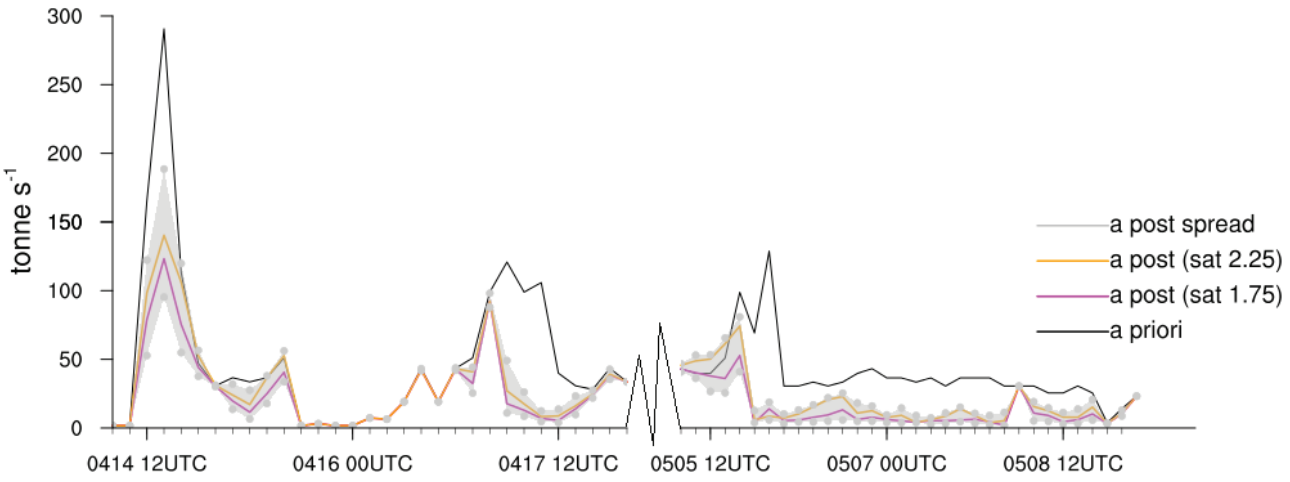

Figure 4: A priori ash emissions and the spread of a posteriori ash emissions calculated by the inversion algorithm using the different uncertainties and satellite data sets during the April and May periods (the break on the x-axis indicate the change in time periods). Magenta and orange lines are a posteriori emissions calculated from inversions assuming a priori uncertainty of 75% and satellite uncertainty set at 100%, using a spread in ash distribution of 1.75 and 2.25 in the satellite retrieval.

Atmos. Chem. Phys. Discuss., doi:10.5194/acp-2016-1075, 2017
Manuscript under review for journal Atmos. Chem. Phys.
Published: 27 January 2017

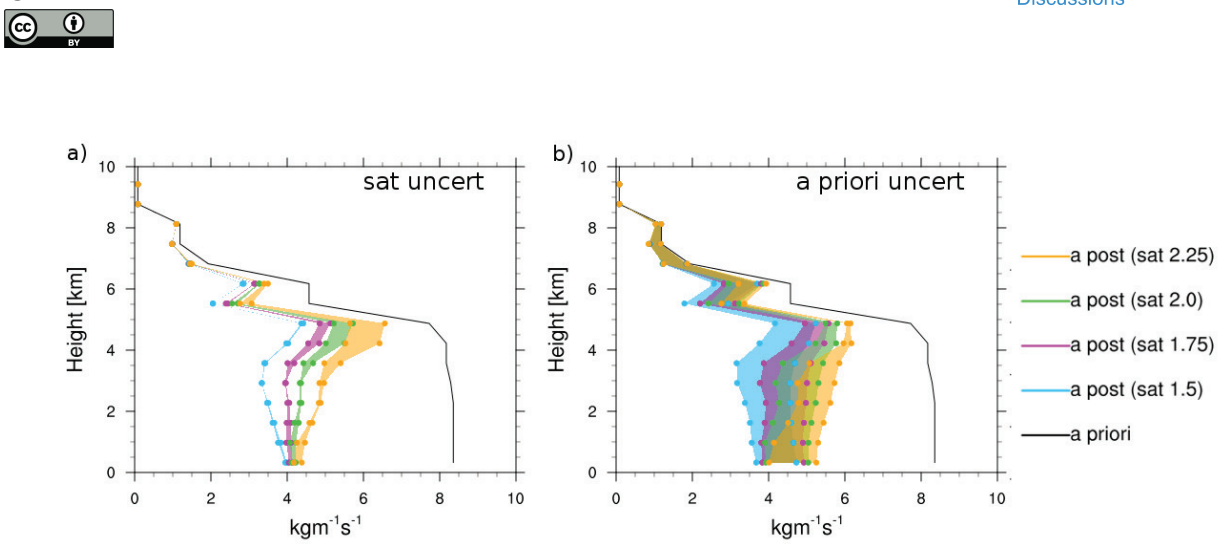

Figure 5: Spread of a posteriori for the four satellite data sets with the four different size distribution assumptions (sat 1.5 – 2.25). Left plot show the spread in a posteriori caused by varying the uncertainty connected to the satellite data, with a priori uncertainty set at 75 %. The right plot shows the spread in a posteriori caused by varying a priori uncertainty, with a constant satellite uncertainty at 100 %.

Atmos. Chem. Phys. Discuss., doi:10.5194/acp-2016-1075, 2017
Manuscript under review for journal Atmos. Chem. Phys.
Published: 27 January 2017

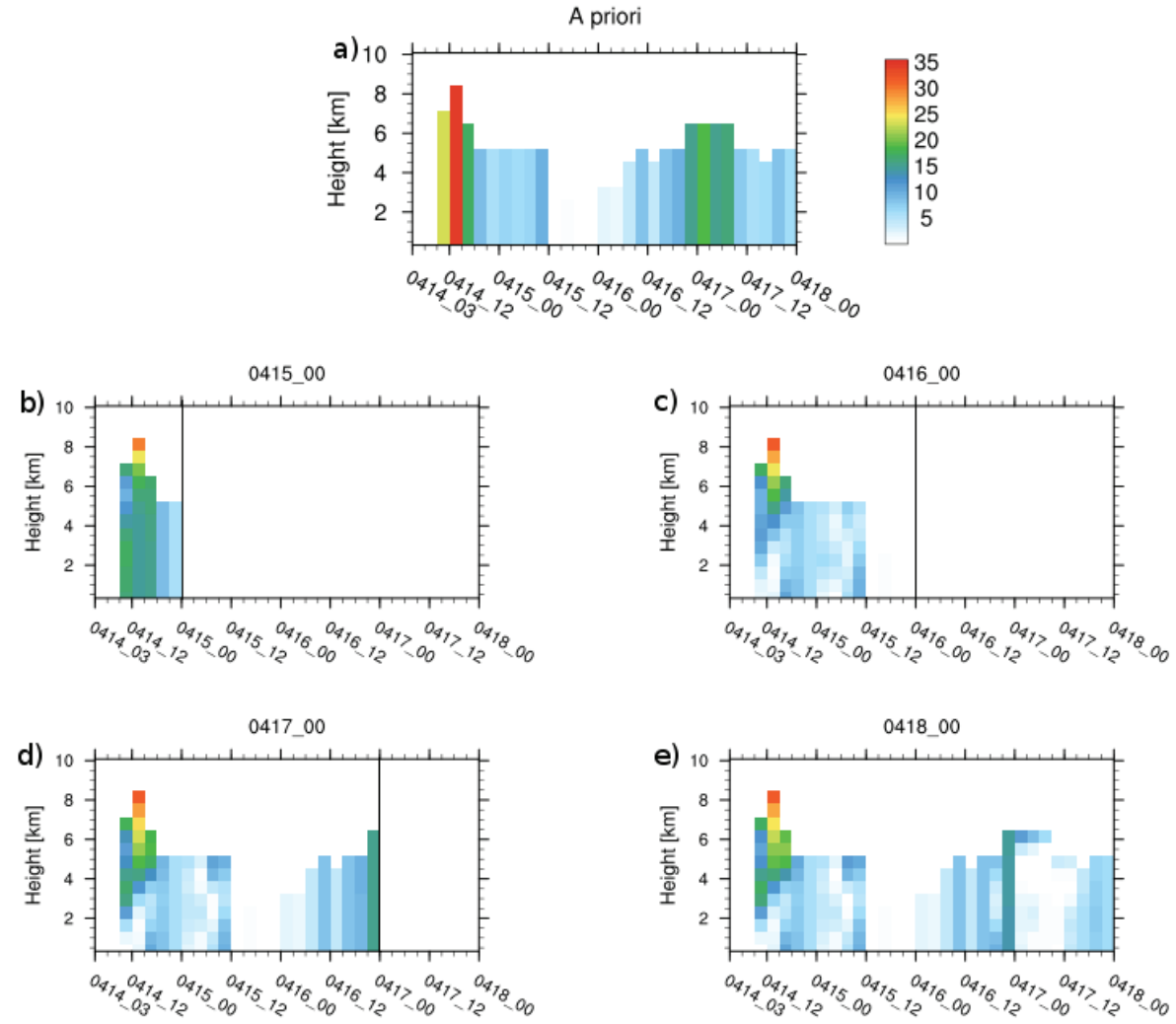

Figure 6: Vertical emission distributions over the volcano with three hour resolution, given in kgm^{-1}s^{-1}. A priori source term (top row) and a posteriori source terms (middle and bottom row) by using satellite observations up until the start of the forecast time (vertical black line) over the April period. Only the a posteriori term for the 00 UTC forecasts are shown.

5

Atmos. Chem. Phys. Discuss., doi:10.5194/acp-2016-1075, 2017
Manuscript under review for journal Atmos. Chem. Phys.
Published: 27 January 2017

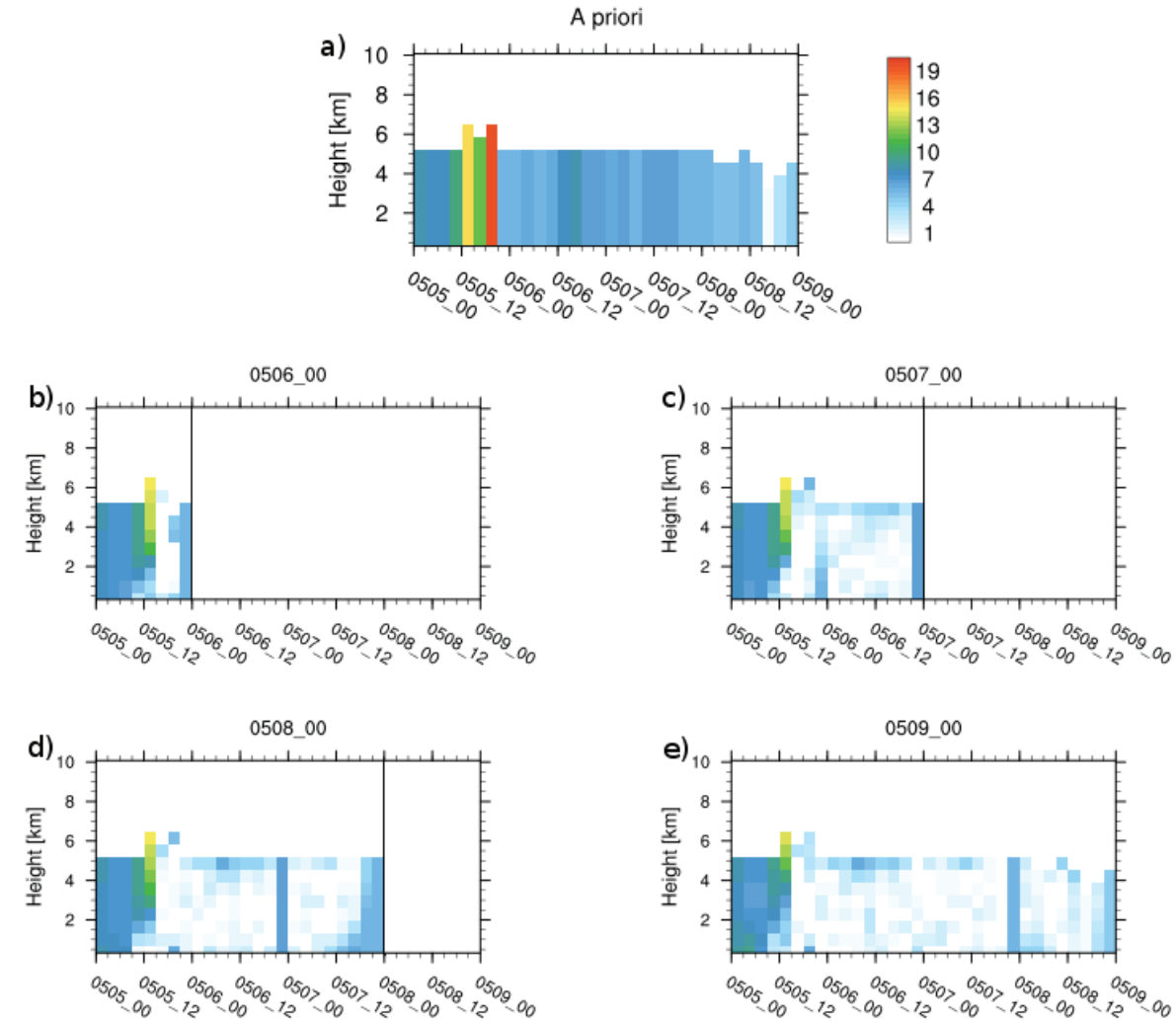

Figure 7: Same as figure 6 but for the May period.

Atmos. Chem. Phys. Discuss., doi:10.5194/acp-2016-1075, 2017
Manuscript under review for journal Atmos. Chem. Phys.
Published: 27 January 2017

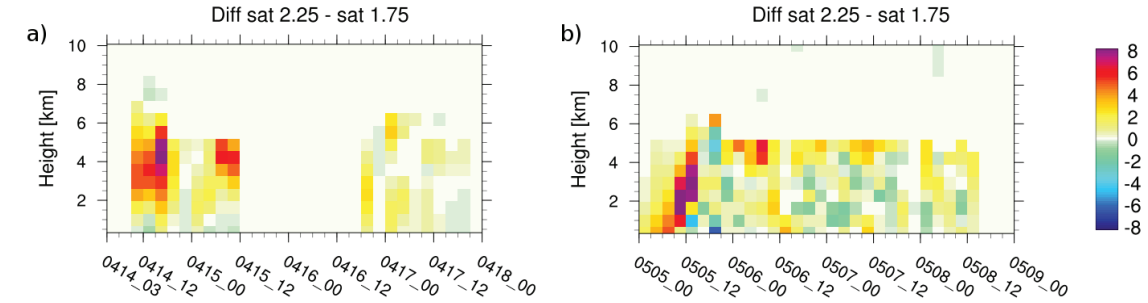

Figure 8: The difference in emissions (kg m^{-1} s^{-1}) between the a posteriori estimates for the inversions using the 2.25 and 1.75 satellite data sets over the two periods in April (left) and May (right).

Atmos. Chem. Phys. Discuss., doi:10.5194/acp-2016-1075, 2017
Manuscript under review for journal Atmos. Chem. Phys.
Published: 27 January 2017

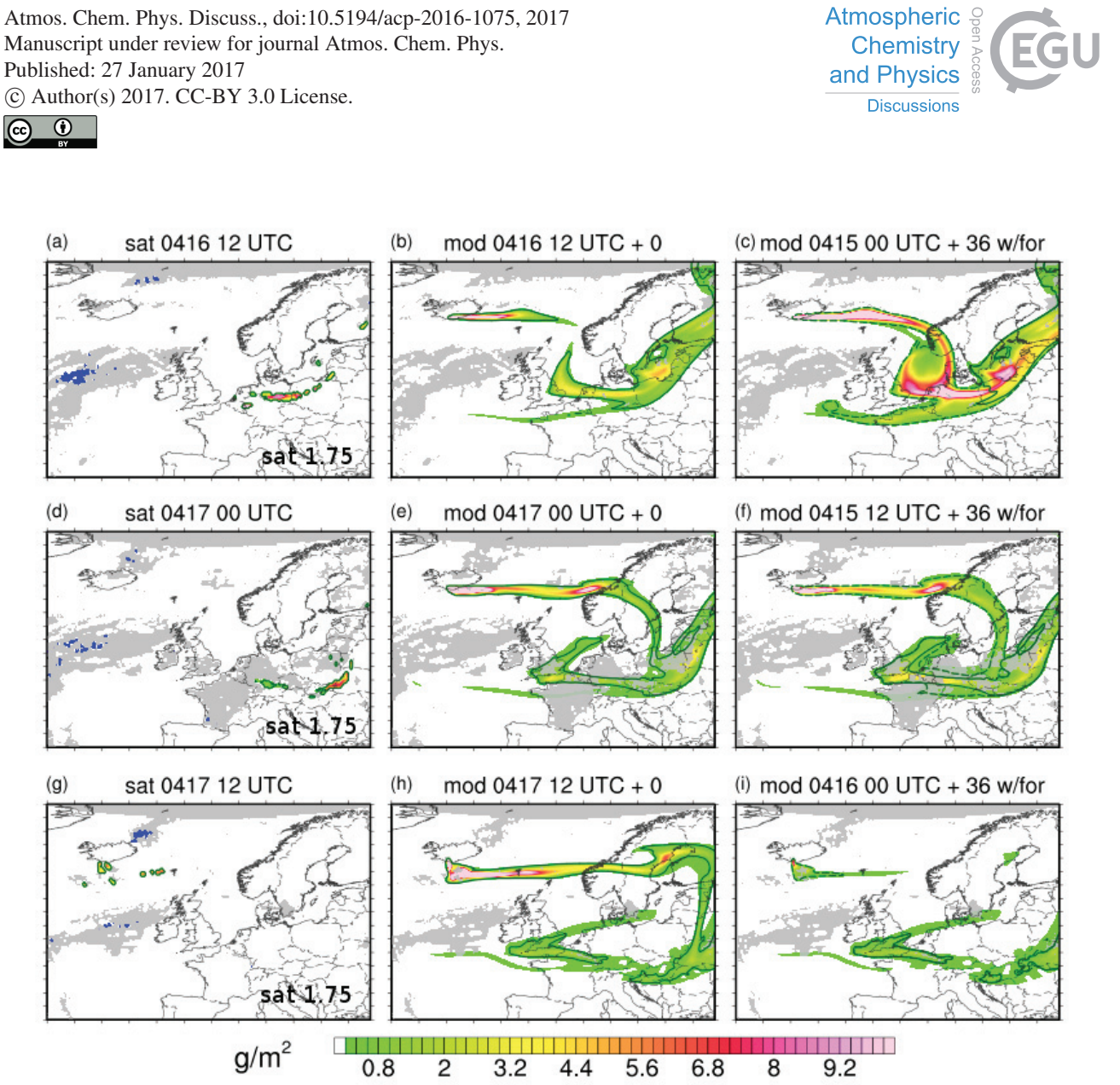

Figure 9: Left column shows SEVIRI satellite retrievals assuming the sat 1.75 size distribution at 16 April 12 UTC (a), 17 April 00 UTC (d) and 17 April 12 UTC (g). Blue areas indicate where the satellite has false positives detection of ash. Middle column shows model simulations with a posteriori emissions calculated from the inversion assuming the 1.75 size distribution, using all satellite retrieval up until the time indicated above the figure (same as satellite). The right column shows model forecasts for the same time as the two first columns, but with a posteriori emissions calculated with satellite observations up to 36 hours before and a forecast emissions term for the remaining 36 hours. The green line encircles objects used for SAL (Structure Amplitude Location) scoring, where ash exceeds 0.5 g m^{-2} limit for model an observed ash. Ash released in the forecast term is shown with a dashed line (only the rightmost column).

Atmos. Chem. Phys. Discuss., doi:10.5194/acp-2016-1075, 2017
Manuscript under review for journal Atmos. Chem. Phys.
Published: 27 January 2017

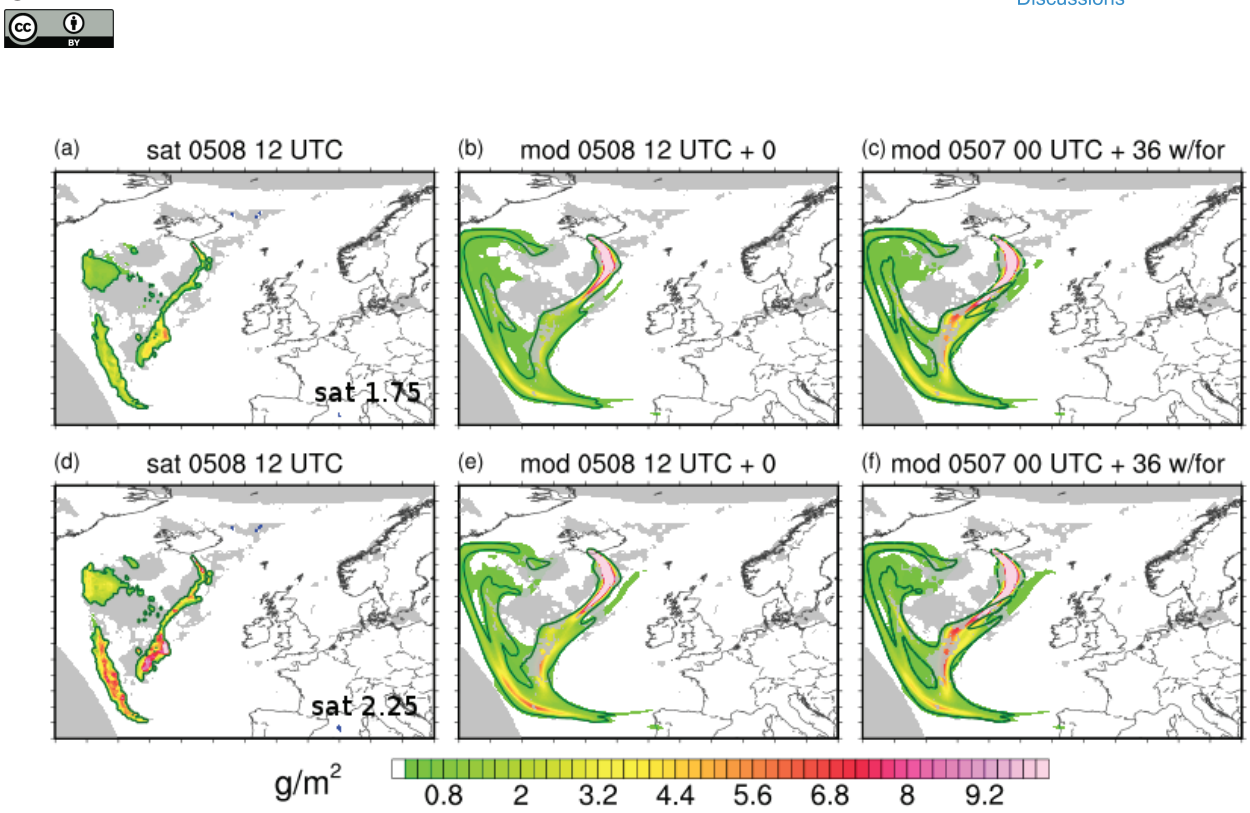

Figure 10: The same as Figure 9 but for 8 May 12 UTC, showing the satellite data (left) and a posteriori model simulations for the first forecast hour (middle) and 36 hour forecasts (right) with inversions for satellite retrieval data with the 1.75 (top row) and 2.25 (bottom row) size distribution assumption.

Atmos. Chem. Phys. Discuss., doi:10.5194/acp-2016-1075, 2017
Manuscript under review for journal Atmos. Chem. Phys.
Published: 27 January 2017

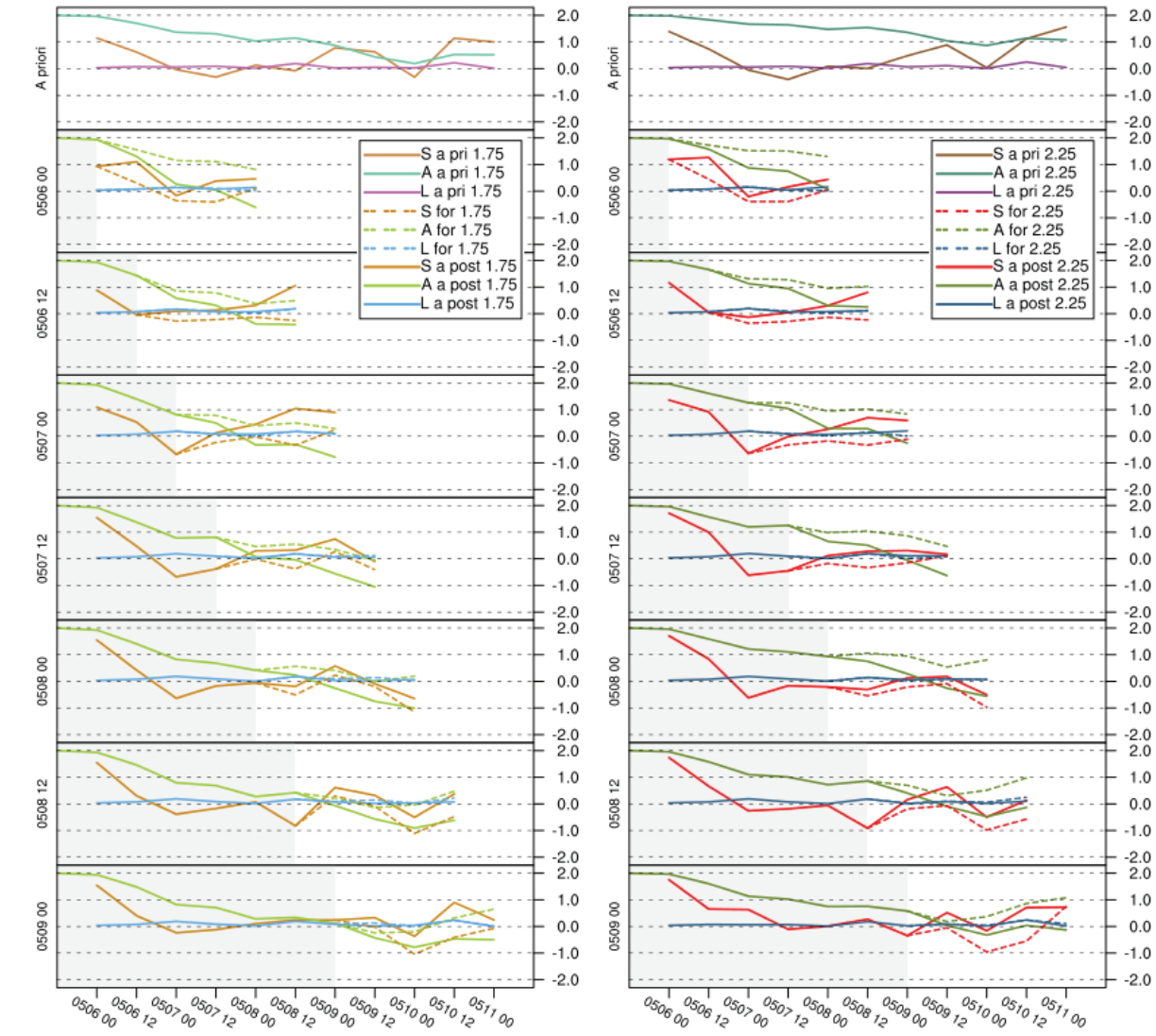

Figure 11: SAL (Structure Amplitude Location) results for model simulations run with the a priori emissions calculated for the 1.75 (left) and 2.25 (right) satellite retrieval (top row), and results for the model simulations using a posteriori emissions started every 12 hours from 6 May 00 UTC to 9 May 00 UTC with a 48 hour forecast using either a forecast emission estimate (dashed lines) or a zero ash emission term in the forecast (straight lines). Grey areas show the assimilation period where the emission estimate is calculated by the inversion. Model simulations with the 1.75 a posteriori source term are compared to the 1.75 satellite observation field, and those with the 2.25 a posteriori emissions are compared to 2.25 satellite retrievals.